Application of Graph Rigidity in Formation Control of Multi-Robot Networks

by

Laura Krick

A thesis submitted in conformity with the requirements
for the degree of Master of Applied Science
Graduate Department of Electrical and Computer Engineering
University of Toronto

Abstract

Application of Graph Rigidity in Formation Control of Multi-Robot Networks

Laura Krick

Master of Applied Science

Graduate Department of Electrical and Computer Engineering

University of Toronto

2007

This thesis designs a formation control for multivehcile systems that uses only local information. Formation control of this type can be applied in mobile sensor networks applications.

The control is derived from a potential function based on an undirected infinitesimally rigid graph. This graph specifies the target formation. Then the potential function is used to specify a gradient control, under which the target formation then becomes a manifold of equilibria for the multivehcile system. The stability of this manifold is studied using a nonlinear coordinate transformation and linearization techniques.

Using these techniques, we show that the infinitesimal rigidity condition of the formation graph provides a sufficient condition to show that the equilibrium manifold is locally asymptotically stable. Finally, a complete study of the stability of the regular polygon formation is presented. These results were validated experimentally.

Acknowledgements

This work would not have be possible without the support and encouragement of my family and friends. In particular, I would like to thank Evangeline Hallam and Paul Tichonczuk.

Additionally, I would like to thank my supervisors Mireille Broucke and Bruce Francis for their patience and guidance in preparing this work. I would also like to thank Manfredi Maggiore for his suggestion to apply center manifold theory in the proof of Theorem 4.5 and Jacek Nawrot for teaching me how to use the experimental apparatus, and for his permission to reprint Figures 7.10 and 7.11.

Contents

Chapter 1

Introduction

Formation control of multi-robot networks is an area of ongoing research in control systems. Formation problems are particularly interesting due to their possible application in multi-robot networks formed using reconfigurable sensor networks.

Sensor networks are comprised of inexpensive devices with computing, communications and sensing capabilities [41]. Each device has a power supply, a computing device with some I/O capabilities and a radio transmitter and receiver. This hardware enables them to form ad-hoc networks. Sensor networks are primarily used to gather data.

A natural extension of sensor networks is to make the network devices mobile, creating a reconfigurable sensor network. This immediately gives rise to a multi-agent control problem. Maintaining a specific formation for a reconfigurable sensor network may be necessary in order to gather data. A particularly useful formation for reconfigurable sensor networks is the regularly spaced polygon. This formation can be used to form a large aperture antenna.

The goal of this work is to design a control law that will stabilize an arbitrary formation of n robots. As a first step, the simple kinematic integrator robot model is considered.

1.1 Literature Review

The simplest multi-robot problem is stabilizing the robots to a common location. This problem is frequently described as the agreement or rendezvous problem and can be viewed as a special case of the formation problem where the target formation is a single point. Many different techniques have been used to solve this problem. Perhaps the simplest scheme is that of cyclic pursuit as described in [26]. Under this control law, each vehicle follows or chases one other vehicle, thereby converging to the centroid of the vehicles. After an initial transient period, the robots move in a spiral motion. Another possible solution to the rendezvous problem is to have the vehicles move based on the positions of the vehicles in the sensor range. A very simple sensor model assumes that each vehicle can sense every other vehicle within a certain radius. As different vehicles move in and out of range, the behaviours of the vehicles change. Reference [10] analyzes the behaviour of such an ad-hoc network.

The solution to the rendezvous problem in [21] is a control law of piecewise constant inputs. The control is a series of "stop and go" maneuvers. During the period when the robot is stopped, its next target location is calculated based on the robots' current neighbours. Although the control is realized as a series of discrete motions, the algorithm does not require that each robot have synchronous stop and go cycles.

The discrete nature and simplicity of the preceding control law has made it especially appealing in sensor network applications. Reference [12] considers a problem of decentralized, self organizing communication nodes with mobility. In this case, the mobility is used to improve communication performance in distributed networks. A variety of networks are considered: single source-destination pair, multiple source and multiple destinations, and many to one. The metrics considered in the evaluation of optimality are power consumption and robustness of transmissions. The control scheme developed is modified from the rendezvous scheme from [21]. The optimization problem considered in [12] has the additional constraint that links between communicating nodes should not

be broken while moving towards an optimal solution.

Another possible goal for mobile sensor networks is to optimize sensor placement by minimizing a cost function. In [11], the solution to this problem involves robots moving to the centroids of convex regions called Voronoi regions. The centroids of these regions are calculated using the cost function as a density function. A specific cost function makes it possible to have the vehicles form certain geometric figures, including polygons. This method is considered to be *decentralized in the sense of Voronoi* as each vehicle must know only the positions of some of the other robots—its Voronoi neighbours—and also to know the cost function. However, this technique requires that the vehicles be contained in a convex region whose boundaries are known and also that there be a global system of coordinates in order to calculate the cost function.

In [40], another goal for sensor networks is explored. In this case, the control goal is to patrol the perimeter of a defined area, with the robots distributed evenly about the boundary. The problem is formulated as a tracking problem on a closed curve, combined with a desired pattern for the vehicles along the curve. The control is designed using control Lyapunov functions and requires global coordinates.

While the techniques of [11] can produce regular polygonal formations, reference [32] considers the problem of producing equilateral formations without global coordinates. In particular, [32] designed a control that makes an equilateral triangle a stable formation. However, for larger groups of robots it is possible to achieve only equilateral polygonal formations, not regular polygonal formations.

The previous papers have all considered problems for mobile networks. Reference [5] studies a problem that is independent of the reconfigurability of the network; namely, the problem of network localization. Network localization is the process of determining the position of each node in a sensor network, given distance measurements between some of the nodes. This problem is of interest for stationary as well as actuated sensor networks. The problem is solvable if the positions can be determined uniquely. The sensor network

is made up of two types of nodes: beacon nodes, whose positions are known; and ordinary nodes. A set of nodes is said to be in a general position for d dimensional space if they do not lie in a proper affine subspace. The network localization problem is solvable if three beacons are in a general position and the graph of known distances is generically globally rigid.

The use of rigidity in [5] shows the interesting relationship between the concept of rigidity and problems involving formations. This leads naturally to the idea of designing a formation control based on rigid graphs. This is the approach to formation control taken by Olfati-Saber and Murray [29]. They use a double integrator model for point mass robots and they propose using rigid graph theory to define the formation. In [29], the concept of an unambiguous graph – essentially a globally rigid graph – is used. They also propose a gradient control law involving prescribed distances. The work in [29] is the closest in spirit to the work of this thesis. Indeed, we use similar ideas based on rigidity theory to formulate a control problem based on distances between agents. As with [29], we derive a gradient control law that is shown to be locally asymptotically stable. However, there are important differences between our work and theirs, and these lie in the methodology and detailed analysis of the problem. Olfati-Saber and Murray give a proof of stability based on the LaSalle invariance theorem. The proof does not analyze all equilibria of the control law. The closed-loop dynamics are not proved to be locally Lipschitz. Also, the control law uses global velocity measurements to stabilize double integrators. Finally, although a set stability result for the equilibrium set is claimed, there is no analysis of stability of points in the equilibrium set.

1.1.1 Gradient Controls

Many of the previously discussed multivehicle controls use a gradient function. We define precisely a gradient control in Section 2.2. Intuitively, gradient controls are those where the system travels down the gradient of a potential function.

In formation control, Olfati-Saber and Muray [29], as well as Zhang and Leonard [40], use the potential function approach in the solutions to their respective multivehicle control problems.

Gradient controls have also been used in flocking problems [35]. Flocking problems are related to formation problems. In flocking, the goal is for the group of agents to form a cohesive group—that is, no agent is far away from all the other agents—but also for the agents to have no collisions. This type of problem mimics the behaviour of a flock of birds or a school of fish. In the control in [35], each agent has an individual potential function based on the location of its neighbours.

A potential function can also be used for path planning problems, as in [30]. The potential function is used both to reach a target destination and to avoid obstacles.

The potential functions used in [29] and [35] are determined by the relative position of the other robots. In [30] the potential function is determine by the features of the environment which are assumed to be static.

Gradient controls are appealing in control problems because such controls have many desirable properties. Some of this properties are discussed in detail in Section 2.2.

1.1.2 Stable Manifolds

The study of formation control is related to the stability of manifolds. As we will see in Section 2.1, manifolds represent specific formations of robots. In formation control our goal is to make the manifold corresponding to the target formation a manifold of equilibria. The study of the stability of a manifold of equilibria is a field of independent interest in dynamics.

A widely used approach to show set stability, and consequently the stability of a manifold, is the application of LaSalle's theorem (Theorem 4.4, p. 128 in [20]). This well-known technique uses a Lyapunov function to show that an invariant set is stable and attractive for initial conditions in a positively invariant set. In practice, the invariant

set is determined by a well chosen Lyapunov function. However, this technique has limitations: one must find a Lyapunov function, and further analysis must be done to determine the behaviour of the trajectories as they approach the manifold.

In [24], Malkin proves an interesting local stability result for an equilibrium manifold. This theorem considers a neighbourhood of a point on an m-dimensional equilibrium manifold. If the Jacobian evaluated at the point has m zero eigenvalues and the rest have negative real parts, trajectories converge to a point on the manifold. The proof of this theorem uses a Lyapunov function and a time-varying change of coordinates. Malkin's result gives more information than local asymptotic stability of the manifold: the manifold is locally asymptotically stable if the distance to the manifold goes to zero—but this does not imply that a limit exists for the trajectory. Malkin's theorem shows that, in this special case, the trajectories do approach a point on the manifold. The limitation of this theorem is that it is a local result about a point on the manifold; further analysis must be done to make any conclusions about the local behavior of the entire manifold. Additionally, Malkin's theorem requires that the dynamics be transformed to a normal form. Finding a coordinate transformation that transforms the dynamics into the form of Malkin may be difficult.

Malkin's proof uses Lyapunov's direct method; in [34] a geometric approach is taken to prove Malkin's theorem. By performing a coordinate transformation, [34] is able to use centre manifold theory to prove Malkin's theorem.

Hale and Massatt extend Malkin's theorem in [15] and consider when the linearization about an equilibrium manifold has no strictly imaginary eigenvalues. Only a one dimensional equilibrium manifold is studied. The result of [15] is to show that if the Jacobian, evaluated at all points on the manifold, has one zero eigenvalue and remaining eigenvalues not on the imaginary axis, then, in a neighbourhood of the manifold, bounded trajectories approach a point on the equilibrium manifold. Centre manifold theory is used to prove the result. This result is appealing as it does not require the dynamics to

be transformed into a normal form.

In [6], Aulbach extends the results of [15] to an equilibrium manifold of any dimension. This result is obtained using centre manifold theory. Aulbach also discusses when these conditions are, in fact, necessary for trajectories to converge to an equilibrium manifold.

In [24], [15] and [6], the stability of equilibrium manifolds is studied using linearization techniques. In [31], Ryashko and Shnol consider the more general problem of the stability of a compact manifold that is invariant—but not an equilibrium. This means there may be dynamics on the manifold of interest; thus linearization techniques are not suitable for the problems considered in [31]. The authors of [31] consider under what conditions an invariant manifold is exponentially stable. Ryashko and Shnol show that if the dynamics transverse to the manifold tend to zero exponentially then the manifold itself is exponentially attractive. This result is obtained using a Lyapunov function.

Under certain conditions, the zero level set of a function is a manifold. For instance, we will construct functions later in this work where the zero level set represents the target formation. In [1], Absil and Kurdyka consider the stability of zero level sets of a function f, where the dynamics of the system are the gradient of f. This type of system is referred to as a gradient system and is discussed in detail in Section 2.2. Absil and Kurdyka show that for a real analytic f, stability and local asymptotic stability of an isolated minimum, i.e. a point, of f are equivalent. They show that a minimum of f, not necessarily only a point, is stable under gradient dynamics.

1.2 Notation

We denote the Jacobian of a function $f : \mathbb{R}^n \to \mathbb{R}^m$ evaluated at a point x as $J_f(x)$. In the special case when $f : \mathbb{R}^n \to \mathbb{R}$, the Jacobian of f is the gradient of f and we denote it by $\nabla f(x)$. Occasionally for convenience during calculations of the Jacobian, the notation

$\frac{\partial}{\partial x}$ will be used to represent

$$J_f(x) = \frac{\partial}{\partial x} f(x).$$

Associated with a mapping $F : \mathcal{S} \to \mathcal{T}$ is the special pre-image set

$$F^{-1}(d) : \{\ p \in \mathcal{S} \mid F(p) = d\ \}.$$

1.3 Illustrative Example

In this work, we design and study controls to stabilize formations. As a preliminary step, we design a control to stabilize two robots so that they are separated by a specified distance d. The robots are modeled using a kinematic point model; that is, robot i's state is $z_i \in \mathbb{R}^2$ and

$$\dot{z}_i = u_i.$$

The combined state of the system is $z = (z_1, z_2) \in \mathbb{R}^4$. If $d = 0$, then the goal is for the robots to be collocated. The set of states where the robots have the same location is

$$\mathcal{S} = \{\ z \in \mathbb{R}^4 \mid z_1 = z_2\ \}.$$

This set is a subspace, and we can use a linear control to stabilize it. Our interest is in controls that use only onboard sensors. That is to say, there are no global coordinates and each robot has only information about the relative positions of the other robots. One possible solution to stabilize $\mathcal{S}$ is for each robot to drive towards the other. Then the control of agent i is $u_i = z_j - z_i$, so

$$\dot{z}_i = z_j - z_i.$$

The coincident formation is a special case: in general the formation will not be char-

acterized by a subspace. When $d \neq 0$, then the formation of interest is

$$\mathcal{M} = \{\ z \in \mathbb{R}^4 \mid \|z_1 - z_2\| = d\ \}.$$

It can be shown that $\mathcal{M}$ is a differential manifold. In this case, the control goal is not a subspace, and we must use a nonlinear control to make $\mathcal{M}$ stable. In particular, when designing a control, we might try scaling our linear control to obtain

$$\dot{z}_i = (\|z_j - z_i\|^2 - d^2)(z_j - z_i). \tag{1.1}$$

This control makes $\mathcal{M}$ a set of equilibria. We analyze these equilibria by linearizing at the point $(0, 0, 0, d) \in \mathcal{M}$. Define $\Delta z := z - (0, 0, 0, d)$. The linearized dynamics of Δz have the form

$$\Delta \dot{z} = -2 \begin{bmatrix} 0 & 0 & 0 & 0 \\ 0 & d^2 & 0 & -d^2 \\ 0 & 0 & 0 & 0 \\ 0 & -d^2 & 0 & d^2 \end{bmatrix} \Delta z.$$

The linearized dynamics have three zero eigenvalues and one stable eigenvalue. So the stability of the system is not obvious from linearization analysis. Instead, we perform an analysis of the output, the distance between the robots, of the system.

Let

$$r := \|z_1 - z_2\|^2.$$

Note that $\sqrt{r}$ is the distance between the robots. Then

$$\begin{aligned}
\dot{r} &= (\dot{z}_1 - \dot{z}_2)^T(z_1 - z_2) + (z_1 - z_2)^T(\dot{z}_1 - \dot{z}_2) \\
&= (2\dot{z}_1)^T(z_1 - z_2) + (z_1 - z_2)^T(2\dot{z}_1) && \text{since } \dot{z}_1 = -\dot{z}_2 \\
&= -4(\dot{z}_1)^T(z_2 - z_1) \\
&= -4(\|z_j - z_i\|^2 - d^2)(z_2 - z_1)^T(z_2 - z_1) && \text{from (1.1)} \\
&= -4(r - d^2)r && \text{from the definition of } r.
\end{aligned}$$

From the phase portrait of r we can conclude immediately that $r = d^2$ is a locally stable equilibrium. The region of attraction for the equilibrium $r = d^2$ is $(0, \infty)$. Moreover, if $r = d^2$, then $z \in \mathcal{M}$. Thus, we can conclude that we achieve our goal to stabilize the robots to be a distance d from one another. However, in doing this analysis we have lost some information about the system. Although we know that the robots are a distance d apart, we do not know if they have stopped moving. We can, however, analyze the zero dynamics of the system. The zero dynamics are the possible dynamics of the system when the output of the system $r - d^2 \equiv 0$. From the form of the z dynamics it is immediately clear that the centroid of the robots is stationary. Furthermore, the robots remain on a line. So we can conclude that the zero dynamics are stationary.

Now, consider stabilizing a more complex formation: three robots in an equilateral triangle with side length d. Again the kinematic point model is studied. Then a system with three robots has the combined state $z = (z_1, z_2, z_3)$. If $d = 0$, then the problem has a linear solution. For instance,

$$\dot{z}_i = (z_j - z_i) + (z_k - z_i)$$

will result in a control law that stabilizes the system. When $d \neq 0$, the formation of

interest is

$$\mathcal{M} = \{\ z \in \mathbb{R}^6 \mid \|z_1 - z_2\| = \|z_2 - z_3\| = \|z_3 - z_1\| = d\ \}.$$

Again, it can be shown that the set $\mathcal{M}$ is a manifold.

In order to have the robots converge to $\mathcal{M}$ we can scale each term by the error term $(\|z_i - z_j\|^2 - d^2)$, obtaining the following controlled system for robot i

$$\dot{z}_i = (\|z_i - z_j\|^2 - d^2)(z_j - z_i) + (\|z_i - z_k\|^2 - d^2)(z_k - z_i).$$

From the form of z_i, it is clear that $\mathcal{M}$ is a set of equilibria. Again the linearized dynamics have three zero eigenvalues, with the remaining eigenvalues being stable. For three robots, the dynamics of the inter-robot distances are unwieldy, so output analysis is not an attractive approach. Note that the set $\mathcal{M}$ is a three dimensional equilibrium manifold, the same as the number of zero eigenvalues. The working hypothesis is that these two facts are related and that it is possible to obtain a stability result from the linearization analysis around a point in an equilibrium manifold.

1.4 Contributions of the Thesis

Our goal is to stabilize particular formations with each robot using only relative information. We first present some mathematical preliminaries on manifolds, gradient systems and graph theory. Next we design a gradient law for a simple robot model to stabilize formations. We discuss in detail properties of equilibrium manifolds. In particular we show that for certain types of equilibrium manifolds there exists a nonlinear change of coordinates to transform the system into the normal form needed to apply Malkin's theorem. This change of coordinates allows us to apply Malkin's theorem, which we use to prove stability of this type of equilibrium manifold. Finally, we apply the stability results to our gradient system.

Chapter 2

Background

The study of formation control applies results from several diverse topics in mathematics. We will review some key results in the literature of differential manifolds, gradient systems and graph rigidity relevant to the current work.

2.1 Differential Geometry

Differential geometry, in particular manifold theory, is useful in the current work because manifolds characterize formations. As we saw in Section 1.3, the set where three agents form an equilateral triangle is a manifold. In fact, most formations can be described by manifolds. We will review some properties of smooth manifolds needed for the study of robot formations. For a rigorous treatment see [9].

2.1.1 Manifolds

An m-dimensional manifold $\mathcal{M}$ is a topological space with a collection of open neighbourhoods $\{\mathcal{U}_i\}$ (note that the index i is countable but not necessarily finite) that cover the entire manifold, with $\mathcal{U}_i \subset \mathcal{M}$, and a collection of diffeomorphisms $\varphi_i : \mathcal{U}_i \to \mathbb{R}^m$. Additionally, for any two neighbourhoods $\mathcal{U}_i$ and $\mathcal{U}_j$ the map $\varphi_j \circ \varphi_i^{-1}$ must be a diffeo-

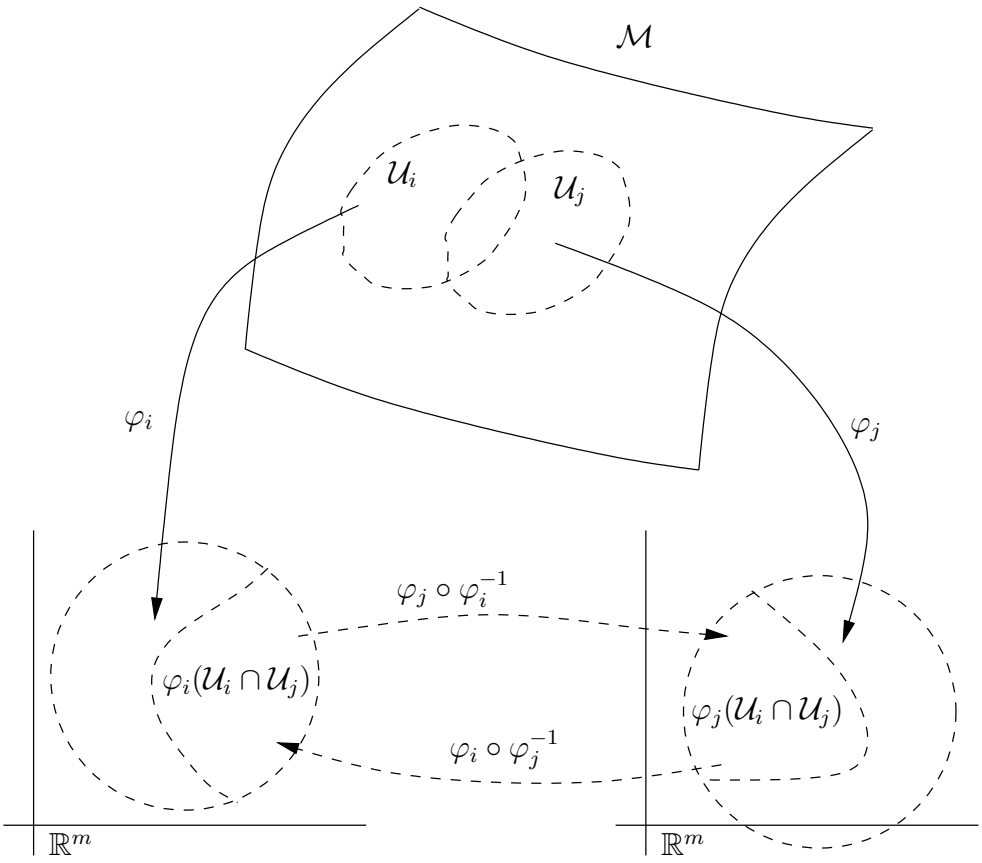

Figure 2.1: An m-dimensional manifold $\mathcal{M}$ and coordinate charts.

morphism from $\varphi_i(\mathcal{U}_i \cap \mathcal{U}_j)$ to $\varphi_j(\mathcal{U}_i \cap \mathcal{U}_j)$ as illustrated in Figure 2.1; likewise $\varphi_i \circ \varphi_j^{-1}$ must be a diffeomorphism from $\varphi_j(\mathcal{U}_i \cap \mathcal{U}_j)$ to $\varphi_i(\mathcal{U}_i \cap \mathcal{U}_j)$. The pair $(\mathcal{U}_i, \varphi_i)$ is called a coordinate chart.

Trivially, $\mathbb{R}^m$ is an m-dimensional manifold; any neighbourhood of a point in $\mathbb{R}^n$ is topologically equivalent to $\mathbb{R}^n$. From the definition it is clear that each $\mathcal{U}_i$ is topologically equivalent to $\mathbb{R}^m$. For instance, a sphere is a 2-dimensional manifold; locally, each point on the manifold appears to be in a plane; a phenomenon that may have led to the erroneous conclusion that the Earth is flat.

Many common geometric structures are manifolds and can be given coordinate charts.

For example, consider the unit circle

$$S^1 := \{\ x \in \mathbb{R}^2 \mid \|x\| = 1\ \}.$$

We can cover the set S^1 with the two open neighbourhoods

$$\mathcal{U}_1 = \{\ x \in S^1 \mid x \neq (1,0)\ \}$$
$$\mathcal{U}_2 = \{\ x \in S^1 \mid x \neq (-1,0)\ \}.$$

Associated with these neighbourhoods are the diffeomorphisms $\varphi_1 : \mathcal{U}_1 \to (0, 2\pi)$ and $\varphi_2 : \mathcal{U}_2 \to (-\pi, \pi)$. Both functions $\varphi_i(x)$ are defined to map x to the angle between x and the positive x_1 axis.

2.1.2 Tangent Space

Define $\mathcal{M}$ to be an m dimensional manifold in $\mathbb{R}^n$. We now consider some vector spaces associated with a manifold $\mathcal{M}$. Each point $p \in \mathcal{M}$ has an associated vector space referred to as the tangent space, $T_p\mathcal{M}$. Although it is possible to define the tangent space of a manifold without using coordinates, as in [9], in this work the manifolds considered will always be subsets of $\mathbb{R}^n$.

The *tangent space* at a point $p \in \mathcal{M}$ is a translated subspace of dimension m that is tangent to the manifold at p. For the manifold S^1, the tangent space at a point p is the line tangent to the circle at p as shown in Figure 2.2. Next consider the sphere S^2. The tangent space T_pS^2 at a point p on the sphere is the plane tangent to p, see Figure 2.3.

We refer to the set $T(\mathcal{M}) := \bigcup_{p\in\mathcal{M}} T_p\mathcal{M}$ as the *tangent bundle* of $\mathcal{M}$. The tangent bundle can also be given the structure of a manifold.

If we have a parametrization of a manifold in $\mathbb{R}^n$ on a neighbourhood $\mathcal{U}$ of $p \in \mathcal{M}$,

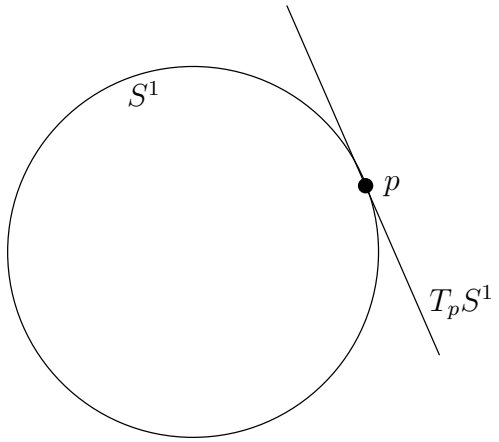

Figure 2.2: The tangent space at the point p for a circle, the manifold S^1.

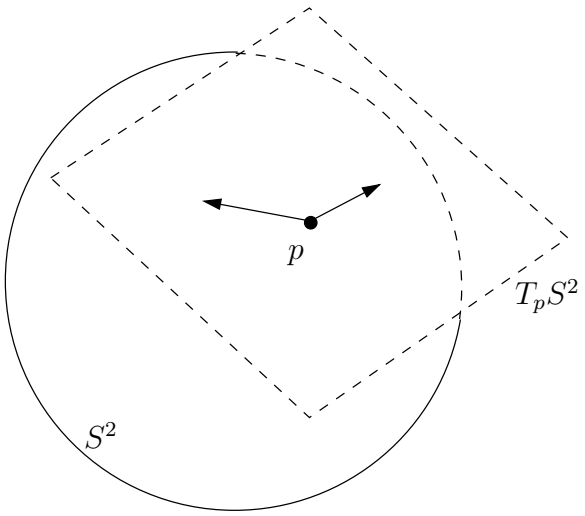

Figure 2.3: The sphere S^2 with the tangent space at p, T_pS^2.

i.e. there exists $h : \mathbb{R}^m \to \mathbb{R}^n$ such that

$$\mathcal{M} \cap \mathcal{U} = h(\mathbb{R}^m) \tag{2.1}$$

then the m columns of $J_h(\theta)$ form a basis for $T_p\mathcal{M}$, (p. 112, [9]).

Let's return to S^2 and calculate a basis for the tangent space at the point $p = (\frac{\sqrt{3}}{4}, \frac{3}{4}, \frac{1}{2})$. A parametric representation of the sphere in the positive orthant is

$$h(\theta) = \begin{bmatrix} \cos(\theta_1)\cos(\theta_2) \\ \cos(\theta_1)\sin(\theta_2) \\ \sin(\theta_1) \end{bmatrix}.$$

Note that $h(\frac{\pi}{6}, \frac{\pi}{3}) = p$. Define $\theta_p = (\frac{\pi}{6}, \frac{\pi}{3})$. The Jacobian of $h(\theta)$ is

$$J_h(\theta) = \begin{bmatrix} -\sin(\theta_1)\cos(\theta_2) & -\cos(\theta_1)\sin(\theta_2) \\ -\sin(\theta_1)\sin(\theta_2) & \cos(\theta_1)\cos(\theta_2) \\ \cos(\theta_1) & 0 \end{bmatrix}.$$

At θ_p,

$$J_h(\theta_p) = \begin{bmatrix} \frac{1}{4} & -\frac{3}{4} \\ -\frac{\sqrt{3}}{4} & \frac{\sqrt{3}}{4} \\ \frac{1}{2} & 0 \end{bmatrix}.$$

Then at the point p a basis for $T_p\mathcal{M}$ is

$$\begin{bmatrix} \frac{1}{4} \\ -\frac{\sqrt{3}}{4} \\ \frac{1}{2} \end{bmatrix} \text{ and } \begin{bmatrix} -\frac{3}{4} \\ \frac{\sqrt{3}}{4} \\ 0 \end{bmatrix}.$$

The plane formed by the span of these two vectors is shown in Figure 2.3.

2.1.3 Normal Space

If $\mathcal{M}$ is a manifold in $\mathbb{R}^n$, then, in addition to the tangent space $T_p\mathcal{M}$ associated with a point p, there is a second vector space associated with the point p, the normal space $N_p\mathcal{M}$. The normal space $N_p\mathcal{M}$ at a point $p \in \mathcal{M}$ is the orthogonal complement in $\mathbb{R}^n$ to the tangent space $T_p\mathcal{M}$. Analogous to the tangent bundle, we refer to the set $N(\mathcal{M}) := \cup_{p\in\mathcal{M}} N_p\mathcal{M}$ as the *normal bundle* of $\mathcal{M}$. The normal bundle can also be given the structure of a manifold.

In certain circumstances, for instance when the normal bundle is trivial, it is possible to calculate the normal bundle without solving for the orthogonal complement of the tangent space; this simplifies the calculation of the normal bundle. The normal bundle of an m-dimensional manifold $\mathcal{M}$ is *trivial* when it is diffeomorphic to $\mathcal{M} \times \mathbb{R}^m$, (p.76, [13]). That is to say the normal space to any point on the manifold can be determined globally using some diffeomorphism. The following lemma describes the conditions for a manifold $\mathcal{M}$ in $\mathbb{R}^n$ to have a trivial normal bundle. First we require a definition. Define $g_i : \mathcal{M} \to \mathbb{R}$. Let $G(x) = (g_1(x), \ldots, g_k(x))$. The functions g_i are *independent* at $p \in \mathbb{R}^k$ if $\nabla g_1(q), \ldots, \nabla g_k(q)$ are linearly independent, for all $q \in G^{-1}(p)$. Note that the rows of $J_G(q)$ are linearly independent when evaluated at every point $q \in G^{-1}(p)$.

Lemma 2.1: *(From [13], p. 77) Let $\mathcal{M} \subset \mathbb{R}^n$ be an $n-k$ dimensional manifold. The normal bundle of $\mathcal{M}$ is trivial if and only if there exist k independent globally defining functions for $\mathcal{M}$ on some open set $\mathcal{U}$ in $\mathbb{R}^n$ such that*

$$\mathcal{M} = \{\ x \in \mathcal{U} \mid g_1(x) = g_2(x) = \ldots = g_k(x) = 0\ \}, \tag{2.2}$$

where $g_i : \mathcal{U} \to \mathbb{R}$ is $\mathcal{C}^\infty$. Moreover

$$\{\nabla g_1(x)^T, \ldots, \nabla g_k(x)^T\}$$

is a basis for $N_x\mathcal{M}$, $\forall x \in \mathcal{M}$.

Let's continue with the example of S^2 and calculate the normal space N_pS^2 where $p = (\frac{\sqrt{3}}{4}, \frac{3}{4}, \frac{1}{2})$. The manifold S^2 has one globally defining function, $\|x\| - 1 = 0$, with $x \in \mathbb{R}^3$ and $\mathcal{U} = \mathbb{R}^3$, and thus Lemma 2.1 applies. A basis for N_pS^2 is

$$\left\{ \begin{bmatrix} \frac{\sqrt{3}}{4} \\ \frac{3}{4} \\ \frac{1}{2} \end{bmatrix} \right\}.$$

It is clear that N_pS^2 is the vector space spanned by p and thus is a ray that is normal to the sphere, as expected.

2.1.4 Functions on Manifolds

Let $\mathcal{M}$ and $\mathcal{N}$ be manifolds with the coordinate charts $(\mathcal{W}_i, \varphi_i)$ on $\mathcal{M}$ and $(\mathcal{U}_j, \psi_j)$ on $\mathcal{N}$. The mapping $F : \mathcal{M} \to \mathcal{N}$ is C^∞ if $\psi_j \circ F \circ \varphi_i^{-1} \in C^\infty$ for any coordinate charts such that $F : \mathcal{W}_i \to \mathcal{U}_j$.

The *rank* of a mapping $F : \mathcal{M} \to \mathcal{N}$ at a point $p \in \mathcal{M}$ is defined to be

$$\text{rank } F = \text{rank } J_{\psi \circ F \circ \varphi^{-1}}(p),$$

where $(\mathcal{W}, \varphi)$ is a coordinate chart such that $p \in \mathcal{W}$ and $(\mathcal{U}, \psi)$ is a coordinate chart such that $F(p) \in \mathcal{U}$.

The rank of a function is useful for studying features of functions on manifolds. In particular, we often consider the rank of a function on an inverse set. For a smooth mapping $F : \mathcal{M} \to \mathcal{N}$, a point $p \in \mathcal{N}$ is a *regular value* if $rank(F(q)) = \dim(\mathcal{N})$, for all $q \in F^{-1}(p)$.

2.1.5 Submanifolds

Analogous to a subspace of a vector space, we can also have a submanifold of a manifold. In the current study, we will be considering submanifolds of $\mathbb{R}^n$. Unlike subspaces, there is more than one class of submanifold. In particular, we are interested in a class of submanifolds referred to as *embedded submanifolds*.

Let $\mathcal{M}$ and $\mathcal{N}$ be two manifolds in $\mathbb{R}^N$ with $\dim(\mathcal{M}) = m$ and $\dim(\mathcal{N}) = n$, as shown in Figure 2.4. The manifold $\mathcal{N}$ is an embedded submanifold of $\mathcal{M}$ if $\mathcal{N} \subset \mathcal{M}$ and for every $p \in \mathcal{N}$ there exists a coordinate chart $(\mathcal{W}, \varphi)$ of $\mathcal{M}$, with $p \in \mathcal{W}$ such that

$$\mathcal{N} \cap \mathcal{W} = \{\ q \in \mathcal{W} \mid \varphi_1(q) = \varphi_2(q) = \ldots = \varphi_{m-n}(q) = 0\ \}, \tag{2.3}$$

where φ_i are the components of φ. So $\varphi(\mathcal{N} \cap \mathcal{W})$ is contained in an n-dimensional subspace in $\mathbb{R}^m$. For this reason $\mathcal{N}$ is often called an n-dimensional slice of $\mathcal{W}$. Locally, $\mathcal{N}$ is the zero level set of the function $F(p) := (\varphi_1(p), \ldots, \varphi_{m-n}(p))$. By definition it is clear that F maps from $\mathcal{W} \to \mathbb{R}^{m-n}$. Thus, we can view an n-dimensional embedded submanifold locally as the level set of an $(m-n)$-dimensional function. Notice the close resemblance between (2.3) and (2.2). In fact, (2.2) is a global version of (2.3) where the larger manifold is $\mathbb{R}^n$. Unfortunately, the definition of an embedded submanifold does not provide an easy algebraic test to determine if a particular submanifold is embedded.

Consider the function $h : \mathbb{R} \to \mathbb{R}^2$ where

$$h(t) = \begin{cases} (t, 0) & t \leq 0 \\ (\sin t, \cos t - 1) & 0 < t \leq \frac{3\pi}{2} \\ (-1, \frac{3\pi}{2} t^{-1}) & t > \frac{3\pi}{2} \end{cases}$$

Figure 2.5 shows a plot of the map h. The image of h is not an embedded submanifold of $\mathbb{R}^2$ because the manifold does not have the required form in the neighbourhood of $(-1, 0)$. In this case, the value of h at $t = -1$ and in the limit as $t \to \infty$ are both $(-1, 0)$. In

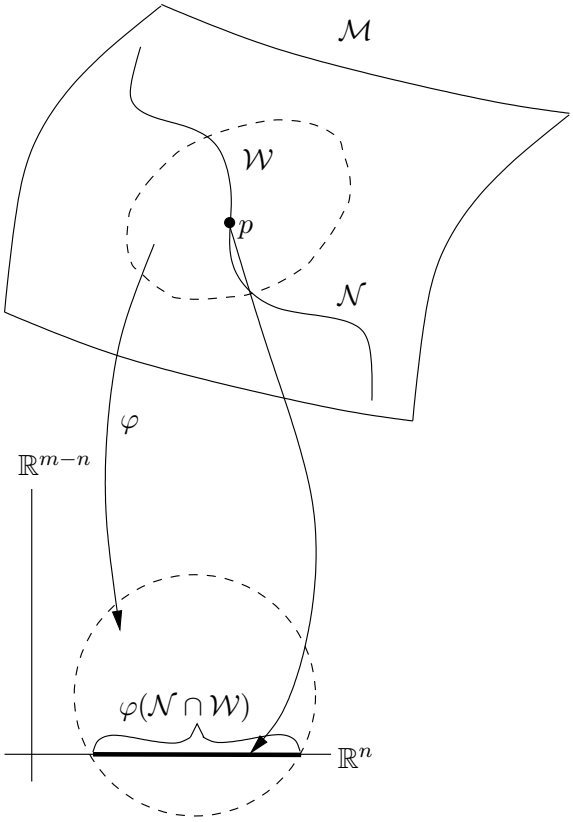

Figure 2.4: An m-dimensional manifold $\mathcal{M}$ with an n-dimensional embedded submanifold $\mathcal{N}$. The set $\mathcal{N} \cap \mathcal{W}$ is mapped to a subset of an n-dimensional plane.

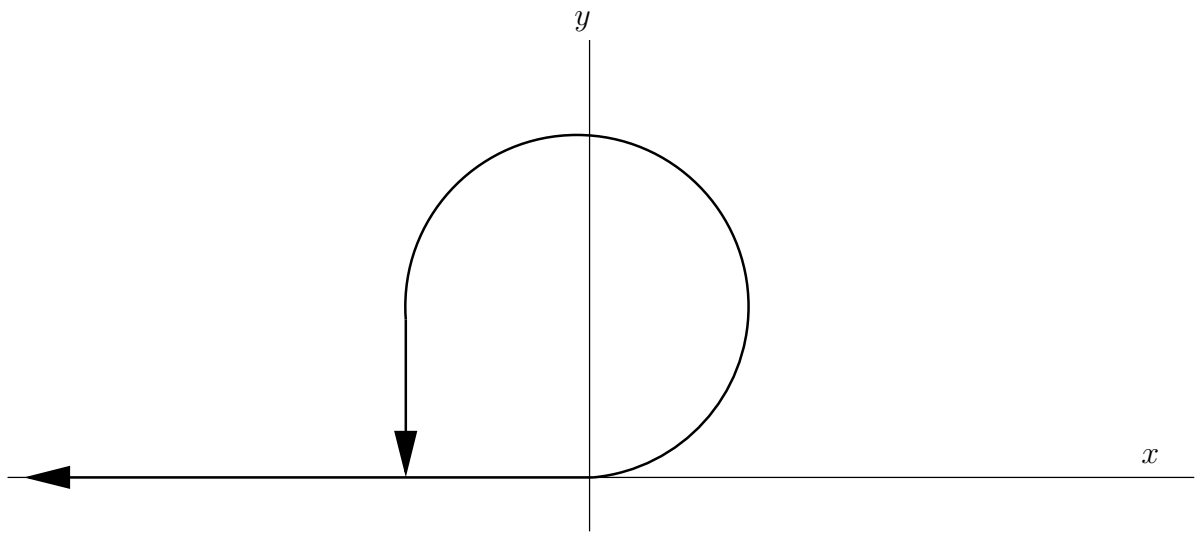

Figure 2.5: Example of a submanifold of $\mathbb{R}^2$ that is not embedded.

any neighbourhood of the point $(-1, 0)$ the manifold has a 'T' shape. It is impossible for this 'T' to be diffeomorphic to a one dimensional subspace, so the embedded submanifold definition does not hold.

We have seen that an embedded submanifold is locally the zero level set of a function. This leads to the question, if a set is the level set of a sufficiently smooth function, is it an embedded submanifold? The following theorem from [9] gives a condition when a level set of a function is also an embedded submanifold.

Theorem 2.1 (Preimage Theorem, [9], p. 79) : *Let $\mathcal{N}$ and $\mathcal{M}$ be two manifolds, with $\dim \mathcal{N} = n$ and $\dim \mathcal{M} = m$. Let $F : \mathcal{M} \to \mathcal{N}$ be a C^∞ mapping. If rank $F = k$ for all points in $\mathcal{M}$, then, for all $q \in F(\mathcal{M})$, $F^{-1}(q)$ is a closed embedded submanifold of $\mathcal{M}$ with dimension $m - k$.*

In [9] there is also a useful corollary to the Preimage Theorem.

Corollary 2.1 ([9], p. 80) : *Let $\mathcal{N}$ and $\mathcal{M}$ be two manifolds, with $\dim \mathcal{N} = n$ and $\dim \mathcal{M} = m$, with $n \leq m$. Let $F : \mathcal{M} \to \mathcal{N}$ be a C^∞ mapping. If for some point $q \in F(\mathcal{M})$ rank $F = n$ for all points in $F^{-1}(q)$, then $F^{-1}(q)$ is a closed embedded submanifold of $\mathcal{M}$ with dimension $m - n$.*

Corollary 2.1 has a less restrictive condition on the rank of F—it must have constant rank only on a subset of $\mathcal{N}$. However, because the rank is maximal, there exists a neighbourhood of $F^{-1}(q)$ with constant rank. The Preimage Theorem can then be applied on this neighbourhood to obtain Corollary 2.1. We will use this corollary in the proof of Theorem 5.1.

Let's continue with the example of the circle to show that the unit circle is an embedded submanifold of $\mathbb{R}^2$. Define $F(x, y) := \|(x, y)\|^2$. Note that $F : \mathbb{R}^2 \to \mathbb{R}$, so in this example $\mathcal{M} = \mathbb{R}^2$ and $\mathcal{N} = \mathbb{R}$. Then the unit circle is the set $F^{-1}(1)$. If we check the rank of F, using φ as the identity map, we obtain

$$\text{rank } F = \text{ rank } \begin{bmatrix} x & y \end{bmatrix}$$

The rank of F equals 1 except at the origin, when rank $F = 0$. On $F^{-1}(1)$, F has constant maximal rank, so by applying Corollary 2.1 we can conclude that the set $F^{-1}(1) = S^1$ is an embedded submanifold of $\mathbb{R}^2$.

In fact, there is an interesting result, the Whitney embedding theorem (p. 197, [9]), that shows that any manifold can be embedded into a sufficiently large Euclidean space. For instance, the 1-dimensional manifold in Figure 2.5 can be embedded in $\mathbb{R}^3$. Consider the function $h : \mathbb{R} \to \mathbb{R}^3$ where

$$h(t) = \begin{cases} (t, 0, 0) & t \leq 0 \\ (\sin t, \cos t - 1, -t) & 0 < t \leq \frac{3\pi}{2} \\ (-1, \frac{3\pi}{2} t^{-1}, -t) & t > \frac{3\pi}{2} \end{cases}$$

Figure 2.6 shows a plot of the map h. The image of h is an embedded submanifold of $\mathbb{R}^3$.

The results in subsequent chapters will involve embedded submanifolds which are level sets of smooth functions. In this special case, the normal and trivial space have

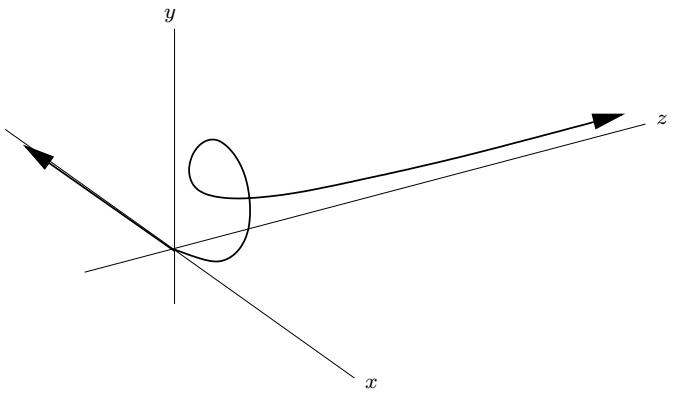

Figure 2.6: Example of an embedded manifold in $\mathbb{R}^3$ that is diffeomorphic to the manifold from Figure 2.5.

some interesting properties. Let $g_i : \mathbb{R}^n \to \mathbb{R}$, $i = 1, \ldots, k$ be smooth functions. We then define $\mathcal{M} \subset \mathbb{R}^n$ such that

$$\mathcal{M} = \{\ x \in \mathbb{R}^n \mid g_1(x) = g_2(x) = \ldots = g_k(x) = 0\ \},$$

and zero is a regular value. Note that $\mathcal{M}$ has exactly the form of (2.2). We have seen in Lemma 2.1, when the functions g_i are globally defining and independent, then there is a simple method to obtain a basis for the normal bundle. In addition, recall from Section 2.1.2 for embedded submanifolds, the tangent space at a point has an explicit local basis obtained from a parametric representation of the submanifold. The form of $\mathcal{M}$ is not a parametric representation, but we can construct a parametric representation.

In particular, the submanifold $\mathcal{M}$ can also be represented as the image of an embedding as in Theorem 3.1 (p. 21, [18]). To construct such an embedding, we begin with the functions $g_1, \ldots, g_k$ defining $\mathcal{M}$. Let $p \in \mathcal{M}$. Then, by the implicit function theorem, there exists a neighborhood $\mathcal{U} \subset \mathbb{R}^n$ of p and a set of functions $\psi_1, \ldots, \psi_{n-k}$, with $\psi : \mathcal{U} \to \psi(\mathcal{U})$, such that the map ψ has the form $\psi := (\psi_1, \ldots, \psi_{n-k}, g_1, \ldots, g_k)$ and ψ is a diffeomorphism (see, for example, Proposition 2.18 from [28]). By construction, $(\mathcal{U}, \psi)$ is a coordinate chart for $\mathbb{R}^n$. In these "preferred coordinates" $\mathcal{M}$ is locally defined

by

$$\mathcal{M} \cap \mathcal{U} = \{\ x \in \mathbb{R}^n \mid \psi_{n-k+1}(x) = \cdots = \psi_n(x) = 0\ \},$$

where $\psi_{n-k+i}(x) = g_i(x)$. The preferred coordinates provide a local representation of an embedding $h : \mathcal{V} \to \mathbb{R}^n$ where $\mathcal{V} = \{\theta \in \mathbb{R}^{n-k} \mid (\theta, 0) \in \psi(\mathcal{U})\}$. The embedding is given by

$$h(\theta) := \psi^{-1}(\theta, 0)\,.$$

Thus, h is a local homeomorphism from $\mathcal{V}$ onto $\mathcal{M}$ and a local parametric form for $\mathcal{M}$. In Remark 4.1 we discuss a global version of this result.

For example, let's consider the unit circle S^1 embedded in $\mathbb{R}^3$ such that

$$S^1 = \{\ x \in \mathbb{R}^3 \mid x_1^2 + x_2^2 - 1 = x_3 = 0\ \}.$$

The function g that defines S^1 is $g = (x_1^2 + x_2^2 - 1, x_3)$. On the set $\mathcal{U} := \{\ x \in \mathbb{R}^3 \mid x_2 > 0\}$ we can define ψ_1 to map x to the angle between (x_1, x_2) and the positive x_1 axis. Then $\psi = (\psi_1, g)$, as shown in Figure 2.7 and $(\mathcal{U}, \psi)$ is a coordinate chart of $\mathbb{R}^3$. We define $h(\theta) := \psi^{-1}(\theta, 0)$.

The homeomorphism h can be used to define a basis for the tangent space. If for all $x \in \mathcal{M}$, we define $\theta = h^{-1}(x)$, then from the definition of the tangent space $T_x\mathcal{M} = \mathrm{Im}(J_h(\theta))$.

This leads to the following fact showing that, as expected, the basis vectors for the normal space and tangent space are orthogonal.

Fact 2.1 *For all $x \in \mathcal{M}$, with $\theta = h^{-1}(x)$,*

$$(\nabla g_i(h(\theta))J_h(\theta) = 0$$

for $1 \le i \le k$.

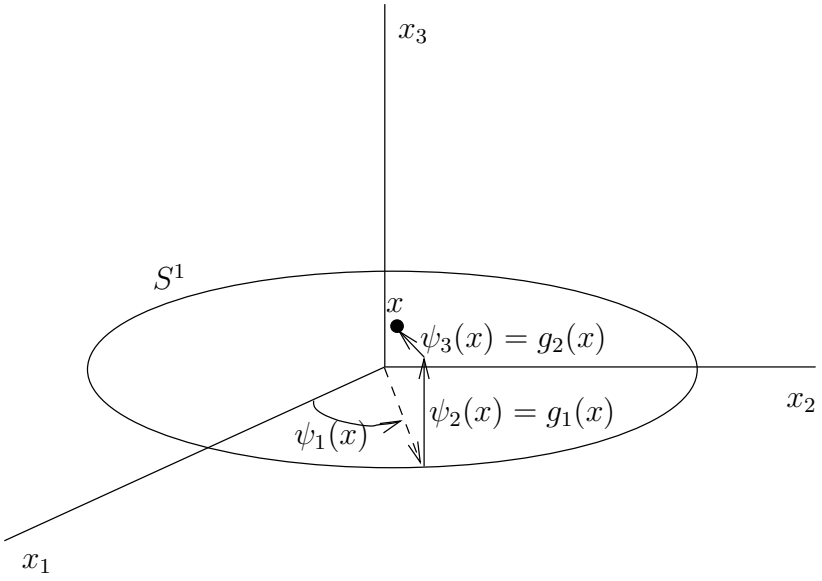

Figure 2.7: Example construction of ψ for S^1 embedded in $\mathbb{R}^3$.

Proof: For any i, and $\forall\theta$, $g_i(h(\theta)) = 0$. If we differentiate with respect to θ we obtain the required result. □

2.2 Gradient Systems

Let $V : \mathbb{R}^n \to \mathbb{R}$ be a continuously differentiable function. Let $f(x) := -\nabla V(x)^T$. Then the system

$$\dot{x} = f(x) \tag{2.4}$$

is a *gradient system*. The function $V(x)$ is referred to as a potential function.

Note that if A is symmetric, the linear system

$$\dot{x} = Ax$$

is a gradient system, with the potential function $V(x) = -\frac{1}{2}x^T Ax$.

Gradient systems have some useful properties that we state below; for proofs see

[19]. In order to describe these properties, we use the *Lie derivative*. The Lie derivative, denoted $L_f V$, is a map from $\mathbb{R}^n \to \mathbb{R}$ and is related to the derivative of $V(x)$ along solutions $x(t)$ of (2.4). We take the time derivative of $V(x(t))$ and find that

$$\begin{aligned}\frac{d}{dt}V(x(t)) &= \nabla V(x(t))\dot{x}(t) \\ &= \nabla V(x(t))f(x(t)).\end{aligned}$$

We then define

$$L_f V(x) := \nabla V(x) f(x).$$

Note that $L_f V(x(t)) = \frac{d}{dt}V(x(t))$. The Lie derivative of a gradient system has the following important property.

Theorem 2.2 ([19], p 200): *The Lie derivative, $L_f V(x)$, satisfies $L_f V(x) \leq 0$ for all x. Furthermore, $L_f V(x) = 0$ if and only if x is an equilibrium of* (2.4).

The proof of Theorem 2.2 follows directly from the fact that $L_f V(x) = -||\nabla V(x)||^2$. From Theorem 2.2 we see that the trajectories of (2.4) either remain on the same level set of V or move down level sets of $V(x)$; the value of $V(x(t))$ cannot increase. Note that this property of the trajectories does not imply stability as we have not restricted $V(x)$ in any way; $V(x)$ may have no minimum value.

Associated with any system of the form (2.4) (not just gradient systems) are two special sets: the α- and ω-limit sets. A point p is an ω-limit point of (2.4) if there exist an initial condition, $x(t_0)$, and a sequence of times t_i, with $t_i \to \infty$ as $i \to \infty$, such that

$$\lim_{i\to\infty} x(t_i) = p. \tag{2.5}$$

The ω-limit set is the set of all ω-limit points. Similarly, an α-limit point is a point p where there exist an initial condition, $x(t_0)$, and a sequence of times t_i, with $t_i \to -\infty$

as $i \to \infty$, such that

$$\lim_{i\to\infty} x(t_i) = p. \tag{2.6}$$

The α-limit set is the set of all α-limit points.

The α- and ω-limit sets of a gradient system have a special property.

Theorem 2.3 ([19], p. 203): *Let z be an α-limit point or an ω-limit point of a trajectory of (2.4). Then z is an equilibrium.*

Theorem 2.3 is particularly interesting because it implies that a gradient system can have no limit cycles or other steady-state periodic behaviour.

Let's consider a simple example using a potential function to stabilize the origin of the system

$$\dot{x} = u,$$

with $x \in \mathbb{R}^n$. A possible potential function is $\frac{1}{2}\|Mx\|^2$, with $M \in \mathbb{R}^{m\times n}$. Then

$$\dot{x} = -M^T M x.$$

The stability of the origin then depends on the size of the kernel of $M^T M$. The following fact shows the relationship between $\ker(M^T M)$ and $\ker(M)$.

Fact 2.2 *For any matrix M, $\ker(M^T M) = \ker(M)$.*

Proof: It is immediate that $\ker(M) \subset \ker(M^T M)$. We now show the converse by letting $x \in \ker(M^T M)$. So $M^T M x = 0$. It follows that

$$x^T M^T M x = 0$$

$$\|Mx\|^2 = 0.$$

So $Mx = 0$ and $x \in \ker(M)$. □

Applying Fact 2.2 we can conclude that if $\ker(M) = 0$ then the origin will be stable.

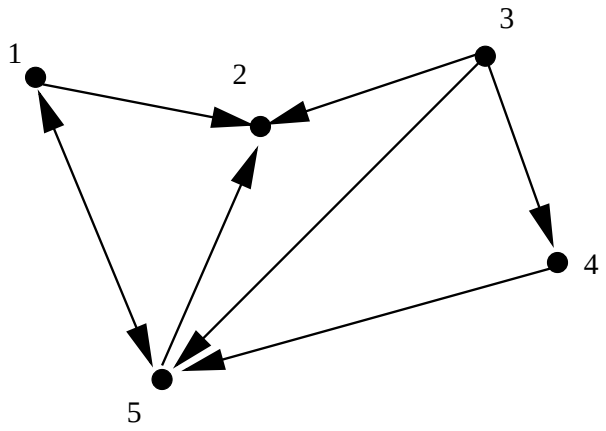

Figure 2.8: Example of a directed graph.

2.3 Graph Theory

The solution to multivehicle problems is strongly dependent on the sensor information each robot knows about its neighbours. For instance, in [22] the robots achieve rendezvous only if there are a sufficient number of sensor connections. A graph is a particularly useful and commonly used way to encode this information.

Typically, set notation is used to describe a graph. A directed graph $G = (V, E)$ is a pair consisting of two sets: a finite set of vertices $V := \{1, \ldots, n\}$ and a set of edges $E \subset V \times V$. We assume the edges are ordered. That is to say that $E = \{1, \ldots, m\}$, where $m \in \{1, \ldots, n(n-1)\}$. Each edge e_i has a source vertex j and a destination vertex k. For example, in Figure 2.8 there is an edge from vertex 1 to vertex 2. We exclude the possibility of self loops: edges with the same source and destination node are not permitted.

An undirected graph is a special case of a directed graph. In an undirected graph if there is an edge e_i from vertex j to vertex k then there is also an edge e_l from vertex k to vertex j. In a directed graph, this is not necessarily the case. For undirected graphs, we will omit the arrows in the pictorial representation of the graph, as in Figure 2.9.

A special undirected graph is the graph K_n, the *complete graph* with n vertices. The

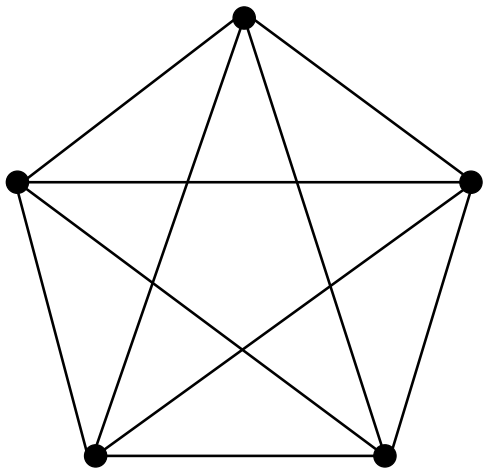

Figure 2.9: The complete graph with five vertices, K_5.

graph K_n has an edge between every pair of nodes. Figure 2.9 shows K_5, the complete graph with five vertices.

We can associate several useful matrices with a graph G. The *adjacency matrix*, $A_G = (a_{ij})$, is a matrix of zeros and ones. There is a 1 in position a_{ij} if there is an edge from vertex i to vertex j. If the graph G is undirected then A_G is a symmetric matrix. A second useful matrix is the *degree matrix*. The degree matrix of a graph G is denoted $D_G = (d_{ij})$ and is defined to be the diagonal matrix where the value of d_{ii} is the number of edges leaving from vertex i. The *incidence matrix*, H_G, is determined by the edges e_i of G: row i of H_G is determined by e_i and has two non-zero entries: a 1 in column k and a -1 in column j. For undirected graphs the location of the 1 and -1 can be chosen arbitrarily. In the graph G then e_i is the edge between vertex j and vertex k. Thus, by definition, $H_G\mathbf{1} = 0$, where $\mathbf{1}$ is the vector with a 1 in each component.

Property 2.1 *The incidence matrix, H_G, has the following properties:*

1. *each row has two non-zero entries: a* 1 *and a* -1,

2. *the rank of H_G is $n-c$ where c is the number of connected components in the graph; see Proposition 4.3 (p. 23) from [8].*

For the remainder of this work we will assume that all graphs we are considering are connected and thus $\ker(H_G)$ is one dimensional. In this work directed graphs are considered connected if the corresponding undirected graph is connected.

Finally, the graph *Laplacian* is $L_G = D_G - A_G$. If G is a symmetric graph then $L = H^T H$ (see Proposition 4.8 p. 27 in [8]). In contexts where the meaning of G is unambiguous, we will drop the subscript.

For the graph in Figure 2.8 the adjacency matrix A and the degree matrix D are

$$A = \begin{bmatrix} 0 & 1 & 0 & 0 & 1 \\ 0 & 0 & 0 & 0 & 0 \\ 0 & 1 & 0 & 1 & 1 \\ 0 & 0 & 0 & 0 & 1 \\ 1 & 1 & 0 & 0 & 0 \end{bmatrix}, \quad D = \begin{bmatrix} 2 & 0 & 0 & 0 & 0 \\ 0 & 0 & 0 & 0 & 0 \\ 0 & 0 & 3 & 0 & 0 \\ 0 & 0 & 0 & 1 & 0 \\ 0 & 0 & 0 & 0 & 2 \end{bmatrix}.$$

For the graph in 2.8 the incidence matrix is

$$H = \begin{bmatrix} -1 & 1 & 0 & 0 & 0 \\ 0 & 1 & -1 & 0 & 0 \\ 0 & 0 & -1 & 1 & 0 \\ 0 & 0 & 0 & -1 & 1 \\ 0 & 0 & -1 & 0 & 1 \\ 0 & 1 & 0 & 0 & -1 \\ 1 & 0 & 0 & 0 & -1 \\ -1 & 0 & 0 & 0 & 1 \end{bmatrix}.$$

2.3.1 Graph Rigidity

In order to consider the rigidity of graphs we view them as frameworks embedded in the plane, $\mathbb{R}^2$. Let $G = (V, E)$ be an undirected graph with vertices V and edges E.

We then *embed* G into $\mathbb{R}^2$ by assigning to each vertex i a location $p_i \in \mathbb{R}^2$. Define the composite vector $p = (p_1, \ldots, p_{|V|}) \in \mathbb{R}^{2|V|}$, where $|V|$ is the cardinality of the set V. Then a framework is a pair (G, p).

We define the *rigidity function* associated with the framework (G, p) as the function $f_G : \mathbb{R}^{2|V|} \to \mathbb{R}^{|E|}$, such that

$$f_G(p) := (\ldots, \|p_k - p_j\|^2, \ldots),$$

with vertices j and k connected by the edge e_i in E. Then the ith component of $f_G(p)$, $\|p_k - p_j\|^2$, corresponds to the edge e_i. Note that this rigidity function is not unique and depends on the ordering given to the edges.

There are several equivalent definitions of rigidity. The definitions below are taken from [4]. Rigidity is related to the isomorphisms of frameworks. Two frameworks are *isomorphic* if they are related by some sequence of translations and rotations in the plane. We will describe a framework as rigid if the only local deformation of the framework is isomorphic to the original framework.

The intuitive idea of rigidity is as follows: Imagine the framework is represented by a collection of magnets and metal bars. Each vertex is represented with a magnet, or some other connector that will allow free movement in the plane, at its location. Then for every edge in the graph we connect the source and destination vertex magnet with a thin metal bar. Now, deform the framework by translating the vertices independently, while maintaining the lengths prescribed by the metal bars. If the graph is embedded as a rigid framework, then the only possible motions of the vertices will result in a framework isomorphic to the original framework.

For example, consider the framework in Figure 2.10(a). It is possible to translate the top two points of the framework while maintaining the four edge lengths to obtain a graph that is not isomorphic to the original graph; the lengths of the diagonals change.

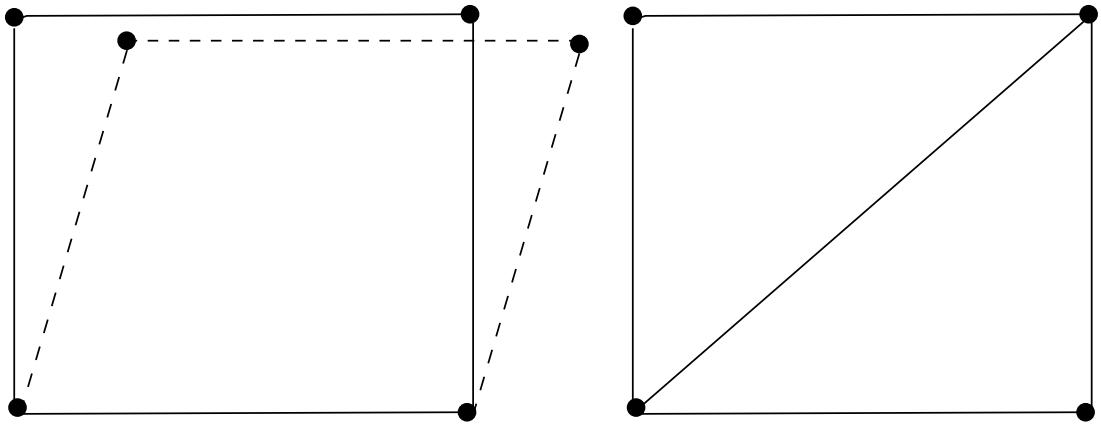

(a) Example of a flexible framework. (b) Example of a rigid framework.

Figure 2.10: Two different frameworks with four nodes.

So the framework in Figure 2.10(a) is not rigid. If we add one more edge to the framework in Figure 2.10(a), we obtain the framework in Figure 2.10(b). For this framework, every perturbation of the vertices that maintains the edge lengths is isomorphic to the original framework. So the graph in Figure 2.10(b) is rigid. Note that in this case, all the edge lengths stay the same, not just the edges specified in the graph.

In particular, the complete graph, K, is always rigid.

Definition 2.1: *A framework (G, p) is rigid if there exists a neighbourhood $\mathcal{U}$ of p such that $f_G^{-1}(f_G(p)) \cap \mathcal{U} = f_K^{-1}(f_K(p)) \cap \mathcal{U}$, where K is the complete graph with the same vertices as G.*

The level set $f_G^{-1}(f_G(p))$ is all the possible locations that have the same edge lengths as the framework (G, p). For the complete graph K the set $f_K^{-1}(f_K(p))$ corresponds to rotations and translations, i.e., rigid body motions, of the framework (K, p). Thus we see that a graph G is rigid if the level set $f_G^{-1}(f_G(p))$ in the neighbourhood of p contains only rotations and translations of the formations corresponding to the point p.

We refer to the matrix $J_{f_G}(p)$ as the *rigidity matrix* of (G, p). The rigidity matrix is useful in defining some other concepts related to graph rigidity.

Definition 2.2: *A point p is a regular point of the graph G with n vertices if*

$$\text{rank}J_{f_G}(p) = \max\left\{ \text{ rank}J_{f_G}(q) \mid q \in \mathbb{R}^{2n} \right\}.$$

In Figure 2.11(a) we see that the graph K_3 is embedded at a regular point. Conversely, Figure 2.11(b) shows the graph K_3 embedded at a point that is not regular.

Next we consider *infinitesimal rigidity*. In this case, we allow the vertices to move infinitesimally, while keeping the rigidity function constant up to first order. Let δp be such an infinitesimal motion of the framework (G, p). Then the Taylor series expansion of f_G about p

$$f_G(p + \delta p) = f_G(p) + J_{f_G}(p)\delta p + \text{ higher order terms.}$$

The rigidity function remains constant up to first order when $f_G(p + \delta p) = f_G(p) + J_{f_G}(p)\delta p = f_G(p)$. This is equivalent to

$$J_{f_G}(p)\delta p = 0.$$

All the possible infinitesimal motions δp such that $f_G(p+\delta p) = f_G(p)$ are in $\ker(J_{f_G}(p))$. Intuitively, the rigidity function remains constant under translations and rotations. For planar graphs, this gives δp three degrees of freedom while keeping $J_{f_G}(p)\delta p$ constant. We will consider a framework to be infinitesimally rigid if the only possible infinitesimal motions correspond to the rigid body motions.

Definition 2.3 ([4]) : *A framework (G, p) is infinitesimally rigid in the plane if* $\dim(\ker J_{f_G}(p)) = 3$*, or equivalently if*

$$\text{rank}J_{f_G}(p) = 2|V| - 3.$$

If a framework is infinitesimally rigid, it implies that it is also rigid. The converse

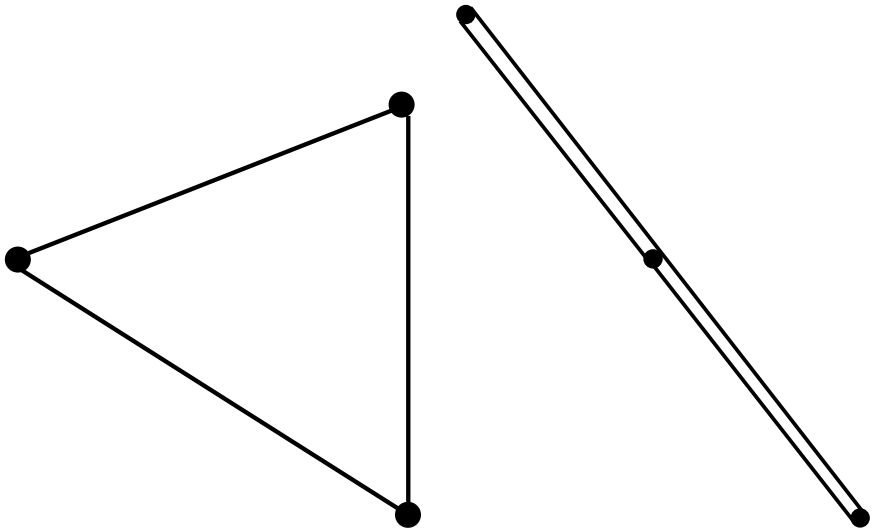

(a) Example of a rigid and infinitesimally rigid framework with K_3 as the underlying graph.

(b) Example of a rigid but not infinitesimally rigid framework with K_3 as the underlying graph.

Figure 2.11: Two different embeddings in the plane of the graph K_3 show that the same graph can be infinitesimally rigid for two frameworks embedded at different points.

is not true. The following theorem outlines when rigidity and infinitesimal rigidity are equivalent.

Theorem 2.4 ([4]) : *A framework (G, p) is infinitesimally rigid if and only if (G, p) is rigid and p is a regular point.*

A final useful concept of graph rigidity is the concept of global rigidity.

Definition 2.4: *A framework (G, p) is globally rigid if $f_G^{-1}(f_G(p)) = f_K^{-1}(f_K(p))$.*

From this definition, and the definition of infinitesimally rigidity, we see that for a graph to be infinitesimally rigid in the plane it must have at least $2|V| - 3$ edges. If it has exactly $2|V| - 3$ edges, we say that the graph is *minimally rigid*.

The two different embeddings of K_3 shown in Figure 2.11 illustrate some of the rigidity properties. Both frameworks shown are embeddings of the complete graph. It follows immediately from the definition of rigidity and global rigidity that the two frameworks

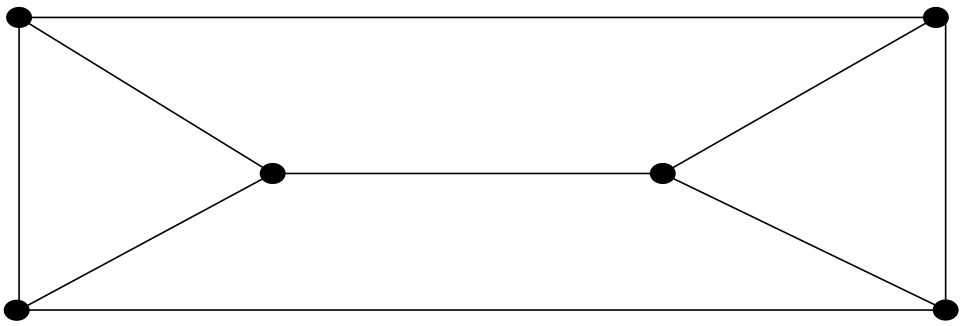

Figure 2.12: Example of a rigid but not infinitesimally rigid graph.

are both rigid and globally rigid. The framework shown in Figure 2.11(a) is also infinitesimally rigid. If we check the rigidity matrix for any point p where the vertices are not collinear we will find it has rank 3. Thus we can conclude for the graph K_3 that any non-collinear point is a regular point.

By changing the positions of the vertices we can obtain the graph in Figure 2.11(b). The framework in Figure 2.11(b) is, as previously noted, rigid and globally rigid, however, unlike Figure 2.11(a), not infinitesimally rigid. We can check this using the rigidity matrix. Let the embedding of the points in the plane be $z_1 = (0, 0)$, $z_2 = (0, 1)$, $z_3 = (0, 3)$. The rigidity function for this graph is

$$f_G(z) = \begin{bmatrix} ||z_1 - z_2||^2 \\ ||z_2 - z_3||^2 \\ ||z_3 - z_1||^2 \end{bmatrix}.$$

Then

$$J_{f_G}(p) = 2 \begin{bmatrix} z_1^T - z_2^T & 0 & z_2^T - z_1^T \\ 0 & z_2^T - z_3^T & z_3^T - z_2^T \\ z_1^T - z_3^T & 0 & z_3^T - z_1^T \end{bmatrix}.$$

If we check the rank at a collinear point p we see rank $J_{f_G}(p) = 2 < 2n - 3$, so the framework is not infinitesimally rigid. As the rigidity matrix does not have maximal

rank, we see that p is not a regular point; consistent with Theorem 2.4, we see that a rigid framework is not infinitesimally rigid at a non-regular point.

In general, frameworks that are rigid but fail to be infinitesimally rigid have collinear or parallel edges. For instance the graph in Figure 2.12 is rigid, but not infinitesimally rigid and has three parallel edges connecting two infinitesimally rigid components—the triangles.

2.3.2 Level Sets of $f_G(p)$

The level sets of $f_G(p)$ are a particularly interesting topological object—they are a real algebraic variety. A *real algebraic variety* is the intersection of the zero level sets of polynomial functions, see [36]. For example the set

$$\{x \in \mathbb{R}^2 \mid x_1 = 0 \text{ and } x_2^2 - x_1 - 1 = 0\}$$

is a real algebraic variety.

A subset $\mathcal{S}$ of a topological space is topologically disconnected if and only if there are two disjoint open sets $\mathcal{U}$ and $\mathcal{V}$ such that $\mathcal{S} \subset \mathcal{U} \cup \mathcal{V}$, $\mathcal{S} \cap \mathcal{U} \neq \emptyset$ and $\mathcal{S} \cap \mathcal{V} \neq \emptyset$. If $\mathcal{S}$ cannot be expressed in this way we say that it is topologically connected (p. 191, [38]). A topological component is a subset of a topological space that is topologically connected.

Lemma 2.2: *([36]) A real algebraic variety has at most a finite number of topological components.*

The set $f_G^{-1}(d)$ is a real algebraic variety. Recall that $p \in f_G^{-1}(d)$ if and only if $f_G(p) - d = 0$. Each component of the function $f_G(z) - d$ is a polynomial in p_i. So the set $f_G^{-1}(d)$ is a real algebraic variety. We now apply Lemma 2.2 to conclude $f_G^{-1}(d)$ has a finite number of topological components. Each component of $f_G^{-1}(d)$ corresponds to one possible embedding of the graph in the plane, up to translations and rotations.

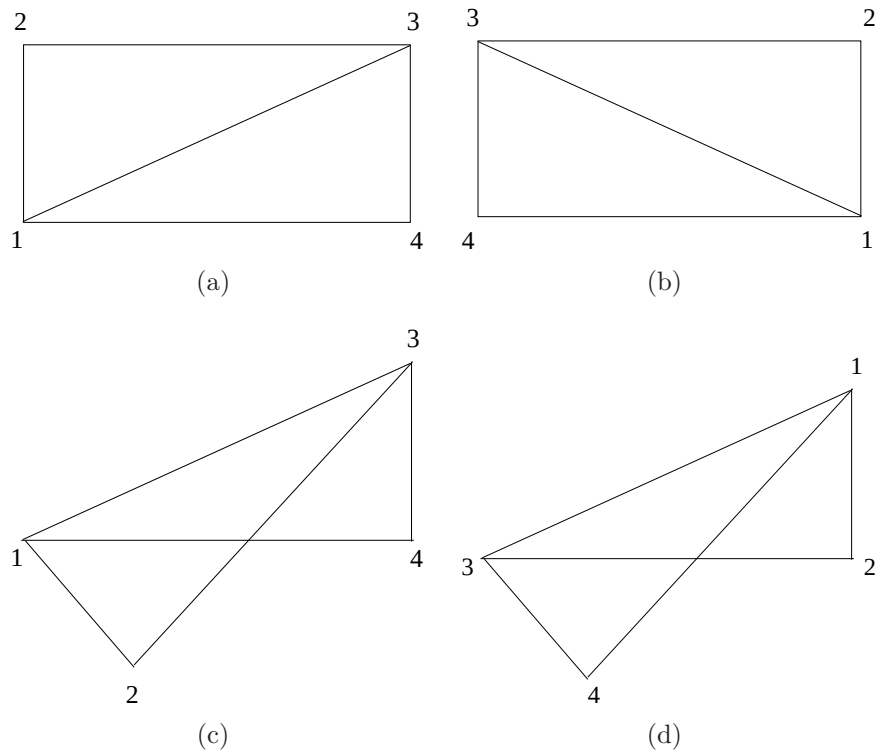

Figure 2.13: Possible unique embeddings of the graph in Example 2.1.

Example 2.1: Let's consider the example of a graph with four vertices and

$$f_G(z) = \begin{bmatrix} ||z_1 - z_2||^2 \\ ||z_2 - z_3||^2 \\ ||z_3 - z_4||^2 \\ ||z_4 - z_1||^2 \\ ||z_3 - z_1||^2 \end{bmatrix} \text{ and } d = \begin{bmatrix} 1 \\ 2 \\ 1 \\ 2 \\ \sqrt{5} \end{bmatrix}.$$

There are four possible distinct frameworks for this graph, as shown in Figure 2.13. Rotating and translating one of these frameworks generates one connected component of $f_G^{-1}(d)$. ◁

If the particular graph being studied is not only rigid, but globally rigid, then $f_G^{-1}(d)$ has only two components. There are only two distinct embeddings of the graph and

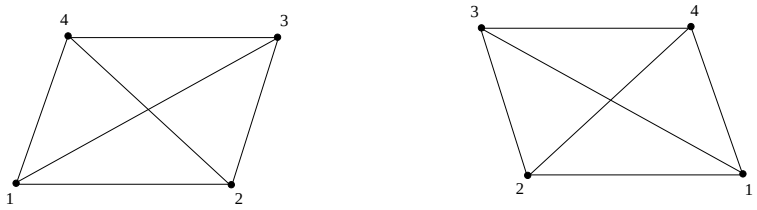

(a) (b)

Figure 2.14: The two possible embeddings of the graph K_4. Note that Figure 2.14(a) is a reflection of Figure 2.14(b).

they are reflections of one another. The complete graph K_4 is globally rigid. Figure 2.14 shows the two distinct embeddings of K_4 for the same edge lengths.

2.3.3 Constructing Rigid Graphs

Any collection of n points in the plane can be connected to form a rigid framework. For instance, we can connect the points using K_n, the complete graph. In subsequent sections we will find that the complexity of the control is proportional to the number of edges in a certain graph. Obviously, using the complete graph will result in a design that is not scalable: as the number of connections needed for n vertices is $\frac{n^2-n}{2}$.

However, from the definition of infinitesimal rigidity, we see a graph can be infinitesimally rigid with only $2n-3$ edges. Since infinitesimal rigidity implies rigidity, we can see a rigid graph can be made with only $2n-3$ edges. For $n > 3$, this is fewer edges than the complete graph.

A rigid graph can be constructed for any embedding of n vertices in the plane in the following manner. First, number all the vertices. Next, add an edge between vertex 1 and vertex 2. If we consider the framework formed by vertex 1 and vertex 2, we see that it is the complete graph, and thus is rigid. The remaining vertices are added in order to the connected component of the graph, connecting each one to the previously connected graph structure by two edges. This operation is sometimes referred to as a *Henneburg*

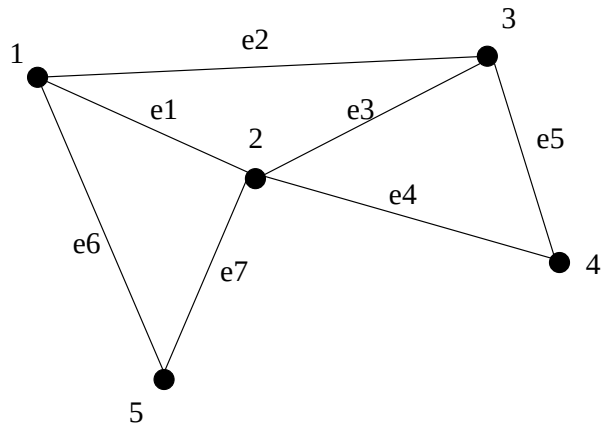

Figure 2.15: Graph created by recursively adding vertices in order. The edges are created in the order $e1, e2, \ldots, e7$. In particular note that there are 7 edges, which equals $2n-3 = 2 \times 5 - 3 = 7$.

insertion, see [7]. This type of insertion preserves graph rigidity because each vertex has two degrees of freedom. By connecting the vertex to the previously connected graph structure by two edges the position of the vertex is subject to two constraints, removing both degrees of freedom. This procedure results in a framework which is not only rigid but also minimally rigid; that is, if we remove any edge the framework is no longer rigid. Figure 2.15 shows a graph created using this procedure.

2.3.4 Graphs in Formation Control

The formation control problem has two associated graphs. The first graph is a *formation graph*; an undirected graph used to specify the desired formation.

We define a *formation* to be a pair (G, d) where G is an undirected graph and $d \in \mathbb{R}^{|E|}$. The vector d specifies the target lengths for the edges. We refer to G as the formation graph. Each robot is represented as a vertex in the graph. The robots achieve the target formation when the length of edge i is the prescribed distance d_i. We assume that the set where the robots achieve the target formation is non-empty. However, if the target distances are chosen arbitrarily it is possible to select a vector d for which there exists no point p such that $f_G(p) = d$. In general, G may not have enough constraints to form a

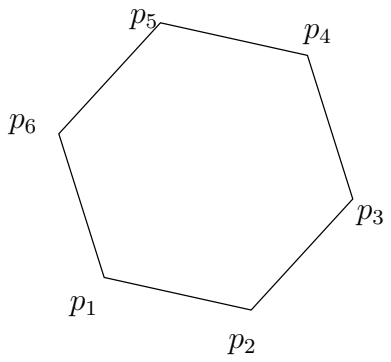

Figure 2.16: A polygon with labeled vertices.

rigid graph. However, the graph can be augmented by additional edges to form a graph which will be infinitesimally rigid if embedded at regular points. Given a formation (G, d), the control goal is for $z(t) \to f_G^{-1}(d)$.

If the target formation is given as an ordered polygon p as in Figure 2.16, the procedure outlined in Section 2.3.3 can be used to construct a rigid framework (G, p). Then the formation is $(G, f_G(p))$.

The second graph in the formation control problem is the *sensor graph*. The sensor graph is a directed graph with each robot represented as a vertex in the graph. The edges in the graph are defined by the closed-loop dynamics of the multi-robot system. Let z_i be the state of the robot i. Further suppose the dynamics of robot i are

$$\dot{z}_i = f(z_i) + g(z_i)u_i.$$

If in the closed loop system, u_i is a function of z_j, where $j \neq i$, then the sensor graph will have an edge between vertex i and vertex j.

Depending on the control the sensor graph may be time varying. This is the case when the robots' control is determined by those robots within a certain radius of the robot. Other multivehicle problems have a fixed sensor graph. This is the situation in the cyclic pursuit law described in [25]. In the present work, the sensor graph will also

be fixed, as we will see in Chapter 5.

Chapter 3

Gradient Control

In this chapter we develop control laws to stabilize robots to nearly arbitrary formations. Then we simulate these laws to gain some intuitive understanding of their behaviour.

Consider N robots in the plane, $\mathbb{R}^2$. The robots are wheeled vehicles with sensors that allow them to measure the relative positions of some of the other vehicles. Such data can be obtained using a camera or a radar system. The simplest model for a wheeled vehicle is the kinematic unicycle. The unicycle has a location in the plane (x, y) and a

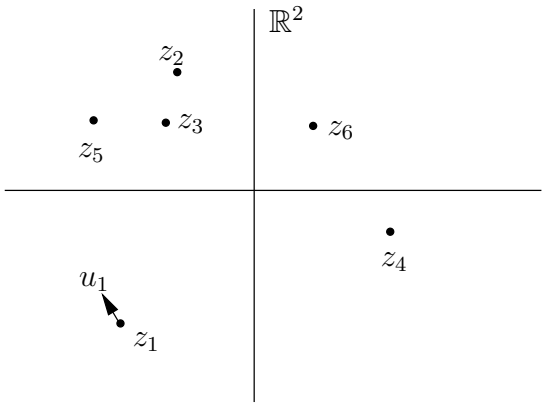

Figure 3.1: Point robots.

heading angle θ. The kinematics are then

$$\dot{x} = v_1 \cos\theta$$
$$\dot{y} = v_1 \sin\theta$$
$$\dot{\theta} = v_2,$$

where $v = (v_1, v_2)$ is the control input.

If we linearize the unicycle model about an arbitrary point equilibrium we find that it is uncontrollable. However, using feedback we can transform the model into a controllable linear model. We do this by considering a point a distance $l > 0$ in front of the unicycle, represented by the outputs

$$\xi_1 = x + l\cos\theta$$
$$\xi_2 = y + l\sin\theta.$$

It follows that

$$\dot{\xi} = A(\theta)v,$$

where $\xi = (\xi_1, \xi_2)$ and

$$A(\theta) = \begin{bmatrix} \cos\theta & -l\sin\theta \\ \sin\theta & l\cos\theta \end{bmatrix}.$$

The determinant of $A(\theta)$ is l, so the matrix $A(\theta)$ is invertible for all θ. Define $w = A(\theta)v$. Then the model becomes

$$\dot{\xi} = w.$$

If we consider only the output dynamics ξ we have a simple kinematic integrator model. The trade-off for this simplification is that we are no longer directly controlling

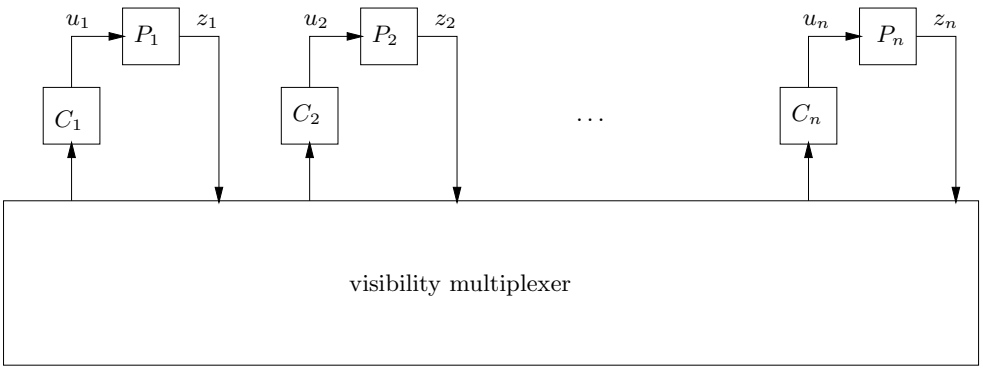

Figure 3.2: The control structure and plant model for the problem.

the unicycle: the point ξ will be at the target location, however the unicycle could be located anywhere on a circle of radius l around the target location. This is a drawback if the goal is to control the precise position of the unicycle. For sensor network applications the end goal of formation control is to precisely place the transmitter and receiver. Thus uncertainty of the location of the unicycle could possibly be overcome by placing the transmitter and receiver at the location l in front of the unicycle.

To simplify the analysis, we assume that the robots' dynamics have been feedback linearized in this way. The robots then have a point kinematic model given by the differential equation

$$\dot{z}_i = u_i, \quad i \in \{1, \ldots, N\} \tag{3.1}$$

where $z_i = (x_i, y_i) \in \mathbb{R}^2$ is the location of the ith robot in the plane and $u_i \in \mathbb{R}^2$ is the control input for the ith robot—see Figure 3.1. We define the composite state vector $z = (z_1, \ldots, z_N)$, as a vector in $(\mathbb{R}^2)^N$.

The control is restricted to be a function only of relative measurements. Each robot's onboard sensors provide relative position measurements of one or more other robots. For example if robot 1 can see robots 3 and 5, then the measurements available to robot 1 are $z_3 - z_1$ and $z_5 - z_1$. Therefore, u_1 can be a function of these two measurements. This defines a distributed control structure, see Figure 3.2. Figure 3.2 shows a visibility multiplexer

that determines the relationship between robot states and each robot's control input. The boxes C_i and P_i model the controller and dynamics of robot i.

Let G be the formation graph and $f_G(z) = d$ be the rigidity function defining the desired formation. Such a graph can be created from several types of specifications as outlined in Section 2.3.4. With this setup, we have the following problem statement: given the system (3.1) and given a target set specified by the equation $f_G(z) = d$, design a distributed control system as described above so that every point z such that $f_G(z) = d$ is a stable equilibrium (the issue of asymptotic convergence will be discussed later).

In Section 2.3.4 we noted that there are two graphs associated with the formation control problem: the formation graph and the sensor graph. In general, these graphs are not related. However, it is particularly advantageous if the two graphs are related. Then when the formation graph is designed, the effect on the sensor graph will be known. To this end, we continue our study with the following assumption.

Assumption 3.1: *A solution to the formation problem exists where the formation graph and sensor graph are the same.*

From Assumption 3.1, we know that when the formation graph and sensor graph are the same, then the sensor graph is undirected. That is to say, if robot i can see robot j, then robot j can see robot i.

Under Assumption 3.1, the goal is to construct a global potential function that defines a distributed gradient control that uses only the relative measurements permitted by the sensor graph such that any z where $f_G(z) = d$ is stable.

Let m be the number of edges in the formation graph. Since the formation graph and sensor graph are the same, there are m available relative positions. We define e_i, $i \in 1, \ldots, m$, to be the available two dimensional relative position measurements with $e_i = z_k - z_j$, where without loss of generality $j < k$. Note that e_i is the direction of edge i[1] and $\|e_i\|^2$ is the ith term in the rigidity function, $f_G(z)$. We also form the composite

[1]The notation e_i is used to refer both to the edge i and the direction of edge i in the framework. In

vector $e = (e_1, \ldots, e_m)$. This vector is a linear function of z and is related to the *incidence matrix*, H, of the graph G. Recall from Property 2.1 that $\ker(H) = \text{span}\{\mathbf{1}\}$ for connected graphs. Additionally, from the definition of H we know that $H \in \mathbb{R}^{m \times N}$.

We define

$$\hat{H} := H \otimes I_2. \tag{3.2}$$

Then e is related to z by

$$e = \hat{H} z. \tag{3.3}$$

For example, let's consider the complete graph K_3. The incidence matrix for this graph is

$$H = \begin{bmatrix} 1 & -1 & 0 \\ 0 & 1 & -1 \\ 1 & 0 & -1 \end{bmatrix}$$

then

$$\hat{H} = \begin{bmatrix} I_2 & -I_2 & 0 \\ 0 & I_2 & -I_2 \\ I_2 & 0 & -I_2 \end{bmatrix}.$$

3.0.5 Special Case: The Rendezvous Problem

The rendezvous problem is a special case of the formation stabilization problem, when $d = 0$. If L is the Laplacian of the sensor graph, and $\hat{L} = L \otimes I_2$, a linear solution to this problem is to let $u = -\hat{L} z$, and then

$$\dot{z} = -\hat{L} z. \tag{3.4}$$

In [22], it is shown that when the sensor graph is connected, rendezvous is achieved with this control law.

this second usage, the vector e_i is also referred to as an error vector.

Recall that if the sensor graph is undirected, the Laplacian is a symmetric matrix.

Lemma 3.1: *The matrix* $\hat{L} = \hat{H}^T\hat{H}$.

For a proof of Lemma 3.1 see Proposition 4.8 (p. 27) in [8]. The form of the Laplacian in Lemma 3.1 leads to the interesting observation that

$$-\hat{L}z = -\left[\nabla\left(\frac{1}{2}\|\hat{H}z\|^2\right)\right]^T.$$

The function $\frac{1}{2}\|\hat{H}z\|^2$ is positive semidefinite. So the control law in (3.4) is not only a gradient control law, as all symmetric linear controls are, but a gradient control law for a positive semidefinite potential function. This suggests considering a gradient control of a positive semidefinite potential function for the general formation stabilization problem.

3.0.6 Control Law

We now consider a gradient control law to maintain an arbitrary formation of robots. First we define a vector norm function $v : \mathbb{R}^{2m} \to \mathbb{R}^m$:

$$v(e) = (||e_1||^2, \ldots, ||e_m||^2).$$

Then using (3.3) we define

$$g(z) := v(e) = v(\hat{H}z). \tag{3.5}$$

Note that $g(z) \equiv f_G(z)$ is the rigidity function for the formation graph in our problem. As a candidate potential function, we consider the positive definite function of $g(z) - d$

$$\phi(z) = \frac{1}{2}\|g(z) - d\|^2. \tag{3.6}$$

Note that $\phi(z)$ is a positive semidefinite function of z and $\phi(z) = 0$ if and only if $g(z) = d$. Inspired by the rendezvous problem, in particular the solution given in (3.4), we propose

the gradient control

$$u = -(\nabla\phi(z))^T.$$

It follows from (3.1) and applying the chain rule to (3.6) that

$$\dot{z} = -J_g(z)^T(g(z) - d), \tag{3.7}$$

where J_g is the Jacobian of $g(z)$.

We now consider some interesting properties of the control. A fairly easy computation using (3.5) gives

$$-[\nabla\phi(z)]^T = -\hat{H}^T(J_v(e))^T(v(e) - d) \tag{3.8}$$

and so the control is a function only of the relative measurements, as required by the problem specification.

If we check the control of each agent we see that

$$\dot{z}_i = -\sum_{j\in\text{edges leaving } i} \frac{1}{2}(\|e_j\|^2 - d_j)e_j,$$

consistent with Assumption 3.1. The sensor graph is the same as the formation graph.

3.1 Simulations

Let's simulate the control law (3.7) for some different graphs, to gain some intuitive understanding about the robots' behaviour.

Example 3.1: Let's start by considering the complete graph K_4 with the rigidity function

$$g(z) = \begin{bmatrix} ||z_1 - z_2||^2 \\ ||z_2 - z_3||^2 \\ ||z_3 - z_4||^2 \\ ||z_4 - z_1||^2 \\ ||z_3 - z_1||^2 \\ ||z_4 - z_2||^2 \end{bmatrix} \text{ and } d = \begin{bmatrix} 1 \\ 2^2 \\ 1 \\ 2^2 \\ 5 \\ 5 \end{bmatrix}.$$

Note that this graph is globally rigid and the set $g^{-1}(d)$ is where the robots form a one by two rectangle. Figure 3.3 shows a trajectory that converges to $g^{-1}(d)$, using $g(z)$ and d to derive the control from (3.7). So we know that under (3.7) some initial conditions converge to the goal formation.

If we continue simulating different initial conditions, we see that some trajectories converge to an equilibrium where the rectangle formed by the robots is "twisted"; the robots converge to an equilibrium that is not in $g^{-1}(d)$. Such a trajectory is shown in Figure 3.4. These equilibria are undesired. From the simulation shown in Figure 3.4, we can conclude that the control in (3.7) has other equilibria than the target formation.

Now let's try initializing the simulation with the robots in a collinear configuration. Such a simulation is shown in Figure 3.5. From the simulation in Figure 3.5 it is clear that the collinear set is invariant and stable collinear equilibria exist.

Clearly, the simulations in Figures 3.4 and 3.5 show that the set $g^{-1}(d)$ is not globally attractive. However, the simulations suggest that it may be locally stable. Figure 3.6 shows a simulation where the robots are started close to the target formation and converge to it. ◁

Example 3.2: Now let's consider the control law derived from the minimally rigid graph

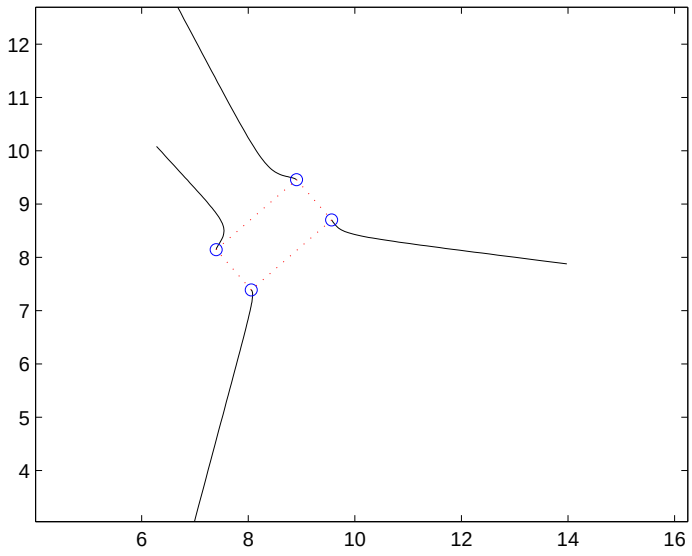

Figure 3.3: Four robots converging to an equilibrium that is in the target formation.

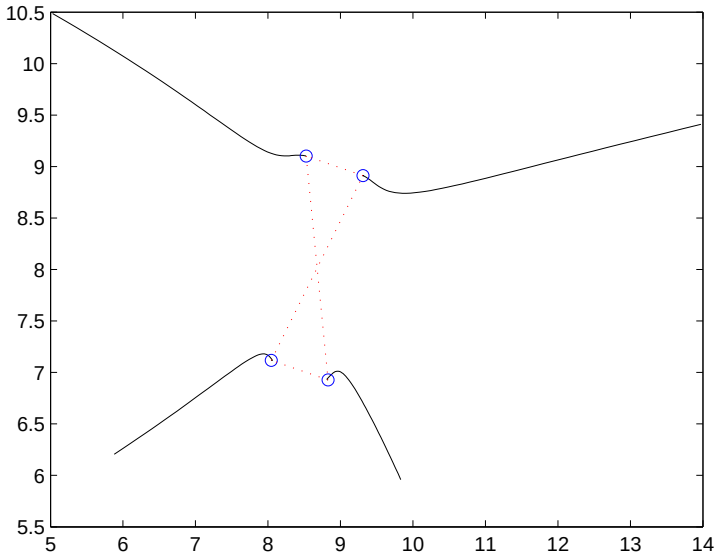

Figure 3.4: Four robots converging to an equilibrium that is not in the target formation.

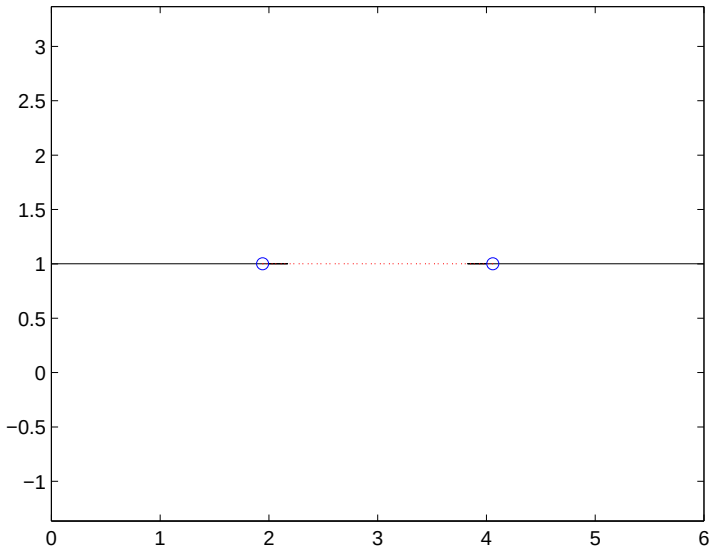

Figure 3.5: Four robots converging to an equilibrium in the collinear set. Note that some robots are coincident in the final configuration.

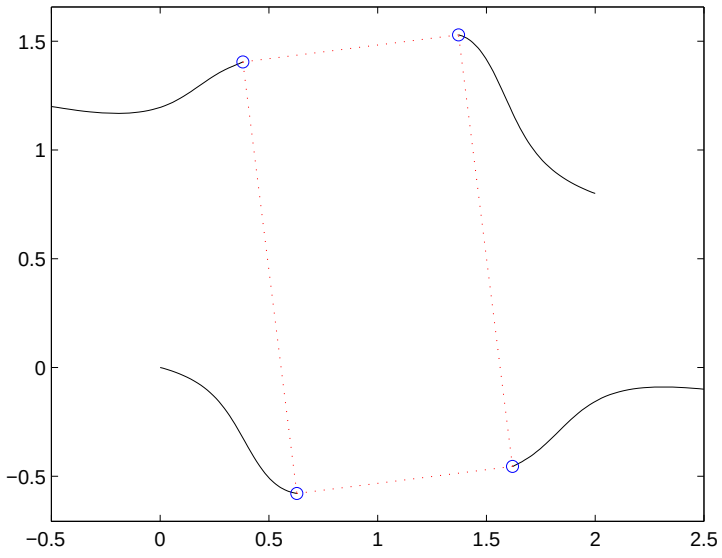

Figure 3.6: Four robots converging to a nearby equilibrium in the target set.

G with four vertices

$$g(z) = \begin{bmatrix} ||z_1 - z_2||^2 \\ ||z_2 - z_3||^2 \\ ||z_3 - z_4||^2 \\ ||z_4 - z_1||^2 \\ ||z_3 - z_1||^2 \end{bmatrix} \text{ and } d = \begin{bmatrix} 1 \\ 2^2 \\ 1 \\ 2^2 \\ 5 \end{bmatrix}.$$

This graph has one less edge than the one used in Example 3.1. Additionally, if we remove any edge the graph will no longer be able to form a rigid graph.

It is interesting to note that this graph is in fact a subgraph of the graph used in the previous simulations, i.e. G is a subgraph of K_4. Due to this relationship we know that the target set from Example 3.1 is a subset of the target set in this example. However, because the two graphs are not equal we know the two target sets are not equal. This is confirmed in the two example simulations shown in Figure 3.7 and Figure 3.8.

Although we have introduced additional equilibria in $g^{-1}(d)$, no twisted or undesired equilibrium has been found in simulation—other than the collinear equilibria. We conjecture that this may be because the minimally rigid framework has no symmetry.

◁

These simulations give us some insight in the behaviour of the multi-robot system. The simulations showed that other equilibria exist—not just the formation that we wish to stabilize. In particular, note that there were collinear equilibria and that if the robots are initialized in a collinear position they converge to a collinear equilibrium. Additionally, the simulations suggest that the formation is locally stable. In the next chapter we will study the stability of equilibrium manifolds in order to understand the multi-robot system analytically.

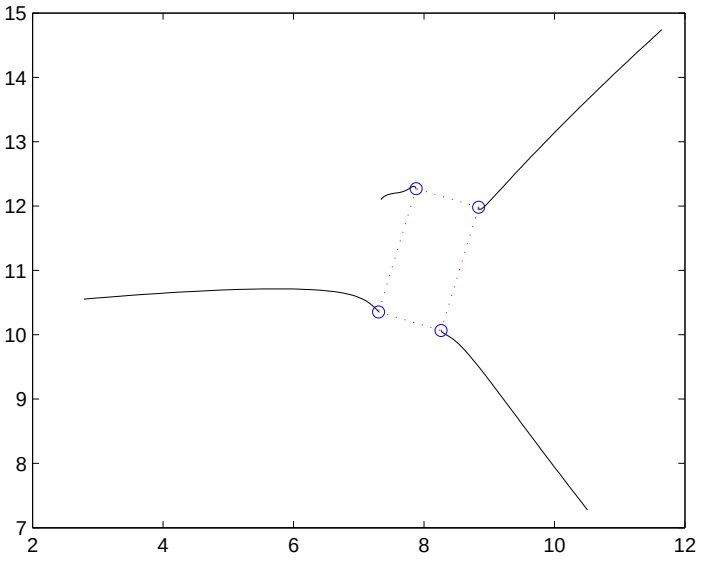

Figure 3.7: Four robots converging to the target formation.

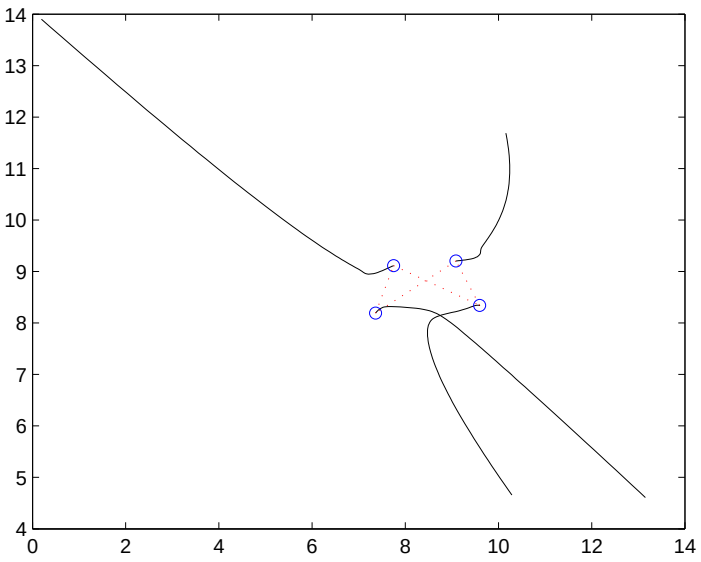

Figure 3.8: Four robots converging to an equilibrium that is not the target formation.

Chapter 4

Stability of Equilibrium Manifolds

In this chapter we study the stability of equilibrium manifolds. In particular, we will use linearization techniques to study the local stability of a point on an equilibrium manifold. From the linearization it is not immediately apparent if the manifold is stable. To reach a conclusion we must analyze the dynamics normal and tangential to the equilibrium manifold. To put the system in this form, we perform a nonlinear change of coordinates, using a property of manifolds with trivial normal bundles. Finally, we study the special case where the manifold of equilibria is the zero level set of a gradient system.

We start our study of equilibrium manifolds with the system

$$\dot{x} = f(x) \tag{4.1}$$

with $x \in \mathbb{R}^n$ and $f \in C^\infty$. Let $\mathcal{E}$ be an isolated $(n-k)$-dimensional manifold of equilibria of the system (4.1).

In order to study the stability of $\mathcal{E}$, we must first define what conditions must hold for the set to be stable. The definition of stability of an isolated equilibrium is well known, for instance see [20]. To precisely define what we mean by set stability we use

the notation $\text{dist}(x, \mathcal{S})$ to define the distance between a point x and a set $\mathcal{S}$:

$$\text{dist}(x, \mathcal{S}) = \inf_{y \in \mathcal{S}} ||x - y||.$$

The following definitions of set stability are from [31].

Definition 4.1 (Stability of a Set): *A set $\mathcal{S}$ is stable if*

$$(\forall \epsilon > 0)(\exists \delta > 0)\ dist(x(0), \mathcal{S}) < \delta \Rightarrow (\forall t \geq 0)\ dist(x(t), \mathcal{S}) < \epsilon.$$

A stronger type of set stability is asymptotic stability, analogous to asymptotic stability of an equilibrium point.

Definition 4.2 (Asymptotic Stability of a Set): *A set $\mathcal{S}$ is locally asymptotically stable if it is stable and if*

$$(\exists \delta > 0)\ dist(x(0), \mathcal{S}) < \delta \Rightarrow \lim_{t \to \infty} dist(x(t), \mathcal{S}) = 0.$$

Finally, we have the strongest definition of set stability, that of exponential stability.

Definition 4.3 (Exponential Stability of a Set): *A set $\mathcal{S}$ is exponentially stable if it is stable and if*

$$(\exists \delta, \alpha, a > 0)\ \ dist(x(0), \mathcal{S}) < \delta \Rightarrow (\forall t \geq 0)\ dist(x(t), \mathcal{S}) < ae^{-\alpha t}.$$

Our goal is to study the stability of the equilibrium manifold $\mathcal{E}$. For an isolated nonlinear equilibrium point p of the system (4.1), a standard way to determine if p is stable is to evaluate the eigenvalues of $J_f(p)$. If $J_f(p)$ is Hurwitz, then we know that the equilibrium p is stable.

Consider instead the Jacobian of (4.1) at a point $p \in \mathcal{E}$. It follows directly that $J_f(p)$ will have at least $n - k$ zero eigenvalues. These zero eigenvalues mean we cannot make a conclusion about the stability of the system, complicating the analysis.

Instead of linearizing the dynamics, we can also use LaSalle's Theorem to analyze the stability of a set as described in [20]. Let's consider some examples to gain some insight into the behaviour of trajectories near stable equilibrium manifolds. We will prove stability of these manifolds by an application of LaSalle's Theorem.

Example 4.1: Consider the system $(\dot{\theta}, \dot{r}) = f(\theta, r)$ where

$$\dot{\theta} = (1-r)^2$$
$$\dot{r} = (1-r).$$

The set $\{(\theta, r) \mid r = 1\}$ is a manifold of equilibrium solutions. We can apply LaSalle's theorem using the Lyapunov function $V(r, \theta) = \frac{1}{2}(1-r)^2$. Then

$$L_f V(\theta, r) = -(1-r)^2,$$

so we can conclude that the manifold is locally stable. If we linearize at a point $(\theta_0, 1)$ we see that

$$J_f(\theta_0, 1) = \begin{bmatrix} 0 & 0 \\ 0 & -1 \end{bmatrix}.$$

The Jacobian has one zero eigenvalue and one stable eigenvalue. If we simulate, we see that trajectories converge to a point on the manifold, as shown in Figure 4.1. ◁

Example 4.2: Consider the system $(\dot{\theta}, \dot{r}) = f(\theta, r)$ where

$$\dot{\theta} = (1-r)^2$$
$$\dot{r} = (1-r)^3.$$

The set $\{(\theta, r) \mid r = 1\}$ is a manifold of equilibrium solutions. We can apply LaSalle's

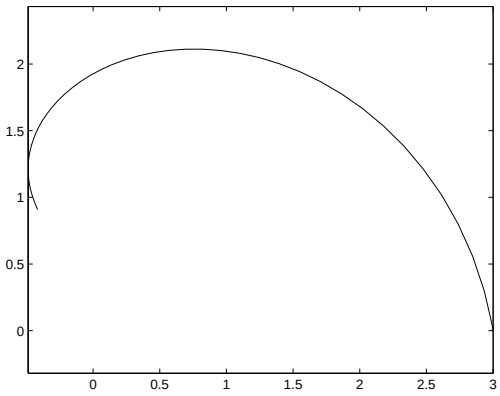

Figure 4.1: Possible trajectory for r and θ, plotted using (r, θ) as polar coordinates. The trajectory converges to a point on the unit circle.

theorem using the Lyapunov function $V(r, \theta) = \frac{1}{2}(1 - r)^2$. Then

$$L_f V(\theta, r) = -(1 - r)^4,$$

so we can conclude that the manifold is locally stable. However if we linearize at a point $(\theta_0, 1)$ we see that

$$J_f(\theta_0, 1) = \begin{bmatrix} 0 & 0 \\ 0 & 0 \end{bmatrix}.$$

This matrix has two zero eigenvalues. If we simulate the system we see that trajectories spiral towards the unit circle without converging to a point, as shown in Figure 4.2. $\lhd$

In both these examples, the unit circle is a stable manifold. However in the first example the trajectories converge to a point on the manifold, and in the second the trajectories do not converge to a point. Note that the dynamics in these two examples have a special form: close to the manifold, the θ dynamics are the dynamics tangent to the manifold, and the r dynamics are the dynamics normal to the manifold. In Example 4.1, close to the manifold the normal dynamics are much faster than the tangential dynamics. Conversely, in Example 4.2, close to the manifold the tangential dynamics are faster than

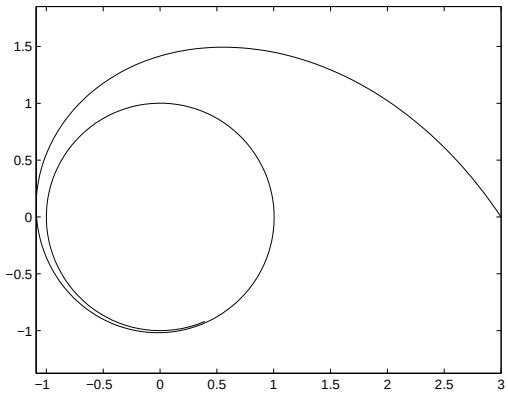

Figure 4.2: Possible trajectory for r and θ, plotted using (r, θ) as polar coordinates. Note that the trajectory does not converge to the unit circle but spirals around it.

the normal dynamics.

For many applications, including the multi-robot formation problem, it is preferable for the trajectory to converge to an equilibrium. Thus, our goal is to study not only when an equilibrium manifold is stable, but also when local trajectories converge to a point on the manifold.

Interestingly, in the example where the manifold is both stable and the trajectories converge to a point the Jacobian has one zero eigenvalue, the same as the dimension of the manifold, and the remaining eigenvalue is stable. For (4.1), if the number of zero eigenvalues is exactly $n - k$ it seems that it might be possible to obtain a stability result based on the linearization by performing some additional analysis of the relative speeds of the tangential and normal dynamics.

In the remainder of this chapter we study equilibrium manifolds in this normal form. In Section 4.1 we study a coordinate transformation that puts a specific class of equilibrium manifolds into such a normal form—where the tangential and normal dynamics are separated. Next in Section 4.2 we study the stability of a point in an equilibrium manifold with dynamics in this normal form. Finally we combine these two results in Section 4.3 to obtain a stability result for a class of equilibrium manifolds.

4.1 Coordinate Transformation

Transforming (4.1) into its normal and tangential components will help us analyze the stability of the system. In general, this may be difficult to do. However, for manifolds with trivial normal bundles, i.e. manifolds that satisfy Lemma 2.1, we can use the following theorem. The result is an adaptation of a technique in [14], p. 214.

Theorem 4.1: *Let $\mathcal{E}$ be an $(n-k)$-dimensional embedded submanifold of $\mathbb{R}^n$ defined on the open set $\mathcal{U} \subset \mathbb{R}^n$ by*

$$\mathcal{E} := \{\ x \in \mathcal{U} \mid g_1(x) = g_2(x) = \ldots = g_k(x) = 0\ \},$$

where each $g_i : \mathcal{U} \to \mathbb{R}$ is C^∞, and $g = (g_1, \ldots, g_k)$ has rank k for all $x \in \mathcal{U}$. Further assume that $\mathcal{E}$ is a set of equilibria of (4.1). Then for each $p \in \mathcal{E}$ there exists an open neighbourhood $\mathcal{W}$ of p, an open set $\mathcal{V} \subset \mathbb{R}^{n-k} \times \mathbb{R}^k$, and a diffeomorphism $\varphi : \mathcal{V} \to \mathcal{W}$ such that

1. *$\mathcal{E} \cap \mathcal{W} = \{\ x \in \mathcal{W} \mid x = \varphi(\theta, 0),\ \ (\theta, 0) \in \mathcal{V}\}$, as shown in Figure 4.3.*

2. *The dynamics of (4.1) in the new coordinate system $(\theta, \rho) = \varphi^{-1}(x)$ have the form*

$$\dot{\theta} = B(\theta, \rho)\rho + \hat{f}_1(\theta, \rho) \tag{4.2}$$

$$\dot{\rho} = A(\theta)\rho + \hat{f}_2(\theta, \rho), \tag{4.3}$$

where A, B, $\hat{f}_1$ and $\hat{f}_2$ are C^∞ and $\hat{f}_1$ and $\hat{f}_2$ satisfy

(a) $\hat{f}_1(\theta, 0) = 0$ and $\hat{f}_2(\theta, 0) = 0$,

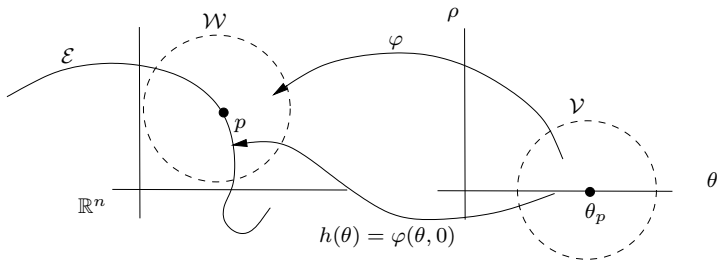

Figure 4.3: The map φ, and the associated sets $\mathcal{W}$ and $\mathcal{V}$.

(b) $\hat{f}_1$ and $\hat{f}_2$ are restricted in order as follows:

$$(\forall\theta) \quad \frac{\hat{f}_1(\theta,\rho)}{\|\rho\|} \to 0 \quad \textit{as } \rho \to 0 \tag{4.4}$$

$$(\forall\theta) \quad \frac{\hat{f}_2(\theta,\rho)}{\|\rho\|} \to 0 \quad \textit{as } \rho \to 0. \tag{4.5}$$

Proof: First we will construct the diffeomorphism $\varphi(\theta, \rho)$. Since $\mathcal{E}$ is an embedded submanifold of $\mathbb{R}^n$, the conditions of Lemma 2.1 hold and we can conclude that for each point $p \in \mathcal{E}$

$$\nabla g_1(p)^T, \ldots, \nabla g_k(p)^T$$

form a basis for $N_p\mathcal{E}$.

From the discussion in Section 2.1.5, for each $p \in \mathcal{E}$ there exists a coordinate chart $(\mathcal{W}_1, \psi)$ for $\mathbb{R}^n$ such that

$$\mathcal{E} \cap \mathcal{W}_1 = \{x \in \mathcal{W}_1 : \psi_{n-k+1}(x) = \cdots \psi_n(x) = 0\},$$

and $h(\theta) := \psi^{-1}(\theta, 0)$ defines a local embedding of $\mathcal{E} \cap \mathcal{W}_1$. The diffeomorphism ψ is related to the defining functions g_i; the last k components of ψ are the functions g_i. Let $\mathcal{V}_1 = \psi(\mathcal{W}_1)$.

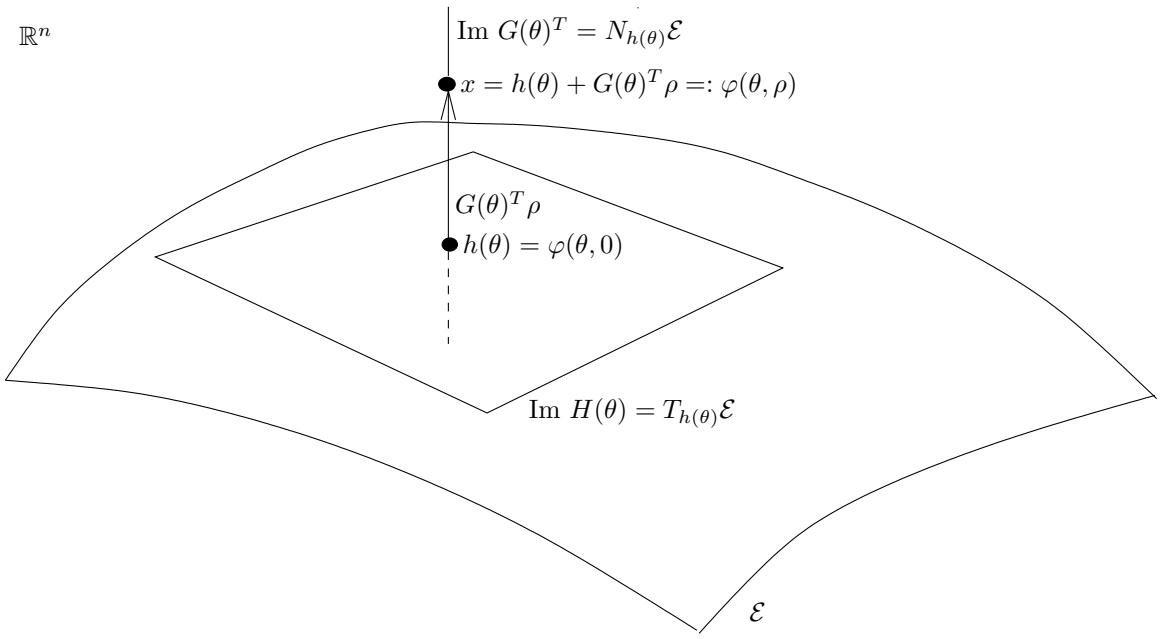

Figure 4.4: The relationship between φ and the normal and tangent spaces of $\mathcal{E}$ at a point $h(\theta)$.

We then define the matrices

$$H(\theta) := \frac{\partial}{\partial\theta}h(\theta) \text{ and } G(\theta) := \begin{bmatrix} \nabla g_1(h(\theta)) \\ \vdots \\ \nabla g_k(h(\theta)) \end{bmatrix}.$$

Note that the columns of $H(\theta)$ are linearly independent, so $\ker(H(\theta)) = 0$. By applying Fact 2.2 we know that $\ker(H(\theta)^T H(\theta)) = 0$, so the square matrix $H(\theta)^T H(\theta)$ is invertible. Likewise, the matrix $G(\theta)G^T(\theta)$ is invertible.

Define the coordinate transformation $\varphi : (\theta, \rho) \mapsto x$ by

$$x = h(\theta) + G(\theta)^T\rho =: \varphi(\theta, \rho), \tag{4.6}$$

as shown in Figure 4.4. It is clear that $\varphi(\theta, 0) \in \mathcal{E}$ on $\mathcal{V}_1$. Subsequently, we will see that $\mathcal{V} \subset \mathcal{V}_1$ so Property 1 of φ will be satisfied.

To show that φ is a valid local diffeomorphism, we check the rank of φ. From (4.6) we see that

$$\begin{aligned}\frac{\partial \varphi}{\partial \theta} &= H(\theta) + \frac{\partial G(\theta)^T}{\partial \theta}\rho \\ \frac{\partial \varphi}{\partial \rho} &= G(\theta)^T,\end{aligned}$$

where $\frac{\partial G(\theta)^T}{\partial \theta}$ is a $(n \times k)$-matrix valued function of θ. At any point on p on $\mathcal{E}$ this becomes

$$\begin{aligned}\frac{\partial \varphi}{\partial \theta}(\theta, 0) &= H(\theta) \\ \frac{\partial \varphi}{\partial \rho}(\theta, 0) &= G(\theta)^T.\end{aligned}$$

From Fact 2.1 it follows that $G(\theta)H(\theta) = 0$, so the matrix

$$\begin{bmatrix} H(\theta) & G(\theta)^T \end{bmatrix} \in \mathbb{R}^{n \times n}$$

is invertible. Since

$$\begin{bmatrix} H(\theta) & G(\theta)^T \end{bmatrix}$$

is the Jacobian of $\varphi(\theta, \rho)$ at $(\theta, 0)$, we can apply the inverse function theorem and conclude that at $(\theta, 0)$, φ is a local diffeomorphism on a neighbourhood $\mathcal{V}_2$ of $(\theta, 0)$. Without loss of generality, assume $\mathcal{V}_2 \subset \mathcal{V}_1$.

We now derive expressions for $\dot{\theta}$ and $\dot{\rho}$ in order to show that they have the required form. As a first step we substitute $x = \varphi(\theta, \rho)$ into (4.1). Taking the derivative of (4.6) with respect to time, we find the dynamics in transformed coordinates are

$$\left(H(\theta) + \frac{\partial G(\theta)^T \rho}{\partial \theta}\right)\dot{\theta} + G(\theta)^T \dot{\rho} = f(h(\theta) + G(\theta)^T \rho). \tag{4.7}$$

In order to isolate $\dot{\theta}$, we project both sides of (4.7) onto $\varphi^{-1}(\mathcal{E})$ by taking the inner product with the columns of $H(\theta)$, obtaining

$$\left(H(\theta)^T H(\theta) + H(\theta)^T \frac{\partial G(\theta)^T \rho}{\partial \theta}\right) \dot{\theta} = H(\theta)^T f(h(\theta) + G(\theta)^T \rho). \tag{4.8}$$

Define the matrix

$$C(\theta, \rho) := H(\theta)^T H(\theta) + H(\theta)^T \frac{\partial G(\theta)^T \rho}{\partial \theta}.$$

Note that $G(\theta)^T \rho$ can be expanded to

$$G(\theta)^T \rho = \rho_1 \nabla g_1(h(\theta))^T + \ldots + \rho_k \nabla g_k(h(\theta))^T,$$

where ρ_i are the components of ρ. It follows that

$$\frac{\partial G(\theta)^T \rho}{\partial \theta} = \rho_1 \frac{\partial}{\partial \theta}(\nabla g_1(h(\theta))^T + \ldots + \rho_k \frac{\partial}{\partial \theta} \nabla g_k(h(\theta))^T$$

When we evaluate $\frac{\partial G(\theta)^T \rho}{\partial \theta}$ at $\rho = 0$ we see that

$$\left.\frac{\partial G(\theta)^T \rho}{\partial \theta}\right|_{\rho=0} = 0.$$

It follows that $\operatorname{rank}(C(\theta_p, 0)) = \operatorname{rank}(H(\theta_p)^T H(\theta_p))$ and so $C(\theta_p, 0)$ is invertible. From continuity of $C(\theta, \rho)$, there exists a neighbourhood $\mathcal{V}$ of $(\theta_p, 0)$ where $C(\theta, \rho)$ is invertible. Without loss of generality, assume $\mathcal{V} \subset \mathcal{V}_2$. Define $\mathcal{W} := \psi^{-1}(\mathcal{V})$. We will now show that $\varphi : \mathcal{V} \to \mathcal{W}$ provides the required form of dynamics and order arguments specified in the theorem statement.

On $\mathcal{V}$ we can rewrite (4.8) as

$$\dot{\theta} = C(\theta, \rho)^{-1} H(\theta)^T f(h(\theta) + G(\theta)^T \rho). \tag{4.9}$$

The Taylor series expansion with respect to ρ of $f(h(\theta) + G(\theta)^T\rho)$ at a point $(\theta, 0)$ is

$$f(h(\theta)) + \frac{\partial f}{\partial x}(h(\theta))G(\theta)^T\rho + r(\theta, \rho). \tag{4.10}$$

The remainder function r is C^∞, consists of higher order terms in ρ, and has the property that

$$\lim_{\rho \to 0} \frac{r(\theta, \rho)}{\|\rho\|} = 0. \tag{4.11}$$

From $f(h(\theta)) = 0$ and (4.10), (4.9) becomes

$$\dot{\theta} = B(\theta, \rho)\rho + \hat{f}_1(\theta, \rho) \tag{4.12}$$

where

$$B(\theta, \rho) := C(\theta, \rho)^{-1}H(\theta)^T\frac{\partial f}{\partial x}(h(\theta))G(\theta)^T$$

and

$$\hat{f}_1(\theta, \rho) := C(\theta, \rho)^{-1}H(\theta)^T r(\theta, \rho).$$

Note that $\hat{f}_1, C \in C^\infty$.

Let's check that $\hat{f}_1(\theta, \rho)$ satisfies (4.4). The term $H(\theta)$ is independent of ρ. Additionally, we know that since $C(\theta, \rho)$ is invertible so $\|C(\theta, 0)^{-1}\| \neq 0$. It follows from the order of $r(\theta, \rho)$, (4.11), that

$$\lim_{\rho \to 0} \frac{\hat{f}_1(\theta, \rho)}{\|\rho\|} = C(\theta, 0)^{-1}H(\theta)^T \lim_{\rho \to 0} \frac{r(\theta, \rho)}{\|\rho\|} = 0$$

as required for (4.4).

From the order requirement on $r(\theta, \rho)$ it follows immediately that $r(\theta, 0) = 0$. Thus, $\hat{f}_1(\theta, 0) = 0$, as required.

To calculate $\dot{\rho}$ we multiply (4.7) by $G(\theta)$, similar to our calculation of $\dot{\theta}$, obtaining

$$G(\theta)\frac{\partial G(\theta)^T\rho}{\partial\theta}\dot{\theta} + G(\theta)G(\theta)^T\dot{\rho} = G(\theta)f(h(\theta) + G(\theta)^T\rho). \tag{4.13}$$

Define $D(\theta) := (G(\theta)G(\theta)^T)^{-1}$ and substitute $\dot{\theta}$ from (4.12), to simplify (4.13) to

$$\dot{\rho} = D(\theta)G(\theta)\left(-\frac{\partial G(\theta)^T\rho}{\partial\theta}(B(\theta,\rho)\rho + \hat{f}_1(\theta,\rho)) + f(h(\theta) + G(\theta)^T\rho)\right). \tag{4.14}$$

Again from (4.10), (4.14) can be simplified to

$$\dot{\rho} = A(\theta)\rho + \hat{f}_2(\theta,\rho) \tag{4.15}$$

where

$$A(\theta) := D(\theta)G(\theta)\frac{\partial f}{\partial x}(h(\theta))G(\theta)^T$$

and

$$\hat{f}_2(\theta,\rho) := D(\theta)G(\theta)\left(r(\theta,\rho) - \frac{\partial G(\theta)^T\rho}{\partial\theta}(B(\theta,\rho)\rho + \hat{f}_1(\theta,\rho))\right).$$

Note that $\hat{f}_2(\theta,0) = 0$ and $\hat{f}_2(\theta,\rho), A(\theta) \in C^\infty$. From (4.11),

$$\lim_{\rho\to 0}\frac{\hat{f}_2(\theta,\rho)}{\|\rho\|} = D(\theta)G(\theta)\lim_{\rho\to 0}\frac{1}{\|\rho\|}\left(r(\theta,\rho) - \frac{\partial G(\theta)^T\rho}{\partial\theta}(B(\theta,\rho)\rho + \hat{f}_1(\theta,\rho))\right) = 0$$

as required for (4.5). □

Note that the form obtained using this coordinate transformation transforms the system so that the θ coordinates are tangent to the manifold and ρ coordinates are normal to the manifold.

We call the equations (4.2)-(4.3) the canonical coordinates for the dynamics near $\mathcal{E}$. This canonical form exposes the dynamics off the submanifold (the ρ-dynamics) and the dynamics on the submanifold (the θ-dynamics), analogous to what is done with

subspaces with respect to linear dynamics. Our main stability result will follow from conditions on the eigenvalues of the Jacobian linearization of the canonical equations (4.2)-(4.3). Because of the order conditions given in (4.4)-(4.5), the Jacobian linearization is obtained by truncating the terms $\hat{f}_1(\theta, \rho)$ and $\hat{f}_2(\theta, \rho)$ in (4.2)-(4.3) and evaluating A and B at a point on $\mathcal{E}$. Thus, the analysis method involves first performing the nonlinear coordinate transformation φ to obtain the canonical form (4.2)-(4.3), followed by a Jacobian linearization at an equilibrium point on $\mathcal{E}$. It is easily shown that this is equivalent to first performing a Jacobian linearization on the original dynamics and then applying a linear coordinate transformation which is precisely J_φ, the differential of φ. That is to say, $(J_\varphi)^{-1} = J_{\varphi^{-1}}$ and the diagram in Figure 4.5 commutes.

Remark 4.1: *A global version of the previous results can be obtained for manifolds diffeomorphic to a generalized cylinder by applying the following facts. Using Lemma 2, (p. 274) from [2], it can be shown that a manifold $\mathcal{M}$ of dimension n is diffeomorphic to a generalized cylinder $S^\kappa \times \mathbb{R}^{n-\kappa}$ if and only if there exist n pairwise commutative*[1] *and linearly independent vector fields defined on $\mathcal{M}$. By flowing along these vector fields one can define a set of global curvilinear coordinates on $\mathcal{M}$ (see [33] Theorem 14 (p. 219)). These coordinates, denoted ψ, define an embedding of $S^\kappa \times \mathbb{R}^{n-\kappa}$ onto $\mathcal{M}$ given by $h(\theta) = \psi^{-1}(\theta)$. Using $h(\theta)$ defined over the entire manifold, one obtains a formula for the coordinate transformation* (4.6) *that can be used at any point of the manifold and this coordinate transformation is a local diffeomorphism for each point on the manifold.*

4.2 Malkin's Theorem

Now that we have transformed the system (4.1) into the canonical coordinates—the normal and tangential basis—at a point on the manifold, we must analyze when the

[1]Two vector fields f and g are said to be pairwise commutative if their Lie bracket, or commutator, is zero. For vector fields the Lie bracket of f and g at a point p is $[f, g](p) = J_g(p)f(p) - J_f(p)g(p)$; see [2] or [28] for more details on the Lie bracket.

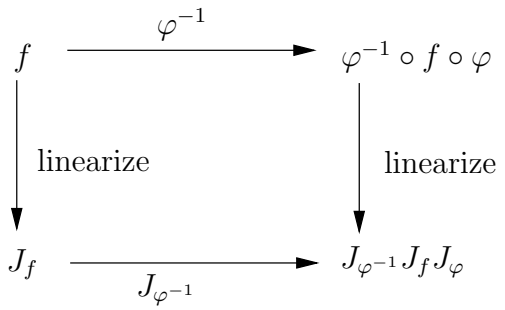

Figure 4.5: Commutative diagram for linearizing the dynamics in the two different coordinate systems.

manifold is both stable and a limit exists for the trajectories. The next theorem uses the linearized dynamics when the equilibrium manifold has this specific form.

Consider a system with a decomposition of the form

$$\dot{\theta} = f_1(\theta, \rho) \tag{4.16}$$

$$\dot{\rho} = A\rho + f_2(\theta, \rho), \tag{4.17}$$

where $\theta \in \mathbb{R}^{n-k}$, $\rho \in \mathbb{R}^k$, the matrix A is Hurwitz, and the functions $f_1, f_2 \in C^\infty$. Additionally, $f_1(\theta, 0) = 0$ and $f_2(\theta, 0) = 0$. From these conditions it is clear that the set $\{ (\theta, \rho) \mid \rho = 0 \}$ is an equilibrium manifold. Moreover, the dynamics are such that the θ-coordinates are tangential to the equilibrium manifold, and ρ-coordinates are normal to the equilibrium manifold.

The functions f_1 and f_2 are restricted in order such that

$$\lim_{\rho \to 0} \frac{f_1(\theta, \rho)}{\|\rho\|} = b_1(\theta) \tag{4.18}$$

$$\lim_{\rho \to 0} \frac{f_2(\theta, \rho)}{\|\rho\|} = b_2(\theta), \tag{4.19}$$

where $b_1, b_2 \in C^\infty$ and $b_2(0) = 0$.

Note that the form in (4.16)-(4.17) is the same as that obtained from the transfor-

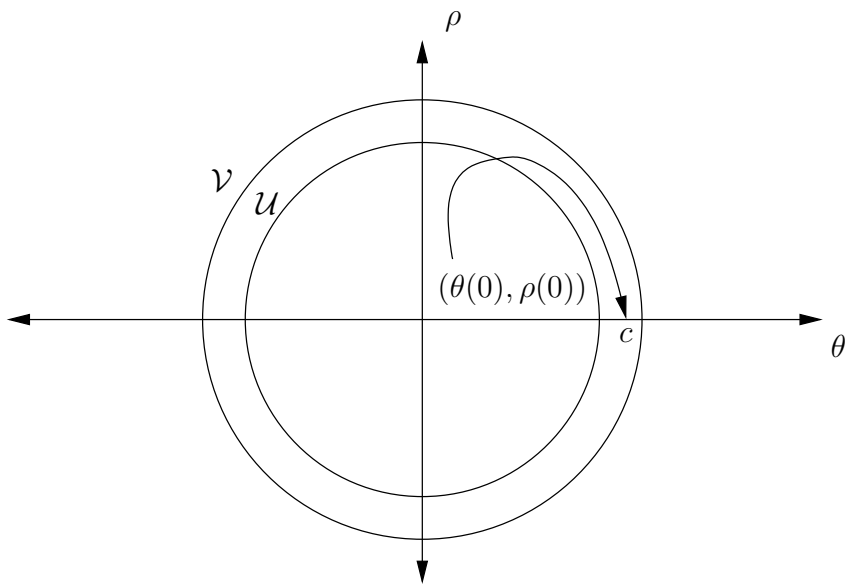

Figure 4.6: Sets associated with Malkin's theorem, and a possible trajectory.

mation in Theorem 4.1 when $A(\theta)$ is both constant and Hurwitz and the $B(\theta, \rho)\rho$ term has been incorporated into f_1.

We also define the useful functions

$$g_1(\theta, \rho) := \begin{cases} \frac{f_1(\theta,\rho)}{\|\rho\|} & \text{if } \rho \neq 0 \\ b_1(\theta) & \text{if } \rho = 0, \end{cases}$$

and

$$g_2(\theta, \rho) := \begin{cases} \frac{f_2(\theta,\rho)}{\|\rho\|} & \text{if } \rho \neq 0 \\ b_2(\theta) & \text{if } \rho = 0. \end{cases}$$

Note from (4.18) and (4.19) that the functions $g_1(\theta, \rho)$ and $g_2(\theta, \rho)$ are continuous. In particular, notice that $g_2(0, 0) = 0$.

Theorem 4.2 (Malkin's theorem, [24], p. 106): *For the system* (4.16)-(4.17)*, the point* $(0, 0)$ *is a stable equilibrium. Moreover, for every neighbourhood* $\mathcal{V}$ *of the origin there exists a neighbourhood* $\mathcal{U} \subset \mathcal{V}$ *of the origin such that for every* $(\theta(0), \rho(0)) \in \mathcal{U}$ *there exists a*

point $c \in \mathbb{R}^{n-k}$ *such that* $(c, 0) \in \mathcal{V}$ *and*

$$\lim_{t\to\infty}(\theta(t), \rho(t)) = (c, 0). \tag{4.20}$$

The proof that follows for Malkin's theorem is an adaptation of his original proof from [24]. Malkin's proof shows that $\|\rho\|$ is exponentially bounded by performing a time varying change of coordinates. In the following proof we show an exponential bound for $\|\rho\|$ by an application of the comparison lemma.

Proof: Let $\mathcal{V}$ be an open neighbourhood of the origin. First, we show that on a neighbourhood of the origin inside $\mathcal{V}$ here exists a positive semidefinite function that has a negative definite Lie derivative. Since A is a Hurwitz matrix, there exists a positive definite matrix P such that $A^TP + PA = -I$. Let $V(\theta, \rho) = \rho^T P\rho$ be a candidate Lyapunov function. Then along a solution of (4.16)-(4.17)

$$\begin{aligned}\frac{d}{dt}V(\theta(t), \rho(t)) &= \dot\rho(t)P\rho(t) + \dot\rho(t)P\rho(t)\\ &= \rho(t)(A^TP + PA)\rho(t) + 2\rho(t)^TPf_2(\theta(t), \rho(t))\\ &= -\|\rho(t)\|^2 + 2\rho(t)^TPf_2(\theta(t), \rho(t)).\end{aligned}$$

Define the function $\dot V(\theta, \rho)$ to be the Lie derivative:

$$\dot V(\theta, \rho) := -\|\rho\|^2 + 2\rho^TPf_2(\theta, \rho).$$

From the definition of $g_2(\theta, \rho)$ we know that

$$\|f_2(\theta, \rho)\| = \|\rho\|\ \|g_2(\theta, \rho)\|. \tag{4.21}$$

Since $g_2(\theta, \rho)$ is continuous and $g_2(0, 0) = 0$, for every $\gamma > 0$ it is possible to select a

closed ball $\overline{B_r} := \{(\theta, \rho) \mid \|(\theta, \rho)\| \leq r\}$ such that

$$\|g_2(\theta, \rho)\| \leq \gamma, \quad \forall (\theta, \rho) \in \overline{B}_r. \tag{4.22}$$

Without loss of generality, we assume $B_r \subset \mathcal{V}$. From (4.21) and (4.22), it follows that on the open ball B_r we have

$$\|f_2(\theta, \rho)\| \leq \gamma \|\rho\|, \quad \forall (\theta, \rho) \in B_r.$$

Then the Lie derivative of V is bounded by

$$\dot{V}(\theta, \rho) \leq -\|\rho\|^2 + 2\gamma \|P\| \, \|\rho\|^2, \quad \forall (\theta, \rho) \in B_r.$$

By selecting γ such that

$$\gamma \leq \frac{1}{4\|P\|}$$

then $\dot{V}(\theta, \rho)$ is a negative semidefinite function on B_r.

Next, we show that on the ball B_r, $\rho(t)$ is exponentially bounded. From the Lipschitz continuity of the vector field, we know that the solutions to (4.16)-(4.17) are continuous functions of time, and we can conclude that if $(\theta(0), \rho(0)) \in B_r$ then, for some interval $T = [0, t_1)$, $(\theta(t), \rho(t)) \in B_r, \forall t \in T$.

Let λ_{min} be the minimum eigenvalue of P and λ_{max} be the maximum eigenvalue of P. Th, that hold on B_r,e following bounds, that hold on B_r,, that hold on B_r,

$$\lambda_{min} \|\rho\|^2 \leq V(\theta, \rho) \leq \lambda_{max} \|\rho\|^2 \tag{4.23}$$

$$\dot{V}(\theta, \rho) \leq -\left(1 - \gamma 2\|P\|\right) \|\rho\|^2 \leq -\frac{1}{2}\|\rho\|^2 \tag{4.24}$$

allow us to apply the Comparison Lemma [20], as in Theorem 4.10 of [20]. First we note

that on B_r from (4.23) and (4.24)

$$\dot{V}(\theta,\rho) \leq -\frac{1}{2\lambda_{max}} V(\theta,\rho). \tag{4.25}$$

We apply the Comparison Lemma to (4.25) to obtain

$$V(\theta(t),\rho(t)) \leq V(\theta(0),\rho(0))e^{-2\alpha t}, \tag{4.26}$$

where $\alpha := \frac{1}{4\lambda_{max}}$. It follows from (4.23) and (4.26) that

$$\begin{aligned} \|\rho(t)\|^2 &\leq \frac{V(\theta(0),\rho(0))}{\lambda_{min}} \mathrm{e}^{-2\alpha t} \\ &\leq \frac{\lambda_{max}\|\rho(0)\|^2}{\lambda_{min}} \mathrm{e}^{-2\alpha t}. \end{aligned}$$

Define $a := \sqrt{\lambda_{max}/\lambda_{min}}$. Then

$$\|\rho(t)\| \leq a\|\rho(0)\|\mathrm{e}^{-\alpha t} \leq a\|\rho(0)\|, \quad \forall t \in T. \tag{4.27}$$

This inequality provides the exponential bound on the growth of $\rho(t)$.

Now we will show that $\theta(t)$ is bounded. From the definition of $g_1(\theta,\rho)$ we know that

$$\|f_1(\theta,\rho)\| = \|\rho\| \, \|g_1(\theta,\rho)\|.$$

Since g_1 is continuous, its norm has a maximum m on the set $\overline{B_r}$. It follows that

$$\|f_1(\theta,\rho)\| \leq m\|\rho\|, \quad \forall (\theta,\rho) \in B_r.$$

Thus from (4.27)

$$\|f_1(\theta(t),\rho(t))\| \leq ma\|\rho(0)\|\mathrm{e}^{-\alpha t}, \quad t \in T. \tag{4.28}$$

So we can bound the value of $\|\theta(t)\|$ by

$$\begin{aligned}\|\theta(t)\| &\leq \|\theta(0)\| + \int_0^{t_1} \|f_1(\theta,\rho)\| d\tau && \text{from (4.16)}\\ &\leq \|\theta(0)\| + a\|\rho(0)\| m \int_0^{t_1} \mathrm{e}^{-\alpha t} d\tau && \text{from (4.28)}\\ &\leq \|\theta(0)\| + \frac{a\|\rho(0)\| m}{\alpha}.\end{aligned}$$

For $(\theta(0),\rho(0)) \in B_r$, while $(\theta(t),\rho(t))$ continues to remain in B_r, the following inequality holds

$$\|\theta(t)\| \leq \|\theta(0)\| + \frac{a\|\rho(0)\| m}{\alpha}. \tag{4.29}$$

Having bounded $\theta(t)$ and $\rho(t)$ while they remain in B_r, we now restrict $\theta(0)$ and $\rho(0)$ so that the trajectories remain in B_r. First select a value $r^* > 0$ such that

$$r^* + \frac{ar^* m}{\alpha} + ar^* < r. \tag{4.30}$$

Let $\mathcal{U} := B_{r^*}$ and let $(\theta(0),\rho(0)) \in \mathcal{U}$. Then there exists an interval $T = [0, t_1)$ where $(\theta(t),\rho(t))$ is in B_r. Towards a contradiction, assume that $t_1 < \infty$ and at t_1, $(\theta(t),\rho(t))$ reaches the boundary of B_r. Up until t_1 the bounds (4.27) and (4.29) hold so it follows that

$$\|(\theta(t),\rho(t))\| \leq \|\theta(t)\| + \|\rho(t)\| \leq r^* + \frac{ar^* m}{\alpha} + ar^*.$$

Then from (4.30) we have

$$\|(\theta(t),\rho(t))\| < r, \quad \forall t \in T$$

a contradiction to the trajectory being on the boundary of B_r at $t = t_1$. So the solution $(\theta(t),\rho(t))$ remains in B_r for $t \in [0,\infty)$.

From (4.27), we see that

$$\lim_{t\to\infty} \rho(t) = 0.$$

The limit of $\theta(t)$ is

$$\lim_{t\to\infty} \theta(t) = \theta(0) + \int_0^\infty f_1(\theta(\tau), \rho(\tau))d\tau.$$

This integral converges because from (4.28) the integrand is exponentially bounded, so we can conclude that $\theta(t)$ converges to some $c \in \mathbb{R}^{n-k}$. From the bound (4.30) we know that $(c, 0) \in B_r$. □

4.2.1 Center Manifold Theory

Malkin's theorem is in fact a special case of center manifold theory. As seen in the proof of Theorem 4.2, Malkin's theorem provides a stability result using standard Lyapunov theory arguments, without resorting to the more general theory of center manifolds. Nevertheless, we include some background on center manifold theory to clarify the strong relationships between the two approaches.

Consider a modification of the equations (4.16)-(4.17) as follows

$$\dot{\theta} = C\theta + f_1(\theta, \rho) \tag{4.31}$$

$$\dot{\rho} = A\rho + f_2(\theta, \rho), \tag{4.32}$$

where C has eigenvalues only on the imaginary axis, A is Hurwitz, $f_1(0,0) = 0$ and $f_2(0,0) = 0$. The functions f_1 and f_2 are restricted in order such that $J_{f_1}(0,0) = 0$ and $J_{f_2}(0,0) = 0$. Note that in (4.16) the linear term in θ in (4.31) is zero; i.e. $C = 0$. From the conditions on (4.31) and (4.32) it is clear that the set $\{\ (\theta, \rho) \mid \rho = 0\ \}$ is not necessarily an equilibrium manifold.

An invariant manifold $\mathcal{M}$ is a center manifold of (4.31)-(4.32) if there exists an embedding

$$\mathcal{M} := \{(\theta, \rho) \in \mathcal{U} \mid h(\theta)\}$$

where $h(\theta)$ has the form

$$h(\theta) = (\theta, h_2(\theta)).$$

That is to say, $\mathcal{M}$ has the local form

$$\mathcal{M} := \{\ (\theta, \rho) \in \mathcal{U} \mid \rho = h_2(\theta)\ \}$$

where $\mathcal{U}$ is a sufficiently small neighbourhood of the origin, $h_2(0) = 0$, and $J_{h_2}(0) = 0$. The conditions of A make $\mathcal{M}$ an invariant manifold close to the origin.

The following theorem from [37] shows that for (4.31)-(4.32) a center manifold always exists.

Theorem 4.3 ([37], p. 195) : *A centre manifold exists for* (4.31)-(4.32) *. Moreover, the dynamics of* (4.31)-(4.32) *restricted to the center manifold are*

$$\dot{\xi} = C\xi + f_1(\xi, h_2(\xi)) \tag{4.33}$$

for a sufficiently small $\xi \in \mathbb{R}^{n-k}$.

The stability of the system (4.31)-(4.32) can then be analyzed from the dynamics on the centre manifold using the next theorem.

Theorem 4.4 ([37], p. 195) : *If the origin is stable under* (4.33)*, then the origin of* (4.31)-(4.32) *is also stable. Moreover there exists a neighbourhood* $\mathcal{W}$ *of the origin such that if* $(\theta(0), \rho(0)) \in \mathcal{W}$ *then there is a solution* $\xi(t)$ *of* (4.33) *such that*

$$\theta(t) = \xi(t) + f_1(t)$$
$$\rho(t) = h_2(\xi(t)) + f_2(t),$$

where there exits $c_i > 0$ *such that* $\|f_i(t)\| < c_1 e^{-\gamma t}$ *for some* $\gamma > 0$.

Malkin's theorem can be proved using centre manifold theory as in [34]. In (4.16)-(4.17) the center manifold can be explicitly found, and is in fact the θ-axis. From the application of Theorem 4.4 we know that the θ-axis is attractive and the origin is stable.

4.3 Main Result

Now we combine the results of Theorem 4.1 and Theorem 4.2 to obtain a local stability result for manifolds with a trivial normal bundle.

Theorem 4.5: *Let $\mathcal{E}$ be a compact, $(n-k)$-dimensional equilibrium manifold of* (4.1) *defined on the open set $\mathcal{U} \subset \mathbb{R}^n$ by*

$$\mathcal{E} := \{\ x \in \mathcal{U} \mid g_1(x) = \cdots = g_k(x) = 0\ \},$$

where $g_i : \mathcal{U} \to \mathbb{R}$ is C^∞, and the functions g_i are independent. If, for all $x_0 \in \mathcal{E}$, $J_f(x_0)$ has all stable eigenvalues, except for $(n-k)$ eigenvalues at zero, then $\mathcal{E}$ is locally asymptotically stable under (4.1). *Moreover, there exists a neighbourhood $\mathcal{N} \subset \mathcal{U}$ of $\mathcal{E}$ such that for each $x(0) \in \mathcal{N}$ there exists a point $p \in \mathcal{E}$ where*

$$\lim_{t\to\infty} x(t) = p.$$

Proof: We begin by transforming the system (4.1) into the canonical coordinates, followed by an application of Malkin's theorem. Then we show that stability in the transformed coordinates implies stability in the original coordinates.

Let $x_0 \in \mathcal{E}$. From Theorem 4.1, there exists a neighbourhood $\mathcal{W}_0$ of x_0 and an open set $\mathcal{V}_0 \subset \mathbb{R}^{n-k} \times \mathbb{R}^k$, and a diffeomorphism $\varphi : \mathcal{V}_0 \to \mathcal{W}_0$ such that dynamics (4.1) in the new coordinates $(\theta, \rho) = \varphi^{-1}(x)$ have the form (4.2)-(4.3). Define $(\theta_0, 0) := \varphi^{-1}(x_0)$. Without loss of generality, assume $\theta_0 = 0$.

We now show the (θ, ρ) dynamics have the form required by Theorem 4.2. First we take the Taylor series expansion of the term $A(\theta)$ from (4.3) about the point $\theta = 0$. The Taylor series of $A(\theta)$ at 0 has the form

$$A(\theta) = A(0) + R(\theta)$$

where

$$R(0) = 0.$$

Define $A_0 := A(0)$. Then the dynamics of the system are

$$\dot{\theta} = B(\theta, \rho)\rho + \hat{f}_1(\theta, \rho) =: f_1(\theta, \rho) \tag{4.34}$$

$$\dot{\rho} = A_0\rho + R(\theta)\rho + \hat{f}_2(\theta, \rho) =: A_0\rho + f_2(\theta, \rho). \tag{4.35}$$

Let's check that the order requirements for Malkin's theorem are met. It is immediate from Theorem 4.1 that

$$B(\theta, 0)0 + \hat{f}_1(\theta, 0) = f_1(\theta, 0) = 0$$

and

$$R(\theta)0 + \hat{f}_2(\theta, 0) = f_2(\theta, 0) = 0.$$

So both terms satisfy the requirement to make $\rho = 0$ an equilibrium manifold. Note that

$$\lim_{\rho \to 0} \frac{f_1(\theta, \rho)}{\|\rho\|} =: b_1(\theta)$$

and

$$\lim_{\rho \to 0} \frac{f_2(\theta, \rho)}{\|\rho\|} =: b_2(\theta),$$

with $b_2(0) = 0$. Thus the dynamics satisfy the order requirements of Theorem 4.2 at $(0, 0)$.

Next we show that A_0 is Hurwitz. If we linearize the (θ, ρ) dynamics from (4.34)-(4.35) at the point $(0,0) = \varphi^{-1}(x_0)$ on $\mathcal{E}$ we obtain

$$\begin{bmatrix} \dot{\delta\theta} \\ \dot{\delta\rho} \end{bmatrix} = J_{\varphi^{-1} \circ f \circ \varphi}(0,0) \begin{bmatrix} \delta\theta \\ \delta\rho \end{bmatrix} = \begin{bmatrix} 0 & B(0,0) \\ 0 & A_0 \end{bmatrix} \begin{bmatrix} \delta\theta \\ \delta\rho \end{bmatrix}.$$

The eigenvalues of $J_{\varphi^{-1} f \varphi}(0,0)$ include $(n-k)$ zero eigenvalues as well as the eigenvalues of A_0. Since the transformation φ to (θ, ρ)-coordinate system is a local diffeomorphism, $J_{\varphi f \varphi^{-1}} = J_{\varphi^{-1}} J_f J_\varphi$. So we can conclude that J_φ is the similarity transformation between $J_{\varphi^{-1} f \varphi}(0,0)$ and $J_f(x_0)$. Thus the matrices $J_{\varphi^{-1} f \varphi}(0,0)$ and $J_f(x_0)$ have the same eigenvalues. The matrix $J_{\varphi^{-1} f \varphi}(0,0)$ is block triangular, with $n-k$ zero eigenvalues in the first $n-k$ rows. So the eigenvalues in the remaining block A_0 are the remaining eigenvalues of $J_f(x_0)$. From the assumption on the eigenvalues on $J_f(x_0)$ we know that A_0 is Hurwitz.

From Theorem 4.2 we know that there exists a neighbourhood $\mathcal{U}_0$ of $(0,0)$ such that

$$(\theta(0), \rho(0)) \in \mathcal{U}_0 \Rightarrow (\forall t > 0)\ (\theta(t), \rho(t)) \in \mathcal{V}_0. \tag{4.36}$$

So the point $(0,0)$ is stable. Additionally from Theorem 4.2, there exists $c \in \mathbb{R}^{n-k}$, such that $(c,0) \in \mathcal{V}_0$ and $(\theta(t), \rho(t)) \to (c,0)$. That is to say, $\rho \to 0$.

Now, let $x_0 \in \mathcal{E}$ and let φ_{x_0} be the coordinate transformation at x_0. Recall from Theorem 4.1, (4.6), that

$$x = h(\theta) + G(\theta)^T \rho := \varphi_{x_0}(\theta, \rho)$$

where $h(\theta) \in \mathcal{E}$. From the compactness of $\mathcal{E}$, we know that there exists a ε-neighbourhood $\mathcal{N}_\varepsilon$ of $\mathcal{E}$, [13], where each point $p \in \mathcal{N}_\varepsilon$ will have a unique closest point in $\mathcal{E}$. Since the coordinate ρ measures the distance along the directions orthogonal to $\mathcal{E}$ then on $\mathcal{W}_0 \cap \mathcal{N}_\varepsilon$

$$\operatorname{dist}(x, \mathcal{E}) = \|G(\theta)^T \rho\|.$$

Define $\rho(x) = \rho$. It follows from the compactness of $\mathcal{E}$ and since $G(\theta)$ is a continuous function of θ, that there exist constants $c_2 > c_1 > 0$ such that for all $x \in \mathcal{N}_\varepsilon$

$$c_1\|\rho(x)\| \leq \text{dist}(x, \mathcal{E}) \leq c_2\|\rho(x)\|. \tag{4.37}$$

Then given an $\epsilon > 0$, (4.36) implies that there exists a $\delta_\epsilon(x_0) > 0$ such that

$$\|\rho(x(0))\| < \delta_\epsilon(x_0) \Longrightarrow \|\rho(x(t))\| < \epsilon \ \ \forall t \geq 0 \text{ and } \lim_{t\to\infty} \|\rho(x(t))\| = 0. \tag{4.38}$$

Select

$$\delta_\epsilon := c_1 \min_{x\in\mathcal{E}} \delta_{\epsilon/c_2}(x).$$

This minimum exists because $\mathcal{E}$ is compact and $\delta_\epsilon(x)$ is continuous. Then from (4.37) and (4.36) and using the compactness of $\mathcal{E}$, we obtain

$$\begin{aligned}
&\text{dist}(x(0), \mathcal{E}) < \delta_\epsilon \\
\Longrightarrow &\|\rho(x(0))\| \leq \frac{1}{c_1} c_1 \min_{x_0\in\mathcal{E}} \delta_{\epsilon/c_2}(x_0) && \text{from (4.37)} \\
\Longrightarrow &\|\rho(x(t))\| \leq \frac{\epsilon}{c_2}, \quad \forall t \geq 0 && \text{from (4.38)} \\
\Longrightarrow &\text{dist}(x(t), \mathcal{E}) \leq \epsilon \quad \forall t \geq 0 && \text{from (4.37) .}
\end{aligned}$$

Thus, $\mathcal{E}$ is stable. Additionally, we know that

$$\lim_{t\to\infty} \text{dist}(x(t), \mathcal{E}) = 0,$$

so $\mathcal{E}$ is asymptotically stable. Finally, define $p = \varphi(c, 0)$, with $\lim_{t\to\infty} x(t) = p$. □

Remark 4.2: *It is clear from the conditions of Theorem 4.2 that the set $\rho = 0$ is locally isolated from any other sets of equilibria. The dynamics in the two coordinate systems*

are related by a diffeomorphism. So we know that equilibria in the original coordinate system are mapped to equilibria in the (θ, ρ)-coordinates, [37]. Additionally, since φ is a diffeomorphism we know that isolated points in the (ρ, θ) coordinates cannot correspond to the same point in the x-coordinates.

Theorem 4.5 provides sufficient conditions for when an equilibrium manifold is not only stable, but also that local trajectories converge to points on the manifold. This result will be key in our study of the multi-robot system.

Comment 4.1: It is possible to prove Theorem 4.5 using center manifold theory directly. Without loss of generality, assume $0 \in \mathcal{E}$. Then rewrite the dynamics near $0 \in \mathcal{E}$ as

$$\dot{x} = J_f(0)x + (f(x) - J_f(0)x).$$

From the eigenvalue assumption in Theorem 4.5, there exists a matrix M that puts $J_f(0)$ into block diagonal form where the first block is an $n-k \times n-k$ block of zeros. Define $(\theta, \rho) = Mx$. Then the θ, ρ dynamics have the form

$$\begin{aligned}\dot{\theta} &= f_1(\theta, \rho) \\ \dot{\rho} &= A\rho + f_2(\theta, \rho),\end{aligned}$$

where $f_1(0,0) = 0$ and $f_2(0,0) = 0$ and $J_{f_1}(0,0) = 0$ and $J_{f_2}(0,0) = 0$. From the eigenvalue assumption in Theorem 4.5, A is Hurwitz.

It follows directly that $M(\mathcal{E})$ is a center manifold for the transformed system. Thus, there exist a function $h(\theta)$ such that in a neighbourhood $\mathcal{U}$ of (θ_0, ρ_0)

$$M(\mathcal{E}) \cap \mathcal{U} = \{\ (\theta, \rho) \mid \rho = h(\theta)\ \}.$$

Since $M(\mathcal{E})$ is an equilibrium manifold, we know that $f_1(\theta, h(\theta)) \equiv 0$ on $\mathcal{U}$. It follows

that

$$\dot{\xi} = 0,$$

and thus $\xi(t) = \xi(0)$. From Theorem 4.4, the solution for (θ, ρ) is then

$$\theta(t) = \xi(0) + f_1(t)$$
$$\rho(t) = h_2(\xi(0)) + f_2(t),$$

where there exits $c_i > 0$ such that $\|f_i(t)\| < c_1 e^{-\gamma t}$ for some $\gamma > 0$. The result of Theorem 4.5 then follows directly. ◁

4.4 Alternate Proof Techniques

As discussed at the beginning of the chapter, LaSalle's Theorem can be used to prove stability of a set. Let's review LaSalle's Theorem from [20].

Theorem 4.6 LaSalle ([20], p. 128) : *Let $\mathcal{U}$ be a compact set that is positively invariant with respect to* (4.1). *Define $V : \mathcal{U} \to \mathbb{R}$ to be a continuously differentiable function where $L_f V \leq 0$ on $\mathcal{U}$. Let $\mathcal{M}$ be the largest invariant set in $\{ x \in \mathcal{U} \mid L_f V(x) = 0 \}$. If $x(0) \in \mathcal{U}$, then $x(t) \to \mathcal{M}$ as $t \to \infty$.*

In order to apply LaSalle's Theorem, the equilibrium manifold of interest must be contained in an invariant set with no other equilibria—at every equilibrium point $L_f V(x) = 0$ so we will be unable to conclude which equilibrium set the trajectories converged to. Thus the equilibrium set of interest must be isolated from other equilibria. For gradient systems, we can use the following technique to show that an equilibrium manifold is isolated. Since the particular control we are studying in the multi-robot problem results in the gradient system (3.7), equilibrium manifolds of gradient systems are of particular interest for this work.

Equilibrium manifolds of gradient systems are a special case of the dynamics in (4.1) where $V : \mathbb{R}^n \to \mathbb{R}$ and

$$\dot{x} = -\nabla V(x)^T. \tag{4.39}$$

Assume that for all x such that $V(x) = 0$, it also holds that $\nabla V(x) = 0$. This implies the zero level set is a set of equilibria. For a gradient system we are interested in studying the stability of this zero level set of equilibria. As a preliminary step we wish to know if this set is isolated from all the other equilibria in the system. By applying the following inequality we can show that in most cases it is isolated.

We consider a set $\mathcal{S}_1$ to be isolated from $\mathcal{S}_2$ if the distance between the two sets has a positive lower bound.

From [23] (Theorem 17, see also [1] for an English version) we know

Lemma 4.1: *(Łojawiewicz's inequality) Let $V : \mathbb{R}^n \to \mathbb{R}$ be a real analytic function on a neighbourhood of a point z in $\mathbb{R}^n$. Then there are constants $c > 0$ and $p \in [0, 1)$ and a neighbourhood $\mathcal{U}$ of z such that*

$$\|\nabla V(x)\| \geq c|V(x) - V(z)|^p, \quad \forall x \in \mathcal{U}.$$

Now we further assume that $V : \mathbb{R}^n \to \mathbb{R}$ is a real analytic non-negative-valued function. Assume that for all x such that $V(x) = 0$ it also holds that $\nabla V(x) = 0$. In [1] such a non-negative-valued function is considered. By using Lemma 4.1, [1] shows that an isolated local minimum is asymptotically stable. In an extension of the techniques of [1], Lemma 4.1 can be used to show that a compact equilibrium set is isolated.

Theorem 4.7: *If $\mathcal{S} := V^{-1}(0)$ is a compact set, then $\mathcal{S}$ is isolated from all other equilibria of the system* (4.39).

Proof: The conditions of Lemma 4.1 hold at each point in $\mathcal{S}$. So it is possible to find a neighbourhood $\mathcal{U}_z$ of each point $z \in \mathcal{S}$. The neighbourhoods $\{\mathcal{U}_z\}$ form an open cover of

$\mathcal{S}$. From the compactness of $\mathcal{S}$ it is possible to select a finite set of points $z_1, \ldots, z_n$ such that the sets $\mathcal{U}_{z_i}$ cover $\mathcal{S}$, i.e.,

$$\mathcal{S} \subset \bigcup_{i=1}^{n} \mathcal{U}_{z_i}.$$

Define

$$\mathcal{U} := \bigcup_{i=1}^{n} \mathcal{U}_{z_i}.$$

For each $\mathcal{U}_i$, from Lemma 4.1 we know that there exist c_i and p_i such that for each point $x \in \mathcal{U}_i$ that

$$\|\nabla V(x)\| \geq c_i |V(x) - 0|^{p_i}.$$

From the continuity of V we know that the set $\{\, x \mid |V(x)| < 1 \,\}$ is an open neighbourhood of $\mathcal{S}$. It follows that $\mathcal{U}^* = \mathcal{U} \cap \{\, x \mid |V(x)| < 1 \,\}$ is also an open neighbourhood of $\mathcal{S}$. Let c be the minimum over all the c_i and p be the maximum of all the p_i; then

$$\|\nabla V(x)\| \geq c|V(x)|^p, \quad \forall x \in \mathcal{U}^*.$$

On the set $\mathcal{U}^*$, $\nabla V(x) = 0$ if and only if $V(x) = 0$. So we can conclude there is no other equilibrium to (4.39) in $\mathcal{U}^*$ except $\mathcal{S}$.

Select an open bounded subset $\mathcal{V} \subset \mathcal{U}$ such that $\mathcal{S} \subset \mathcal{V}$. Define $\partial\mathcal{V}$ to be the boundary of $\mathcal{V}$. The set $\partial\mathcal{V}$ is compact. Let δ be the minimum distance between $\mathcal{S}$ and $\partial\mathcal{V}$. A minimum exists because both sets are compact. This minimum must be greater than zero. To see this, assume, towards a contradiction, that $\delta = 0$. Then there exists a point $p \in \mathcal{S}$ that is also in $\partial\mathcal{V}$. Thus, $p \notin \mathcal{V}$, a contradiction to $\mathcal{S} \in \mathcal{V}$.

It follows that

$$(\forall x) \quad \operatorname{dist}(x, \mathcal{S}) < \delta \Rightarrow x \in \mathcal{U}.$$

Thus, the equilibrium set $\mathcal{S}$ is isolated from all other equilibria by a distance δ. □

LaSalle's theorem then shows that the set $V^{-1}(0)$ is stable, by using $V(x)$ as a Lyapunov function and Lemma 4.7 to show that $V^{-1}(0)$ is isolated.

This method has the benefit of not requiring an eigenvalue analysis. However, as we saw from Examples 4.1 and 4.2 the LaSalle technique does not give any information on the behaviour of the trajectories as the distance to the manifold goes to zero. In order to gain a result like that of Theorem 4.5 one must analyze the normal and tangential dynamics of the system.

Chapter 5

Main Results

We now return to the multi-robot formation problem. In this chapter we analyze some properties of control (3.7) and then show that the equilibrium set of interest is locally asymptotically stable.

Let's start by reviewing the problem formulation. Given an undirected graph G and a vector $d \in \mathbb{R}^{|V|}$, our goal is to construct a global potential function that defines a distributed gradient control that uses only the relative measurements permitted by the sensor graph such that any z such that $f_G(z) = d$ is stable. In particular, we are interested in a solution where the sensor graph and the formation graph are the same.

Note that the vector d cannot be selected arbitrarily from $\mathbb{R}^{|V|}$. It must be selected such that the set $f_G^{-1}(d)$ is non-empty. Even for minimally rigid graphs it is possible to select a value for d that cannot be achieved. For instance, consider the complete graph K_3. If we let $d = (1, 1, 9)$, then the control goal is to stabilize to a triangle with side lengths of 1,1 and 3. However, no such triangle exists.

5.1 Summary of Equations

Let's review the control laws we derived in Chapter 3. The robot model for our problem is

$$\dot{z} = u. \tag{5.1}$$

The control is derived from a potential function based on the error vector, e. The error vectors are calculated from $\hat{H} = H \otimes I_2$, where H is the incidence matrix of the graph G, i.e.

$$e = \hat{H}z.$$

Then the potential function is defined using the function of vector norms $v : \mathbb{R}^{2m} \to \mathbb{R}^m$:

$$v(e) = (||e_1||^2, \ldots, ||e_m||^2).$$

It follows that

$$J_v(e) = 2 \begin{bmatrix} e_1^T & \ldots & 0 \\ \vdots & \ddots & \vdots \\ 0 & \ldots & e_m^T \end{bmatrix}. \tag{5.2}$$

For convenience we define

$$g(z) := v(e) = v(\hat{H}z). \tag{5.3}$$

The function $g(z) \equiv f_G(z)$. From the form of g, it follows directly that g is invariant under rigid-body motion, i.e.,

$$g(z) = g(R^*(z + \mathbf{1} \otimes w)) \tag{5.4}$$

where $w \in \mathbb{R}^2$, $R \in \mathbb{R}^{2\times 2}$ is a rotation matrix and $R^* = I_n \otimes R$.

With these definitions, the potential function is

$$\phi(z) = \frac{1}{2}\|g(z) - d)\|^2. \tag{5.5}$$

Note that the potential function is derived from the formation graph via the incidence matrix.

The control input is the gradient of ϕ, that is,

$$u = -\nabla\phi(z)^T.$$

The control and the robot dynamics are combined to derive the closed loop system with the following equations of motion,

$$\begin{aligned} \dot{z} &= -\left(J_g(z)\right)^T \left(g(z) - d\right) \\ &= -\hat{H}^T J_v(\hat{H}z)^T (v(\hat{H}z) - d)\,. \end{aligned} \tag{5.6}$$

5.2 Properties of the Control

To start the analysis of (5.6) we consider some interesting properties of the control. Using $\hat{H}z = e$ in (5.6) gives

$$-[\nabla\phi(z)]^T = -\hat{H}^T(J_v(e))^T(v(e) - d). \tag{5.7}$$

Now we investigate the behaviour of the center of mass $\bar{z}$.

Lemma 5.1: *Let $\overline{z} = \frac{1}{n}\sum_{i=1}^{n} z_i$ be the center of mass of the robots. Then $\dot{\overline{z}} = 0$.*

Proof: We can rewrite $\overline{z}$ as

$$\overline{z} = \frac{1}{n}(\mathbf{1} \otimes I_2)^T z.$$

If we differentiate, we obtain

$$\begin{aligned}\dot{\bar{z}} &= \frac{1}{n}(\mathbf{1}\otimes I_2)^T\dot{z} \\ &= -\frac{1}{n}(\mathbf{1}\otimes I_2)^T\hat{H}^T J_v(\hat{H}z)^T(g(z)-d).\end{aligned}$$

Recall that, from the structure of $\hat{H}$, $\hat{H}(\mathbf{1}\otimes I_2)=0$, and thus $\dot{\bar{z}}=0$. □

The control in (5.6) has the interesting property that it is independent of the system of global coordinates.

Lemma 5.2: *The function* $[\nabla\phi(z)]$ *in* (5.6) *satisfies*

$$\nabla\phi(z+\mathbf{1}\otimes w)=\nabla\phi(z),$$

where $w\in\mathbb{R}^2$*, and also satisfies*

$$\nabla\phi(z)R^{*T}=\nabla\phi(R^*z),$$

where $R^*=I_n\otimes R$*, and* $R\in\mathbb{R}^{2\times 2}$ *is a rotation matrix, i.e.* $R^TR=I_2$*.*

Proof: Equation (5.5) shows the function $\nabla\phi(z)$ is a function of $g(z)$ and thus from (5.3) also a function of $v(\hat{H}z)$. Recall from (5.3) and (5.5)

$$\phi(z)=\frac{1}{2}\|v(\hat{H}z)-d)\|^2.$$

So to show that

$$[\nabla\phi(z+\mathbf{1}\otimes w)]=[\nabla\phi(z)],$$

it suffices to show that

$$\hat{H}(z+\mathbf{1}\otimes w)=\hat{H}z.$$

This follows directly from $H\mathbf{1} = 0$.

Next we show that $R^*\nabla\phi(z) = \nabla\phi(R^*z)$. From the chain rule we obtain

$$\begin{aligned}\phi(R^*z) &= \phi(z)\\ \nabla\phi(R^*z)R^* &= \nabla\phi(z)\\ \nabla\phi(R^*z) &= \nabla\phi(z)R^{*T}.\end{aligned}$$

□

Note that if $\overline{z} = 0$ then the action of R^* is to rotate the formation about its centroid in the plane. If $\overline{z} \neq 0$ then the action of R^* can be viewed as a combination of a rotation of the formation about its centroid and a translation. From Lemma 5.2 we can conclude that the behaviour of the robots is independent of the global system of coordinates used. To see this explicitly, let ξ_i be the position of robot i in the plane using a different global coordinate system. Then $\xi_i = Rz_i + w$, and $\xi = R^*z + \mathbf{1} \otimes w$, where $w \in \mathbb{R}^2$. If we look at the dynamics of ξ we find that

$$\begin{aligned}\dot{\xi} &= R^*\dot{z}\\ &= -R^*\nabla\phi(z)^T\\ &= -\nabla\phi(R^*z)^T\\ &= -\nabla\phi(R^*z + \mathbf{1} \otimes w)^T\\ &= -\nabla\phi(\xi)^T.\end{aligned}$$

So the dynamics in the new coordinate system are the same as in the old.

5.2.1 Collinear Dynamics

An interesting feature of the system (5.6) is the existence of an invariant collinear set. We define the collinear set $\mathcal{C}$ to be the set

$$\mathcal{C} := \{z \in \mathbb{R}^{2N} \mid (\exists w \in \mathbb{R}^2)(\forall i)\ (z_i - \overline{z}) \in \text{span}(w)\}.$$

The set $\mathcal{C}$ is not a differential manifold.

Lemma 5.3: *The set $\mathcal{C}$ is an invariant set.*

Proof: The velocity of robot i has the form

$$\dot{z}_i = \sum_{j=1}^{N} a_{ij}(z_j - z_i).$$

Note that a_{ij} are functions of z. When $z \in \mathcal{C}$ this can be rewritten as

$$\dot{z}_i = \sum_{j=1}^{N} a_{ij}(c_j w - c_i w),$$

where $c_i, c_j \in \mathbb{R}$. Thus, $\dot{z}_i \in \text{span}(w)$. From Lemma 5.1 we know that $\overline{z}$ is stationary. So it follows that $z_i(t) - \overline{z} \in \text{span}(w)$. Thus, the set $\mathcal{C}$ is an invariant set. □

This confirms the observations we made in Section 3.1 when simulating the robots starting in a collinear position. Since $\mathcal{C}$ is an invariant set, and the function $\phi(z)$ has a lower bound, we know that there exist some equilibria in $\mathcal{C}$. Simulations show that these equilibria are attractive for initial conditions in $\mathcal{C}$. An example simulation is in Section 3.1.

5.3 Equilibria

We are interested in studying the equilibria of (5.6). From the structure of (5.6) it is immediately apparent that there are equilibria when $g(z) = d$. Let the set E_1 be defined by

$$E_1 := \{ z \mid g(z) - d = 0 \} \equiv \{ z \mid \phi(z) = 0 \}.$$

The set E_1 represents the desired formations as specified by the formation graph.

Unfortunately, these are not the only equilibria for the system (5.6). There is also a larger set of equilibria

$$E_2 := \{ z \mid J_v(\hat{H}z)^T (g(z) - d) = 0 \}.$$

Note that $E_1 \subset E_2$. The matrix

$$J_v(\hat{H}z)^T = 2 \begin{bmatrix} e_1 & \dots & 0 \\ \vdots & \ddots & \vdots \\ 0 & \dots & e_m \end{bmatrix}$$

has a nontrivial kernel if and only if for some $i \in \{ 1, \dots, m \}$, $e_i = 0$. So for a point z to be an equilibrium in E_2, each $||e_i||^2 = d_i$ or $||e_i||^2 = 0$. That is to say each the edge has the correct length as specified by the formation graph or the edge is zero.

Finally we consider the complete set of equilibria for (5.6)

$$E = \{ z \mid \nabla\phi(z) = 0 \}.$$

Notice $E_1 \subset E_2 \subset E$. Simulation has shown that, in general, $E_2 \neq E$. These extra equilibria are not unexpected: the matrix $\hat{H}^T \in \mathbb{R}^{2N \times 2m}$ where $m > N$. Thus, $\hat{H}^T$ has a nontrivial kernel. In particular, the set E includes equilibria where the robots' positions are collinear.

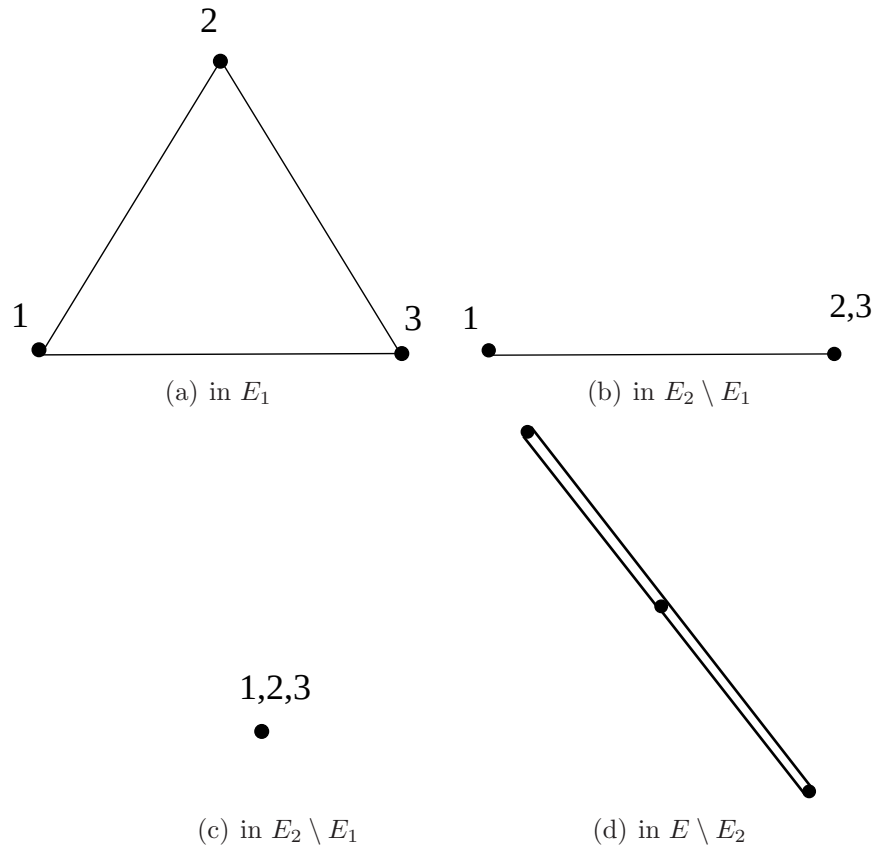

(a) in E_1 (b) in $E_2 \setminus E_1$

(c) in $E_2 \setminus E_1$ (d) in $E \setminus E_2$

Figure 5.1: Possible equilibria when the target formation is an equilateral triangle. The figures show the formations in $\mathbb{R}^2$, whereas the sets E_1, E_2 and E are in $\mathbb{R}^{2n}$.

To gain a better understanding of these sets let's return to the triangle example.

Example 5.1: Let's consider the example of a triangle with

$$g(z) = \begin{bmatrix} ||z_1 - z_2||^2 \\ ||z_2 - z_3||^2 \\ ||z_3 - z_1||^2 \end{bmatrix} \text{ and } d = \begin{bmatrix} 1 \\ 1 \\ 1 \end{bmatrix}.$$

In this case the set E_1 is all the points z where z_1, z_2, z_3 form an equilateral triangle with sides of unit length as in Figure 5.1(a). The set E_2 contains two additional distinct formations: $z_1 = z_2 = z_3$ and when $z_i = z_j$ and the third robot z_k is positioned such that $||z_i - z_k||^2 = 1$. These two configurations are illustrated in Figure 5.1(c) and 5.1(b). Finally, the set E contains collinear equilibria as illustrated in Figure 5.1(d).

Note that the set E_1 contains only points where the three agents are in an equilateral triangle. If we look at the other formations in $E \setminus E_1$ it is clear that E_1 and $E \setminus E_1$ are separated by some finite distance. ◁

5.3.1 Summary of Equilibria Sets

The equilibria are subdivided into three sets:

$$E_1 := \{ z \mid g(z) - d = 0 \} \equiv \{ z \mid \phi(z) = 0 \}$$
$$E_2 := \{ z \mid J_v(Hz)^T (g(z) - d) = 0 \}$$
$$E := \{ z \mid \nabla\phi(z) = 0 \}.$$

By definition $E_1 \subset E_2 \subset E$. The equilibria in E_1 are the desired ones.

5.3.2 Components of E_1

Before we study stability of the equilibrium set E_1, we examine some of its properties. In particular, we are interested in classifying E_1 as a topological object. If we are able to show that the set E_1 is a manifold with a trivial normal bundle we will be able to transform the coordinate system into a set of canonical coordinates (θ, ρ) using Theorem 4.1.

From Section 2.3.2 we know that E_1 has a finite number of topological components. We now turn our attention to classifying the components of E_1 under the following assumption.

Assumption 5.1: *At every point $p \in E_1$ the framework (G, p) is infinitesimally rigid.*

Let's now study the implications of Assumption 5.1.

Theorem 5.1: *If Assumption 5.1 holds, then E_1 is a three dimensional embedded submanifold of $\mathbb{R}^{2N}$. Moreover, on each connected component of E_1 there exist $2N-3$ components of g that are independent on the connected component.*

If there are $2N - 3$ edges in the graph, then the theorem follows immediately from Corollary 2.1. However, if there are more than $2N-3$ edges in the graph, then a slightly more subtle argument is needed. The argument depends on the following fact.

Lemma 5.4: *Suppose that for all $p \in g^{-1}(d)$, the framework (G, p) is infinitesimally rigid. Then the set $\mathcal{S} \subset g^{-1}(d)$ is a topologically connected component of $g^{-1}(d)$ if and only if for each $p, p' \in g^{-1}(d)$, p and p' are related by a combination of rotations and translations of $\mathbb{R}^2$, and moreover, $\mathcal{S}$ is maximal with respect to rotations and translations.*

We say that a manifold $\mathcal{M}$ is maximal with respect to a group of functions if, given a point $p \in \mathcal{M}$, every point $q \in \mathcal{M}$ is related to p by a function in the group and also every point generated by a function in the group acting on p is in $\mathcal{M}$.

The proof of this fact follows from the fact that the level sets of the complete graph corresponding to G are generated by isometries, [3]. If the points in p are not collinear—as they must be for G to be infinitesimally rigid—then it follows directly that any reflection in the plane of p will not be in the same component as p.

Given $p \in \mathbb{R}^{2N}$ let $\mathcal{M}_p$ denote the maximal set of points related by a combination of rotations and translations to p. Now we prove Theorem 5.1.

Proof: Fix $p \in g^{-1}(d)$ and suppose, without loss of generality, that $\hat{g} := (g_1, \ldots, g_{2N-3})$, the first $2N-3$ components of g, satisfy rank $J_{\hat{g}}(p) = 2N-3$. Let $\hat{G}$ denote the reduced graph with edges corresponding to $\hat{g}$. Consider $\mathcal{M}_p$. Let q $in\mathbb{R}^{2N}$. A simple calculation shows that $J_{\hat{g}}(q)$ and $J_{\hat{g}}(p)$ are related by an invertible matrix when $q \in \mathcal{M}_p$. So rank $J_{\hat{g}}(q) = 2N-3$ for all $q \in \mathcal{M}_p$. From Fact 5.4 we know that $\mathcal{M}_p$ is also a connected component of $g^{-1}(d)$. So the required independent components of g exist.

From the rank of $J_{\hat{g}}(q)$ we know that $(\hat{G}, q)$ is infinitesimally rigid, and therefore rigid, for all $q \in \mathcal{M}_p$. This implies there exists an open neighborhood $\mathcal{U}_q$ of q such that $\mathcal{M}_p \cap \mathcal{U}_q = \hat{g}^{-1}(\hat{g}(p)) \cap \mathcal{U}_q$. Let $\mathcal{U} := \cup_{q \in \mathcal{M}_p} \mathcal{U}_q$, a $2N$-dimensional manifold, be an open cover of $\mathcal{M}_p$. Then $\mathcal{M}_p \cap \mathcal{U} = \hat{g}^{-1}(\hat{g}(p)) \cap \mathcal{U}$. Thus, we have that $\hat{g} : \mathcal{U} \to \mathbb{R}^{2N-3}$ has rank $2N-3$ for all $q \in \mathcal{M}_p$. By Corollary 2.1, we obtain that $\mathcal{M}_p$ is a 3-dimensional embedded submanifold of $\mathcal{U} \subset \mathbb{R}^{2N}$. Thus, each connected component of $g^{-1}(d)$ is an embedded submanifold. It follows directly that $g^{-1}(d)$ is a 3-dimensional embedded submanifold also. □

On first reading the infinitesimal rigidity condition in Assumption 5.1 seems difficult to check, since E_1 is not compact. However, to check Assumption 5.1 only a finite number of calculations must be made. From (5.4) it is clear that the Jacobian of $g(z)$ has constant rank on components of E_1. So we must check the rank of the rigidity matrix at only one point on each component of E_1, or on one possible embedding, in order to apply Theorem 5.1.

From Lemma 2.2 we know that level sets of real algebraic varieties, like E_1, have only a finite number of components. So to check that Assumption 5.1 holds only a finite number of tests must be made.

5.4 Existence of Solutions

In order to study the existence of solutions to (5.6) we first perform a linear change of coordinates in order to separate the center of mass dynamics from the dynamics of the rest of the system. Let P be an orthonormal matrix where the first two rows are $\frac{1}{n}\mathbf{1}^T \otimes I_2$. Recall that for an orthonormal matrix P, $P^{-1} = P^T$. We now consider the transformation

$$\tilde{z} = \begin{bmatrix} \overline{z} \\ \check{z} \end{bmatrix} = Pz,$$

where $\bar{z}$ is the centroid of z, as discussed in Lemma 5.1. Define

$$\tilde{H} = \hat{H}P^{-1}. \tag{5.8}$$

From the definition of $\tilde{H}$ it is clear that $\tilde{H}\tilde{z} = \hat{H}z$. We now solve for the $\tilde{z}$ dynamics, obtaining

$$\begin{aligned} \dot{\tilde{z}} &= P\dot{z} \\ &= -P\hat{H}^T \left(J_v(\hat{H}z)\right)^T (g(z) - d) \\ &= -\tilde{H}^T \left(J_v(\tilde{H}\tilde{z})\right)^T (v(\tilde{H}\tilde{z}) - d). \end{aligned} \tag{5.9}$$

So, $\dot{\tilde{z}} = -[\nabla\tilde{\phi}(\tilde{z})]^T$ where $\tilde{\phi}(\tilde{z}) = \frac{1}{2}\|v(\tilde{H}\tilde{z}) - d\|^2$.

Next we consider an interesting property of $\tilde{H}$. Note that since the first two columns of P^{-1} are in $\ker(\hat{H})$, $\tilde{H}$ has the form $\begin{bmatrix} 0 & \check{H} \end{bmatrix}$.

From Property 2.1 of H we know that $\ker(H)$ is one dimensional, thus $\mathrm{Ker}(\hat{H})$ is

two dimensional. Then by using the dimension of $\mathrm{Ker}(\hat{H})$, the invertibility of P and the block form of $\tilde{H}$, we know that $\mathrm{Ker}(\check{H}) = 0$.

We now expand $\tilde{H}\tilde{z}$:

$$\begin{aligned}\tilde{H}\tilde{z} &= \begin{bmatrix} 0 & \check{H} \end{bmatrix} \begin{bmatrix} \overline{z} \\ \check{z} \end{bmatrix} \\ &= \check{H}\check{z}. \end{aligned} \tag{5.10}$$

So the $\tilde{z}$ dynamics from (5.9) can be rewritten using (5.8) and (5.10) as

$$\begin{bmatrix} \dot{\overline{z}} \\ \dot{\check{z}} \end{bmatrix} = - \begin{bmatrix} 0 \\ \check{H}^T \end{bmatrix} \left(J_v(\check{H}\check{z})\right)^T (v(\check{H}\check{z}) - d). \tag{5.11}$$

If we define $\check{\phi}(\check{z}) := \frac{1}{2}\|v(\check{H}\check{z}) - d\|^2$ then $\dot{\check{z}} = -(\nabla\check{\phi}(\check{z}))^T$, and so $\check{z}$ is a gradient system.

We now define the equilibrium sets for the $\check{z}$ system

$$\check{E}_1 = \{\ \check{z} \in \mathbb{R}^{2N-2} \mid v(\check{H}\check{z}) = d\ \},$$

and

$$\check{E} = \{\ \check{z} \in \mathbb{R}^{2N-2} \mid \nabla\check{\phi}(\check{z}) = 0\ \}.$$

Lemma 5.5: *The set $\check{E}_1$ is compact.*

Proof: The set $\mathcal{C} = \{\ e \in \mathbb{R}^m \mid v(e) = d\ \}$ is a compact set because it is m copies of S^1. The set $\check{E}_1 = \{\ \check{z} \mid \check{H}\check{z} \in \mathcal{C}\ \}$. Since $\ker(\check{H}) = 0$, it follows that $\check{E}_1$ is also a compact set. □

The compactness of this set will be key in our application of Theorem (4.5).

Now let's study the existence of solutions in the $(\bar{z}, \check{z})$ coordinates. The $\bar{z}$ dynamics and the $\check{z}$ dynamics are decoupled, so we can analyze existence of solutions independently. From Lemma 5.1 we know that $\dot{\bar{z}}$ is zero. So solutions exist for all time.

Now let's study the dynamics of $\check{z}$. We know that the dynamics of $\check{z}$ are a gradient system with the potential function $\check{\phi}(\check{z})$ and that $\check{\phi}(\check{z})$ is a radially unbounded function. Let's study the level sets of $\check{\phi}(\check{z})$. Define the sublevel set

$$\mathcal{U}_a := \{\ \check{z} \in \mathbb{R}^{2N-2} \mid \check{\phi}(\check{z}) \leq a\}.$$

We can use Lyapunov techniques to study the behaviour of this set. Define the Lyapunov function to be $V(\check{z}) := \phi(\check{z})$. We denote $-L_{\nabla\check{\phi}}V(\check{z})$ to be Lie derivative of $-\nabla\check{\phi}(\check{z})^T$. For the $\check{z}$ system the Lie derivative is $-L_{\nabla\check{\phi}}V(\check{z}) = -\|\nabla\check{\phi}(\check{z})\|^2$, a negative semidefinite function. So the set $\mathcal{U}_a$ is invariant for any $a > 0$. On the set $\mathcal{U}_a$, the function $\nabla\check{\phi}(\check{z})$ is Lipschitz continuous. So we can conclude that a solution $\check{z}(t)$ exists for all time for initial conditions starting in $\mathcal{U}_a$.

5.5 Linearized Dynamics

In order to study the stability of the equilibrium manifold E_1, we will consider the linearized z-dynamics.

Define

$$M(e) := J_v(e)^T J_v(e) = 4\begin{bmatrix} e_1 e_1^T & \dots & 0 \\ \vdots & \ddots & \vdots \\ 0 & \dots & e_m e_m^T \end{bmatrix} \tag{5.12}$$

and

$$K(e) := 2\begin{bmatrix} I_2(||e_1|| - d_1) & \dots & 0 \\ \vdots & \ddots & \vdots \\ 0 & \dots & I_2(||e_m|| - d_m) \end{bmatrix}.$$

Lemma 5.6: *Let f denote the vector field for the z dynamics, i.e., from* (5.6)

$$\dot{z} = f(z) = -\hat{H}^T J_v(\hat{H}z)^T(v(\hat{H}z) - d).$$

Then

$$J_f(z) = -\hat{H}^T(K(e) + M(e))\hat{H}.$$

where $e = \hat{H}z$.

Proof: By applying the chain rule to (5.6), we obtain

$$\begin{aligned} J_f(z) &= -\frac{\partial}{\partial z}\hat{H}^T \left(J_v(\hat{H}z)\right)^T (g(z) - d) \\ &= -\hat{H}^T \frac{\partial}{\partial z} \left(J_v(\hat{H}z)\right)^T (g(z) - d). \end{aligned}$$

The remaining derivative can be calculated in two stages by recalling that $g(z) = v(\hat{H}z) = v(e)$:

$$\frac{\partial}{\partial z} \left(J_v(\hat{H}z)\right)^T (g(z) - d) = \frac{\partial}{\partial e} \left(J_v(e)\right)^T (v(e) - d) \frac{\partial}{\partial z}\hat{H}z. \tag{5.13}$$

From (5.2) we obtain

$$\left(J_v(e)\right)^T (v(e) - d) = 2 \begin{bmatrix} e_1(||e_1|| - d_1) & \dots & 0 \\ \vdots & \ddots & \vdots \\ 0 & \dots & e_m(||e_m|| - d_m) \end{bmatrix}.$$

Note that

$$\frac{\partial}{\partial e_i} 2e_i(||e_i|| - d_i) = 2(||e_i|| - d_i)I_2 + 4e_i e_i^T.$$

Then from the definitions of $M(e)$ and $K(e)$ it follows that

$$\frac{\partial}{\partial e} \left(J_v(e)\right)^T (v(e) - d) = K(e) + M(e). \tag{5.14}$$

Combining (5.13) and (5.14) we obtain

$$J_f(z) = -\hat{H}^T(K(e) + M(e))\hat{H}.$$

□

Theorem 5.2: *The matrix $J_f(z)$ evaluated at a point on E_1 has three zero eigenvalues; the rest are real and negative.*

Proof: Let $z_0 \in E_1$ and define $e_0 = \hat{H} z_0$. It follows that $K(e_0) = 0$. Then $J_f(z_0) = -\hat{H}^T M(e_0) \hat{H}$. From (5.12), it follows that

$$J_f(z_0) = -\hat{H}^T M(e_0) \hat{H} \tag{5.15}$$

$$= -\hat{H}^T J_v(e_0)^T J_v(e_0) \hat{H} \tag{5.16}$$

$$= -J_g(z_0)^T J_g(z_0). \tag{5.17}$$

So the matrix $J_f(z_0)$ is symmetric and thus has real eigenvalues. From the structure of (5.15) we know that $\mathrm{Ker}(J_f(z_0)) = \mathrm{Ker}(J_g(z_0))$. The function $g(z)$ is the rigidity function for the graph and $J_g(z)$ is the rigidity matrix. From Assumption 5.1 we know that the rank of the rigidity matrix is $2N-3$ at all points on E_1. So $\dim(\ker J_g(z_0)) = 3$ and thus $J_f(z_0)$ has three zero eigenvalues. Moreover, the structure of $J_f(z_0)$ implies that it is a negative semidefinite matrix, so the non-zero eigenvalues are negative. □

The existence of the three zero eigenvalues of the Jacobian evaluated at a point on E_1 prevents us from drawing any conclusions about stability from the linearization. However, it is intuitively obvious that the linearization at a point on a manifold of equilibria must have at least as many zero eigenvalues as the dimension of the manifold. The set E_1 is a three dimensional manifold, and the linearization about any point on E_1 has three zero eigenvalues.

It is clear that at each point on E_1 the conditions of the Malkin theorem (Theorem 4.2) hold. We use the fact that $\check{E}_1$ is a compact manifold to prove stability of the set E_1.

Theorem 5.3 (Main Result): *The set E_1 is asymptotically stable. Moreover, there exists a neighborhood $\mathcal{U}$ of E_1 such that for each $z(0) \in \mathcal{U}$ there exists a point $p \in E_1$ where*

$$\lim_{t\to\infty} z(t) = p.$$

Proof: To prove E_1 is stable we study the $(\bar{z}, \check{z})$ dynamics. First perform the linear transformation P to separate the system into $(\bar{z}, \check{z})$ components. The $\bar{z}$ dynamics are stationary, so we study only the reduced $\check{z}$ system. From Lemma 5.5 we know that $\check{E}_1$ is a compact set. To show $\check{E}_1$ is stable we show that each component of $\check{E}_1$ is stable. Let $\mathcal{S}$ be an arbitrary topologically connected component of $\check{E}_1$. Furthermore, let $\check{z}_0 \in \mathcal{S}$. From Theorem 5.1 we know that $\mathcal{S}$ has $2N-3$ globally defining functions.

In order to apply Theorem 4.5 it only remains to show that the Jacobian of the $\check{z}$ dynamics meets the eigenvalues requirement.

Define $\check{f}$

$$\dot{\check{z}} = -\nabla\check{\phi}(\check{z})^T.$$

Now we show that $J_{\check{f}}(\check{z}_0)$ has one zero eigenvalue and the remaining eigenvalues are stable. If we linearize the $(\overline{z}, \check{z})$ dynamics at a point $(\overline{z}_0, \check{z}_0) = Pz_0$ on E_1 we obtain

$$\begin{bmatrix} \dot{\delta\overline{z}} \\ \dot{\delta\check{z}} \end{bmatrix} = \begin{bmatrix} 0 & 0 \\ 0 & J_{\check{f}}(\check{z}_0) \end{bmatrix} \begin{bmatrix} \delta\overline{z} \\ \delta\check{z} \end{bmatrix}.$$

Since the transformation P is invertible it is clear that the matrices PJ_fP^{-1} and $J_f(z_0)$ have the same eigenvalues. The matrix PJ_fP^{-1} is block triangular, with two zero eigenvalues in the first two rows. So the eigenvalues in the remaining block $J_{\check{f}}$ are the remaining eigenvalues of $J_f(z_0)$. From Theorem 5.2 we know these eigenvalues are all stable except for one zero eigenvalue.

Since $J_{\check{f}}$ has one zero eigenvalue and the remaining are stable, the conditions of Theorem 4.5 apply. It follows that $\mathcal{S}$ is asymptotically stable. The set $\mathcal{U} := P^{-1}(\mathbb{R}^2 \times \mathcal{N})$. $\square$

Corollary 5.1: *Let z be a point on E_1. There exists an open ball B centered at z such that if $z(0) \in B$, then $z(t)$ converges to a nearby equilibrium formation.*

This corollary follows directly from Theorem 5.3.

In summary, we see that by using an infinitesimally rigid graph to define a gradient control the formation is locally stable. For (5.6), the infinitesimally rigidity of the underlying graph was key in proving that both that the target set is an embedded submanifold of the state space and that the linearized dynamics has the required form to apply Theorem (4.5). The local stability of the formation implies that if the robots experience small perturbations away from an equilibrium formation they will converge back to another nearby point in the target set.

Comment 5.1: In the introduction, we noted that [29] was closest in spirit to the work of this thesis. However, there are some significant differences.

- Both works use graphs to define formations. The graphs in [29] are globally rigid. The graphs in our work are infinitesimally rigid.
- This work uses a single integrator model. In [29] a double integrator model is used.
- In [29], velocities are used as a control input. Thus the control does not use only local measurements.
- [29] has no topological analysis of the equilibrium set. In particular, [29] does not note that the equilibrium set is not compact.
- [29] uses a LaSalle argument to prove stability. Since the equilibrium set is not compact, this is an unusual use of LaSalle. Additionally, the LaSalle argument does not give any information about the behaviour of the trajectories as they approach the equilibrium set. In particular, it is unknown if under the control in [29] the trajectories have a limit on the equilibrium set.

We noted that the proof in [29] has some problems. Essentially, [29] assumes that the dynamics on the equilibrium manifold can be quotiented out and the formation equilibrium is topologically equivalent to a point. We have seen in our analysis of the formation problem that the situation is not so simple.

Although our work is close in spirit to [29], the previous discussion shows that there are in fact significant differences between the two works.

However, let's consider if it is possible to quotient out the dynamics on the equilibrium manifold. Let's again consider the equation

$$\dot{x} = f(x) \tag{5.18}$$

where $x \in \mathbb{R}^n$ and $\mathcal{E}$ is an $(n-k)$-dimensional manifold of equilibrium solutions.

Quotienting out the dynamics on the manifold is equivalent to asking if there exists a diffeomorphism $\varphi : \mathbb{R}^n \to \mathbb{R}^{n-k} \times \mathbb{R}^k$ such that

$$\dot{\theta} = f_1(\theta, \rho)$$
$$\dot{\rho} = f_2(\rho),$$

where $(\theta, \rho) = \varphi(x)$, $\frac{\partial f_1}{\partial \theta} = 0$ and

$$\mathcal{E} = \{\ x \in \mathbb{R}^n \mid x = \varphi^{-1}(\theta, 0)\ \}.$$

If such a normal form exists then the stability of the equilibrium set becomes a study of the stability of $\rho = 0$.

There are several difficulties in this analysis. The change of coordinates must be global on the manifold $\mathcal{E}$. For the formation problem, the equilibrium manifold is topologically equivalent to a generalized cylinder, so this requirement is unlikely to be a problem. It is not known if such a diffeomorphism exists for the formation problem, and it may

be computationally difficult to show $\frac{\partial f_1}{\partial \theta} = 0$. Clearly, to quotient out the manifold $\mathcal{E}$ requires some additional analysis. $\lhd$

Chapter 6

Applications

6.1 Regular Polygon Formations

An application of the formation stabilization control developed in the previous chapters is to stabilize the robots to a regular polygon. A regular polygon is a useful formation because robots in this configuration can be used to form a large aperture antenna array. For sensor network applications, such an antenna can be used to transmit information back to a base location.

In order to stabilize the robots to a regular polygon we must first design a graph that is infinitesimally rigid. We could use the procedure outlined in Section 2.3.3 to build this graph, but there are other possible graphs. In particular, we are interested in graphs that result in *cyclically homogeneous* controls. Cyclical homogeneity is a special type of symmetry. We consider a control to be cyclically homogeneous if when the indices 1 to N of the robots undergo a cyclic permutation, the control laws are permuted by the same permutation. An example of cyclically homogeneous control laws is cyclic pursuit:

$$u_1 = z_2 - z_1, \quad u_2 = z_3 - z_2, \quad \ldots, \quad u_N = z_1 - z_N.$$

(This control law achieves rendezvous, not a polygon formation.)

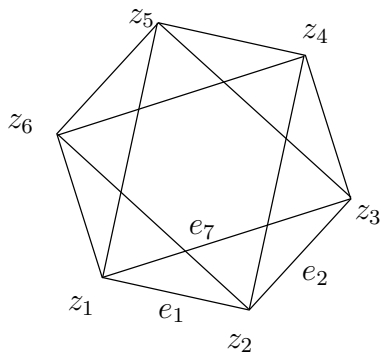

Figure 6.1: The graph G_6^*.

Cyclically homogeneous control laws are identical for each robot except that a known indexing of the robots is required. Cyclically homogeneous controls are desirable because an identical controller on each robot makes implementation easier.

For our two dimensional agents the cyclic homogeneity property can be stated precisely in the following way: we define the $2N \times 2N$ fundamental permutation matrix P^* whose first block row is

$$\begin{bmatrix} 0 & I_2 & 0 & 0 & \dots & 0 \end{bmatrix},$$

where $I \in \mathbb{R}^{2\times 2}$. Then for a closed-loop system of the form

$$\dot{x} = f(x)$$

if it has the interesting symmetry

$$f(P^* z) = P^* f(z),$$

we say that f has the property of *cyclic homogeneity*.

Let's consider the graph where vertex i is connected to vertices $i+1$, $i+2$, $i-1$ and $i-2$. We will refer to such a graph as G_N^*, where N is the number of vertices. In contexts where the number of vertices is implied we will drop the subscript. The graph

G_6^* is shown in Figure 6.1. By definition, the graph G_N^* has $2N$ edges. We order the edges in the graph so that the expanded incidence matrix $\hat{H} = H \otimes I_2$ is

$$\hat{H} := \begin{bmatrix} I_{2N} - P^* \\ I_{2N} - (P^*)^2 \end{bmatrix}.$$

By definition it is clear that $\hat{H} \in \mathbb{R}^{4N \times 2N}$. Note that

$$\hat{H} = \begin{bmatrix} I_{2N} \\ I_{2N} + P^* \end{bmatrix} (I_{2N} - P^*)$$

thus if $e = \hat{H}z$ then

$$\begin{bmatrix} I_{2N} + P^* & -I_{2N} \end{bmatrix} e = 0.$$

Thus the components of e have a special form with $e_{i+N} = e_i + e_{i+1}$ for $i = 1, \ldots, N$.

Let

$$d^* := \begin{bmatrix} c\mathbf{1} \\ c^*\mathbf{1} \end{bmatrix},$$

where $\sqrt{c} \in \mathbb{R}$ is the side length of the regular polygon and

$$c^* := 2c\left(1 - \cos\left(\frac{n\pi - 2\pi}{n}\right)\right).$$

We assume that $c \neq 0$. If p is a point where the robots form a regular polygon, then $f_{G^*}(p) = d^*$. By construction, we can see that the set $f_{G^*}^{-1}(d^*)$ is non-empty. The following lemma discusses the relationship between the robots being in a regular polygon formation and $f_{G^*}^{-1}(d^*)$.

Lemma 6.1: *The robots located at $p \in \mathbb{R}^{2N}$ form a regular polygon if and and only if $p \in f_{G^*}^{-1}(d^*)$.*

Proof: By construction, if the robots form a regular polygon at p than $f_{G^*}(p) = d^*$.

The sufficient condition is true if (G^*, p) is a globally rigid framework. Techniques from graph theory can be used to show that the framework (G^*, p) is globally rigid. However, it can also be shown using some simple geometry. By the definition of e_i, e_{i+1} and e_{i+N} we see that $e_{i+N} = e_i + e_{i+1}$, for $i = 1, \ldots, N$. So the three edges form a triangle. The goal that $\|e_i\|^2 = \|e_{i+1}\|^2 = c$ and $\|e_{i+N}\|^2 = c^*$ uniquely constrains the side lengths of the triangle. Thus the angle between each e_i and e_{i+1} is prescribed. Since the side lengths and interior angles of the polygon are all defined, there is only one possible embedding of the graph G^* that satisfies the edge lengths d^*, and (G^*, p) is globally rigid. □

Lemma 6.1 shows that the regular polygon formation is the only formation in the set E_1 as defined in Section 5.3.1. Thus e_i and e_{i+1}, $i = 1, \ldots, N$, are related by a rotation of $\pm 2\pi/N$. Note that if e_2 is e_1 rotated by $2\pi/N$ then all other $N-1$ edge vectors are related by the same rotation. Likewise if e_2 is e_1 rotated by $-2\pi/N$. These two possible rotations correspond to the two possible embeddings of the globally rigid graph. The formations in these two cases are reflections of one another. Now we must now check the rank of the rigidity matrix on E_1 to check the conditions of Theorem 5.3.

Lemma 6.2: *Let $p \in \mathbb{R}^{2N}$ be a point in $f_{G^*}^{-1}(d^*)$. Then the framework (G^*, p) is infinitesimally rigid.*

Proof: The rigidity matrix is $J_{f_{G^*}}(p) = J_v(e)\hat{H}$, with $e = \hat{H}p$. The graph G^* is connected, so from Property 2.1 of H we know that $\dim(\mathrm{Ker}(\hat{H})) = 2$. The strategy of the proof is to show that $\mathrm{Im}(\hat{H}) \cap \mathrm{Ker}(J_v(e)) = 1$, from which it follows that

$$\dim(\ker J_{f_G^*}(p)) = \dim(\mathrm{Ker}(\hat{H})) + \mathrm{Im}(\hat{H}) \cap \mathrm{Ker}(J_v(e)) = 3^1.$$

We now consider the dimension of $\mathrm{Im}(\hat{H}) \cap \mathrm{Ker}(J_v(e))$.

[1] That is to say that given a set $\mathcal{S}$ and a matrix C that $\dim(C^{-1}(\mathcal{S})) = \dim(\ker C) + \dim(\mathrm{Im}C \cap \mathcal{S})$, [39]

Assume $\xi \in \mathrm{Im}(\hat{H})$ where $\xi = (\xi_1, \ldots, \xi_{2N})$ and each $\xi_i \in \mathbb{R}^2$. Since $\xi \in \mathrm{Im}(\hat{H})$, we know that $\xi_{i+N} = \xi_i + \xi_{i+1}$ for $i = 1, \ldots, N$. We now consider the restrictions on ξ so that it is in $\mathrm{Ker}(J_v(e))$.

Assume $J_v(e)\xi = 0$. First we note from (5.2) that $e_1^T \xi_1 = 0$. This gives ξ_1 one degree of freedom.

Next consider the restrictions on ξ_2. We see that $e_2^T \xi_2 = 0$ and $e_{N+1}^T \xi_{N+1} = e_{N+1}^T(\xi_1 + \xi_2) = 0$. This can be rewritten as

$$\begin{bmatrix} e_2^T \\ e_{N+1}^T \end{bmatrix} \xi_2 = \begin{bmatrix} 0 \\ -e_{N+1}^T \xi_1 \end{bmatrix} = \begin{bmatrix} e_1^T \\ -e_{N+1}^T \end{bmatrix} \xi_1 \tag{6.1}$$

The matrix

$$\begin{bmatrix} e_2^T \\ e_{N+1}^T \end{bmatrix}$$

is non-singular because e_2 and e_{N+1} are not collinear; ξ_2 is then uniquely determined from ξ_1. Solving, we see that $\xi_2 = R\xi_1$, where R is the rotation by $\pm 2\pi/N$ radians such that $e_{i+1} = Re_i$, for $i = 1, \ldots, N$. Let's check to see that ξ_2 does in fact satisfy (6.1). Substituting ξ_2 into the top row we see that

$$e_2^T \xi_2 = e_1^T R^T R \xi_1 = 0$$

as required. If we substitute into the second row we obtain

$$\begin{aligned} e_{N+1}^T(\xi_1 + \xi_2) &= (e_1 + Re_1)^T(\xi_1 + \xi_2) \\ &= (e_1 + Re_1)^T(\xi_1 + R\xi_1) \\ &= e_1^T(2I + R + R^T)\xi_1 \end{aligned}$$

the matrix $R + R^T = \omega I$ for some $\omega \in \mathbb{R}$ so

$$e_{N+1}^T(\xi_1 + \xi_2) = 0.$$

If we continue this process inductively we see that ξ_i is uniquely determined by ξ_{i-1}, for $i = 2, \ldots, N$ with $\xi_i = R\xi_{i-1}$. Combining all expressions for ξ_i we see that

$$\xi = (w, Rw, R^2w, \ldots, R^{N-1}w, (I+R)w, R(I+R)w, \ldots R^{N-1}(I+R)w),$$

where $w \in \mathrm{Ker}(e_1^T)$.

It only remains to show that $\xi \in \mathrm{Im}(\hat{H})$ as assumed. The vector ξ is in $\mathrm{Im}(\hat{H})$ if $(\mathbf{1}^T \otimes I_2)\xi = 0$. To check that this is true we expand to see

$$(\mathbf{1}^T \otimes I_2)\xi = (I + R + R^2 + \ldots + R^{N-1} + (I+R) + R(I+R) + \cdots + R^{N-1}(I+R))\xi_1.$$

Since ξ_1 is a non zero vector, we must show that

$$(I + R + R^2 + \ldots + R^{N-1} + (I+R) + R(I+R) + \cdots + R^{N-1}(I+R)) = 0. \qquad (6.2)$$

Note that

$$\begin{aligned}(I-R)(I + R + R^2 + \ldots + R^{N-1}) &= I + R + R^2 + \ldots + R^{N-1} - R - R^2 - \ldots - R^N \\ &= I - R^N.\end{aligned}$$

If we factor the left side of (6.2), we obtain

$$(I-R)^{-1}(I-R^N) + (I-R)^{-1}(I-R^N)(I_R).$$

The matrix R^N is the rotation by 2π, so $R^N = I$. It follows that $\xi \in \mathrm{Im}(\hat{H})$. Thus the

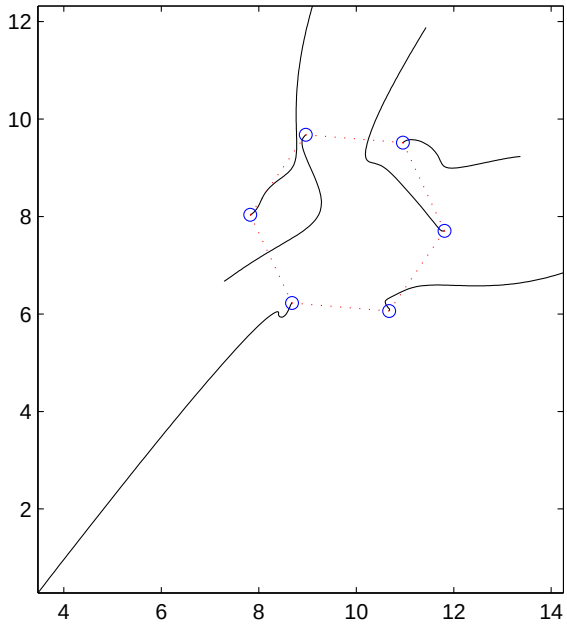

Figure 6.2: Six robots converging to a regular polygon.

dimension of $\mathrm{Im}(\hat{H}) \cap \mathrm{Ker}(J_v(\hat{H}z))$ is one. □

From Lemma 6.2 we see that the graph G^* forms an infinitesimally rigid framework at regular points. Thus the control developed in Chapter 3 can be used to stabilize a regular polygon with the graph G^*.

Figure 6.2 shows six robots converging to a regular polygon using this control. Figure 6.3 shows six robots converging into one of the collinear equilibria in the set $\mathcal{C}$. In simulation, only initial conditions in the set $\mathcal{C}$ have been found to converge to collinear equilibria.

6.2 Formations using Directed Graphs

A drawback to the control designed in Chapter 5 is that it relies on two-way communication. If robot i's control uses the position of robot j, then robot j's uses the position

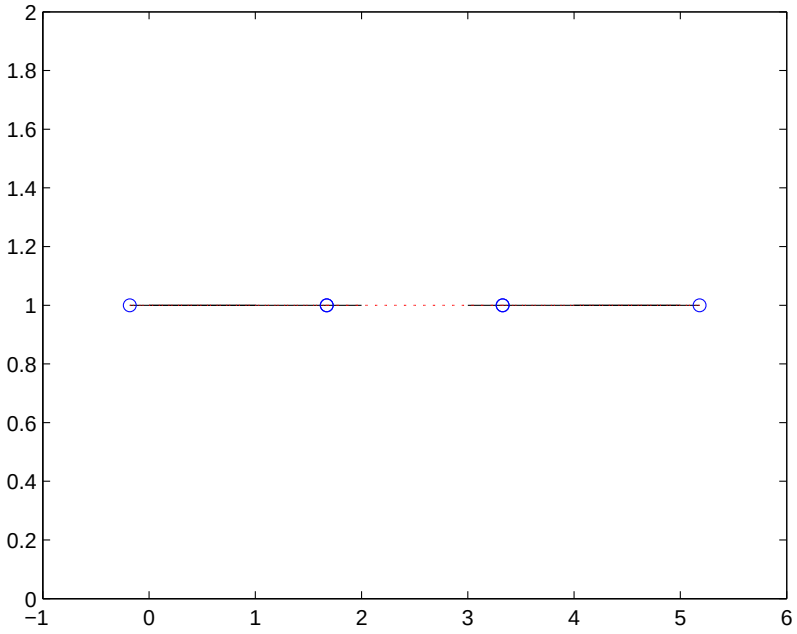

Figure 6.3: Six robots converging to one of the collinear equilibria. Note that there are two sets of robots that are coincident.

of robot i. This makes implementation difficult when using cameras with a limited field of view. When using this type of camera, a control based on a directed graph is easier to implement. Controls based on directed graphs are currently an area of active research in the field of formation control; see [16]. A key development in this theory is the idea of a directed formation graph being persistent. Persistence characterizes directed graphs that produce formations that maintain their shape [17], analogous to the use of rigidity in undirected graphs.

In this section we outline a procedure for how directed graphs can be constructed to stabilize formations.

6.2.1 Rigidity and Persistence

Before we design controls based on directed graphs, we will consider how to define rigidity in the context of directed graphs as well as discuss persistence. Persistence combines two

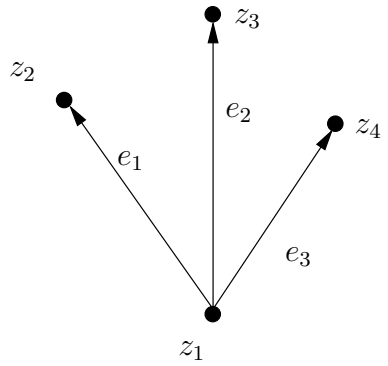

Figure 6.4: A directed graph that is not constraint consistent. Note that this graph is not rigid

ideas: rigidity and constraint consistency. Constraint consistency formalizes achievability of the control goal. In order to define persistence we first define rigidity for directed graphs. Let G be a directed graph. We define a framework for a directed graph to be (G, p), where $p \in \mathbb{R}^{2|V|}$. We denote by $f_G(p)$ the rigidity function, as in Section 2.3.1.

Definition 6.1: *A framework (G, p) is rigid if there exists a neighbourhood of U of p such that $f_G^{-1}(f_G(p)) \cap U = f_K^{-1}(f_K(p)) \cap U$.*

From Definition 6.1, a directed framework is rigid if the corresponding undirected framework is rigid. Similarly, we define a directed framework (G, p) to be *infinitesimally rigid* if rank $J_{f_G}(p) = 2N - 3$.

However, when using a directed graph to maintain a formation it is not enough to have the graph be rigid. There can be situations where some inter-robot distances are correct but it is impossible to satisfy the remaining distance constraints. Figure 6.4 shows such a situation when the framework is not rigid. If vertex z_2 moves such that the length of e_1 changes, while all the other vertices remain in the same position, then there is no location where the lengths of e_1, e_2 and e_3 can all be maintained. If such a situation cannot happen, we describe the graph as constraint consistent. The precise definition of constraint consistence from [16] is complex and beyond what is needed for the implementation proposed in this work. Instead, we will use the following sufficient

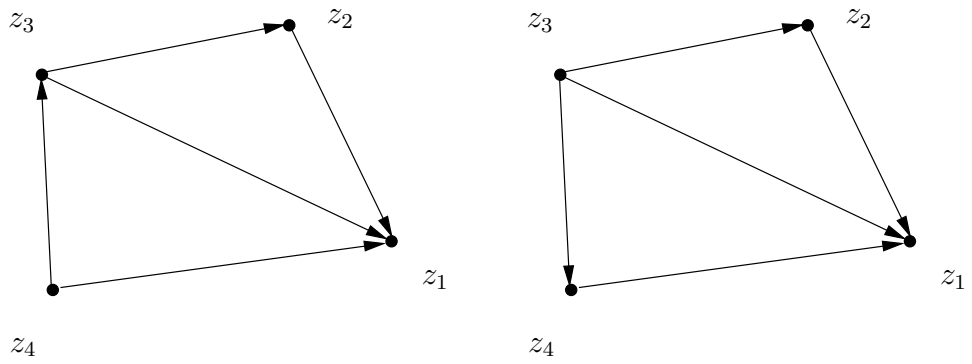

(a) Example of a persistent framework.

(b) Example of a non-persistent but rigid framework.

Figure 6.5: Two different rigid frameworks with four nodes.

condition.

Definition 6.2 ([16]) : *A framework (G, p) is constraint consistent if each vertex has two or fewer outgoing edges.*

Finally, *persistence* is defined in [16] as a framework that is both rigid and constraint consistent. A graph is *minimally persistent* if it is minimally rigid and constraint consistent.

Figure 6.5 shows why constraint consistence is needed in addition to rigidity when considering directed formations. Both graphs in Figure 6.5 are rigid: Figure 6.5(a) is also constraint consistent and thus persistent, whereas Figure 6.5(b) is not. If vertex 4 moves while still maintaining the distance to vertex 1 it is no longer possible for vertex 3 to maintain the lengths of its three outgoing edges.

The following useful theorem characterizes minimal persistence.

Theorem 6.1 (Theorem 4, [16]) : *A rigid graph is minimally persistent if and only if*

1. *There are three vertices that have one outgoing edge, and the remaining vertices have two outgoing edges.*

2. *There is one vertex that has no outgoing edges, one vertex that has one outgoing edge, and the remaining vertices have two outgoing edges.*

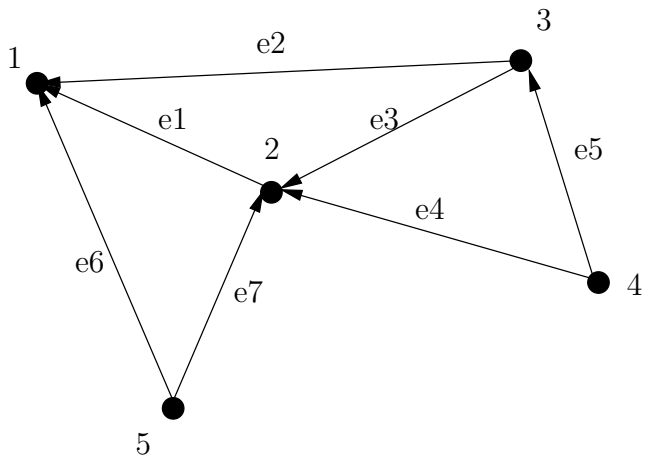

Figure 6.6: Graph created by recursively adding vertices in order. The edges are created in the order $e1, e2, \ldots, e7$. In particular note that there are 7 directed edges, which equal $2 \times 5 - 3$.

6.2.2 Constructing a Persistent Graph

To construct the directed graph we use a modification of the Henneburg insertion technique described in Section 2.3.3. Let p be the location of the vertices in the plane. Again, we number all the vertices. The first step in adding the edges is to add a directed edge from vertex 2 to vertex 1. All remaining vertices are connected to the graph in numerical order by creating two edges leaving the newly connected node whose destination is two distinct vertices that are already in the connected graph structure. Figure 6.6 shows a graph created using this procedure. Note that directed graphs formed by a sequence of Henneburg insertions are persistent and satisfy case 2 in Theorem 6.1.

Now we develop the control law for each robot. Instead of having a global potential function, as in (5.5), we have a potential function for each robot. Let $\phi_i(z)$ be the potential function for robot i and the control goal be $f_G(z(t)) \to d$. If we again define $e := \hat{H}z$, then in the target formation $d_j = \|e_j\|^2$.

In Figure 6.6 robot 1 has no outgoing edges. We define $\phi_1(z) := 0$. Robot 2 has only one outgoing edge, e_1. We define robot 2's potential function to be $\phi_2(z) := \frac{1}{2}(\|e_1\|^2 - d_1)^2$. By construction, all other robots have two outgoing edges. Define the outgoing edges for

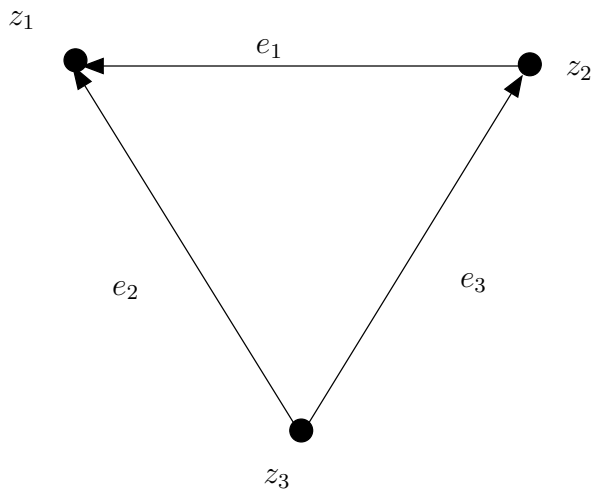

Figure 6.7: An embedding of a directed graph triangle graph.

robot i to be e_j and e_k. By construction, we know that $j < i$ and $k < i$. Then for robot i, where $i \neq 1$ and $i \neq 2$, the potential function is

$$\phi_i(z) := \frac{1}{2}(\|e_j\|^2 - d_j)^2 + \frac{1}{2}(\|e_k\|^2 - d_k)^2.$$

The control for each robot is then

$$u_i = -\frac{\partial}{\partial z_i}\phi_i(z)^T. \tag{6.3}$$

From (5.1) it follows that

$$\dot{z}_i = -\frac{\partial}{\partial z_i}\phi_i(z)^T.$$

Define the closed-loop system to be $\dot{z} =: F(z)$.

Let's consider stabilizing an equilateral triangle using a directed graph and the individual potential functions developed above.

Example 6.1: We construct a triangular graph with three edges:

$$e_1 = z_1 - z_2$$

$$e_2 = z_1 - z_3$$

$$e_3 = z_2 - z_3$$

and $d = (1, 1, 1)$, as shown in Figure 6.7. Then the control law is

$$\dot{z}_1 = 0$$

$$\dot{z}_2 = -2(\|e_1\|^2 - 1)e_1$$

$$\dot{z}_3 = -2(\|e_2\|^2 - 1)e_2 - 2(\|e_3\|^2 - 1)e_3.$$

The Jacobian of F evaluated at a point p such that $f_G(p) = d$ is

$$J_F(p) = 4 \begin{bmatrix} 0 & 0 & 0 \\ e_1 e_1^T & -e_1 e_1^T & 0 \\ e_2 e_2^T & e_3 e_3^T & -e_2 e_2^T - e_3 e_3^T \end{bmatrix}.$$

The matrix $J_F(p)$ is block lower triangular, so we can analyze the eigenvalues of the blocks on the diagonal to study the eigenvalues of $J_F(p)$. The first two rows are zero: the first 2×2 block on the main diagonal has two zero eigenvalues. The second 2×2 block $-e_1 e_1^T$ is a negative semidefinite matrix with rank 1, and so has one zero eigenvalue and one strictly real negative eigenvalue. The third 2×2 block, $-e_2 e_2^T - e_3 e_3^T$, is the sum of two negative semidefinite matrices, and thus is also a negative semidefinite matrix. If e_2 and e_3 are linearly independent, as they are in the triangle problem, then the third block has rank 2 and thus has two negative real eigenvalues. Thus we see that $J_F(p)$ has three zero eigenvalues and three real negative eigenvalues.

If we check the rigidity matrix of the corresponding undirected graph we see that this

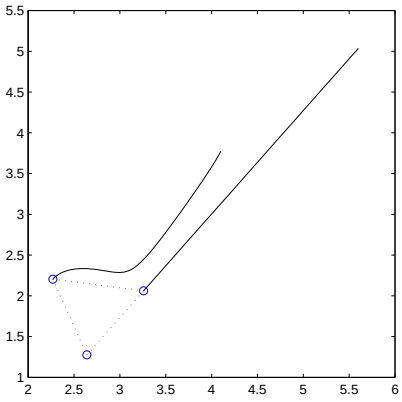

Figure 6.8: Simulation of three robots stabilizing to an equilateral triangle using a control derived from a directed graph. Note that one of the robots remains stationary.

graph is infinitesimally rigid. If we define E_1 as in Section 5.3.1, the condition for E_1 to be an embedded submanifold holds. Thus we can apply the coordinate transformation in Theorem 4.1 and apply Malkin's theorem as in Theorem 5.3 to conclude that E_1 is a locally stable manifold. Figure 6.8 shows a simulation using this control law. $\lhd$

Lemma 6.3: *The Jacobian of the control law* (6.3), $J_F(z)$, *at a point* $p \in f_G^{-1}(d)$ *is block lower triangular.*

Proof: From the definition of $\phi_1(z)$ we see that $\dot{z}_1 = 0$. So the first two rows of $J_F(p)$ are zero.

From the definition of $\phi_2(z)$ we see that

$$\dot{z}_2 = -2(\|e_1\|^2 - d_1)e_1.$$

Differentiating we see that the next two rows of $J_F(p)$ are

$$4 \begin{bmatrix} e_1 e_1^T & -e_1 e_1^T & 0 & \dots & 0 \end{bmatrix}.$$

Note that the block $-e_1 e_1^T$ is on the main diagonal.

When we linearize $\dot{z}_i$ we see there are three non-zero 2×2 blocks: $e_j e_j^T$, $e_k e_k^T$, and along the main diagonal $-e_j e_j^T - e_k e_k^T$. The blocks $e_j e_j^T$ and $e_k e_k^T$ are both below the main diagonal because $j < i$ and $k < i$. Thus $J_F(p)$ has a block lower triangular structure. □

Theorem 6.2: *The matrix $J_F(p)$, where $p \in f_G^{-1}(d)$, has three zero eigenvalues and the rest are real and negative if for each $i > 2$ the edges e_k and e_j leaving vertex i are not collinear.*

Proof: From Lemma 6.3 we know that the matrix $J_F(p)$ is block lower triangular. The first two rows of $J_F(p)$ are zero. Thus the first 2×2 block on the main diagonal has two zero eigenvalues. The second 2×2 block is $-e_1 e_1^T$, a negative semidefinite matrix with rank 1, and so has one zero eigenvalue and one negative real eigenvalue. Each subsequent 2×2 block on the main diagonal has the form $-e_j e_j^T - e_k e_k^T$ and is the sum of two negative semidefinite matrices, and thus is also a negative semidefinite matrix. By the non-collinearity assumption e_j and e_k are linearly independent so the third block has rank 2 and thus has two negative real eigenvalues. Thus we see that $J_F(p)$ has three zero eigenvalues and the rest are real and negative eigenvalues. □

Note that instead of an infinitesimally rigid condition on the graph as in Theorem 5.2, we instead have a non-collinearity condition on the edges leaving a graph. One might wonder if the non-collinearity condition is implied by the infinitesimal rigidity condition. However, Figure 6.9 provides a counterexample, showing a graph may be infinitesimally rigid and have one vertex with two collinear edges leaving it.

Theorem 6.3: *Let G be a directed graph constructed using a sequence of Henneburg insertions. If G is infinitesimally rigid and no vertex has collinear outgoing edges for each point p such that $f_G(p) = d$, then, under the control* (6.3)*, E_1 is locally asymptotically stable.*

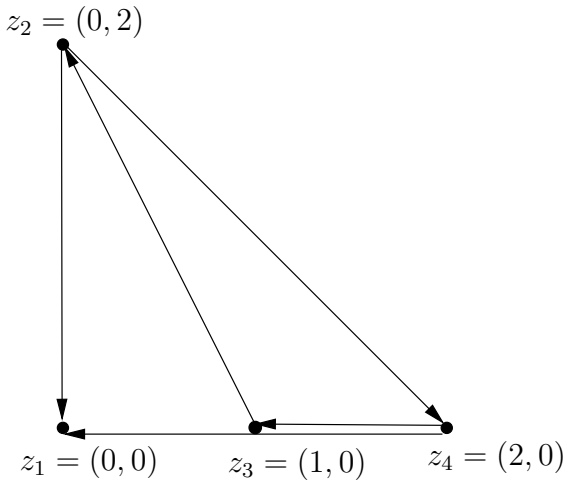

Figure 6.9: A directed graph that is infinitesimally rigid, but has a vertex (z_4) with two parallel outgoing edges.

Moreover, there exists a neighborhood $\mathcal{U}$ *of* E_1 *such that for each* $z(0) \in \mathcal{U}$ *there exists a point* $p \in E_1$ *where*

$$\lim_{t\to\infty} z(t) = p.$$

Proof: The proof largely follows from the results of Chapter 5.

First we separate the stationary z_1 dynamics from the rest of the system. Define

$$P_2 = \begin{bmatrix} I_2 & 0 & 0 & \dots & 0 \\ -I_2 & I_2 & 0 & \dots & 0 \\ -I_2 & 0 & I_2 & \dots & 0 \\ \vdots & \vdots & \ddots & \dots & \vdots \\ -I_2 & 0 & \dots & \dots & I_2 \end{bmatrix}.$$

Further define

$$(z_1, \psi) = P_2 z.$$

Thus $\psi = (z_2 - z_1, \dots, z_N - z_1)$. Note that if $e_i = z_j - z_1$ then $e_i = \psi_j$ and if $e_i = z_j - z_k$

then $e_i = \psi_j - \psi_i$. So it is possible to find a matrix M such that $e = M\psi$. Further define

$$\mathcal{E} := \{\ \psi \in \mathbb{R}^{2N-2} \mid v(e) = v(M\psi) = d\}.$$

Note that $E_1 = \mathbb{R}^2 \times \mathcal{E}$. Additionally, we see that $\mathcal{E}$ is compact and each component is diffeomorphic to S^1. Define $\dot{\psi} = F_\psi(\psi)$ to be the closed loop ψ dynamics.

To prove E_1 is stable we study these ψ dynamics. Thus from the structure of $F(z)$ it is clear that $\mathcal{E}$ is stable if and only if E_1 is stable. To show $\mathcal{E}$ is stable we show that each component of $\mathcal{E}$ is stable. Let $\mathcal{S}$ be an arbitrary topologically connected component of $\mathcal{E}$. Furthermore, let $\psi_0 \in \mathcal{S}$. From Theorem 5.1 we know that $\mathcal{S}$ has $2N-3$ globally defining functions.

In order to apply Theorem 4.5 it remains to show only that the Jacobian of the ψ dynamics meet the eigenvalue requirement.

Now we show that $J_{F_\psi}(\psi)$ has one zero eigenvalue and the remaining eigenvalues are stable. If we linearize the (z_1, ψ) dynamics at a point $(z_1, \psi_0) = P_2 z_0$ on E_1 we obtain

$$\begin{bmatrix} \dot{\delta z_1} \\ \dot{\delta\psi} \end{bmatrix} = \begin{bmatrix} 0 & 0 \\ 0 & J_{F_\psi}(\psi) \end{bmatrix} \begin{bmatrix} \delta z_1 \\ \delta\psi \end{bmatrix}.$$

Since the transformation P_2 is invertible it is clear that the matrices $P_2 J_F P_2^{-1}$ and $J_F(z_0)$ have the same eigenvalues. The matrix $P_2 J_F P_2^{-1}$ is block diagonal, with two zero eigenvalues in the first block. So the eigenvalues in the remaining block, $J_{F_\psi}(\psi)$, are the remaining eigenvalues of $J_F(z_0)$. From Theorem 6.2 we know these eigenvalues are all stable except for one zero eigenvalue.

Since J_{F_ψ} has one zero eigenvalue and the remaining are stable, the conditions of Theorem 4.5 apply. It follows that $\mathcal{S}$ is asymptotically stable. Finally, the set $\mathcal{U} := P_2^{-1}(\mathbb{R}^2 \times \mathcal{N})$. □

Theorem 6.3 shows that the results of Chapter 5 can be extended in the special case of directed graphs constructed using Henneburg insertions.

6.2.3 General Directed Graphs

If an arbitrary directed graph is used to derive the potential functions for each robot the analysis of the linearized dynamics is not so simple. However, if the linearized dynamics have three zero eigenvalues and the rest have negative real parts it is possible to locally apply the results of Chapter 5, most notably we can apply Theorem 4.2 to conclude that the formation is stable.

The following example has linearized dynamics that are not upper triangular, but by checking the eigenvalues numerically we can see that the results of Chapter 5 apply.

Example 6.2: Consider the framework shown in Figure 6.10. Let the location of the vertices be p. If we check the rigidity matrix of the undirected graph we see that the graph is infinitesimally rigid, thus E_1 is an embedded submanifold.

If we linearize we see that for $z \in E_1$

$$J_F(z) = 4 \begin{bmatrix} 0 & 0 & 0 & 0 \\ e_1 e_1^T & -e_1 e_1^T - e_2 e_2^T & e_2 e_2^T & 0 \\ e_3 e_3^T & 0 & -e_2 e_2^T - e_4 e_4^T & e_4 e_4^T \\ 0 & e_5 e_5^T & 0 & -e_5 e_5^T \end{bmatrix}.$$

Note that $J_F(z)$ is not block lower triangular, nor is there any way to permute the indices to make the matrix block lower triangular. The graph in Figure 6.10 could not have been created using the Henneburg insertion method. (Reference [17] discusses other operations that can produce such a directed graph.)

If we evaluate the eigenvalues of $J_F(z)$ numerically we see that there are three zero eigenvalues and the rest are real and stable. Thus the conditions to apply Malkin's

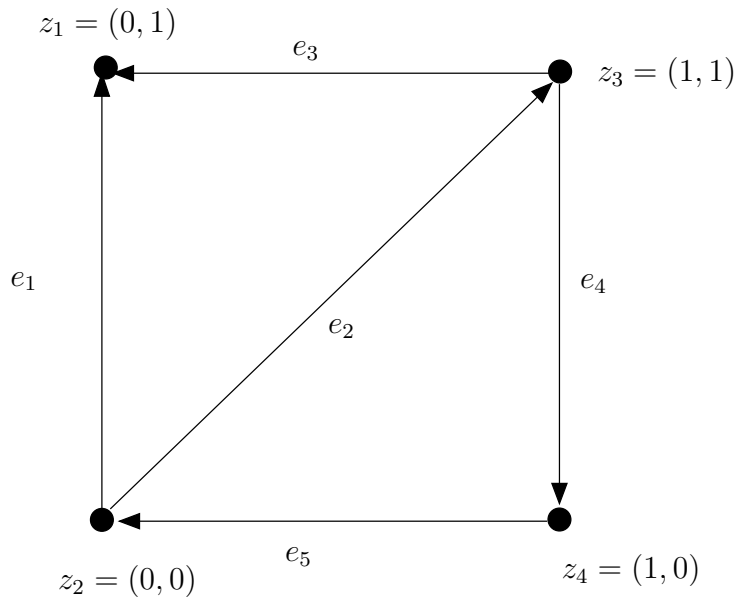

Figure 6.10: An embedding of a directed graph. Due to the arrangement of the edges leaving vertex 3 this graph could not have been created using the Henneburg insertion procedure.

theorem do hold and the formation is stable. ◁

The previous example shows that the procedure in Section 6.2.2 to construct a directed graph to stabilize formations is sufficient but not necessary for stability.

Conversely, there are some directed graphs where we cannot apply the results of Chapter 4.

Example 6.3: Consider the framework shown in Figure 6.11. Let the location of the vertices be p. If we check the rank of the rigidity matrix of the graph we see that the graph is infinitesimally rigid, thus E_1 is an embedded submanifold.

If we linearize at a point $z \in E_1$ we see that

$$J_F(z) = 4 \begin{bmatrix} 0 & 0 & 0 & 0 & 0 & 0 \\ e_1e_1^T & -e_1e_1^T & 0 & 0 & 0 & 0 \\ e_2e_2^T & e_3e_3^T & -e_2e_2^T - e_3e_3^T & 0 & 0 & 0 \\ 0 & 0 & e_5e_5^T & -e_5e_5^T - e_7e_7^T & 0 & e_7e_7^T \\ e_6e_6^T & 0 & 0 & e_9e_9^T & -e_6e_6^T - e_9e_9^T & 0 \\ 0 & e_6e_6^T & 0 & 0 & e_9e_9^T & -e_6e_6^T - e_9e_9^T \end{bmatrix}.$$

If we evaluate the eigenvalues numerically at p we see that there are 4 zero eigenvalues and the rest are real and stable. Thus the conditions to apply Malkin's theorem do not hold as there are more zero eigenvalues than the dimension of the equilibrium manifold and we can make no conclusion about the stability of this formation using this analysis technique. ◁

Due to the four zero eigenvalues, no stability conclusion can be drawn for this control using the linearized results. However if we again consider the placement of the robots at p, we can construct a new directed graph with the edges shown in Figure 6.12. If we check the rank of the rigidity matrix of the graph we see that the graph is infinitesimally rigid, thus E_1 is an embedded submanifold. By linearizing at a point z on the equilibrium manifold E_1,

$$J_F(z) = 4 \begin{bmatrix} 0 & 0 & 0 & 0 & 0 & 0 \\ e_1e_1^T & -e_1e_1^T & 0 & 0 & 0 & 0 \\ e_2e_2^T & e_3e_3^T & -e_2e_2^T - e_3e_3^T & 0 & 0 & 0 \\ e_4e_4^T & 0 & e_5e_5^T & -e_4e_4^T - e_5e_5^T & 0 & 0 \\ e_6e_6^T & 0 & 0 & e_7e_7^T & -e_6e_6^T - e_7e_7^T & 0 \\ 0 & 0 & 0 & e_8e_8^T & e_9e_9^T & -e_8e_8^T - e_9e_9^T \end{bmatrix}.$$

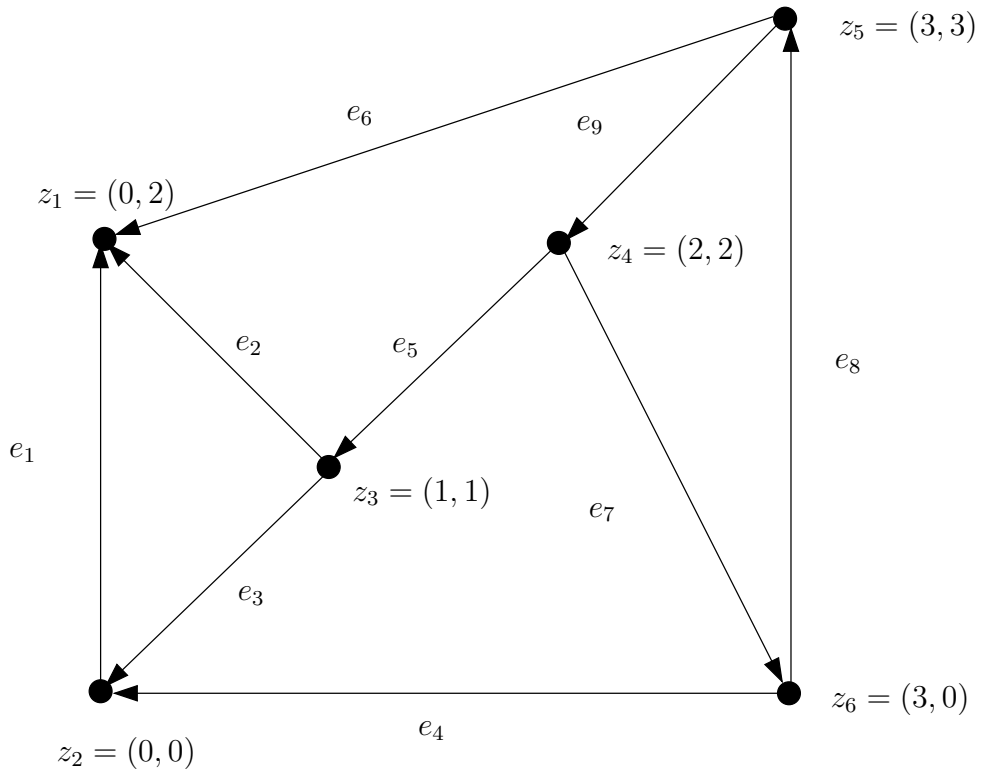

Figure 6.11: An embedding of a directed graph for six robots.

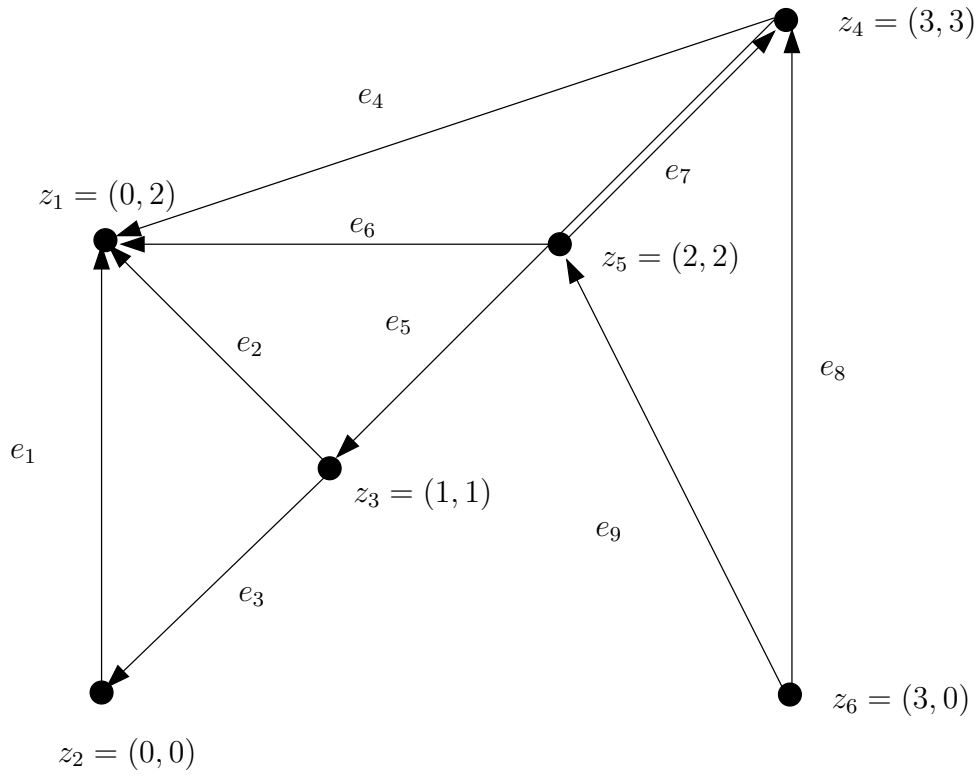

Figure 6.12: An embedding of a directed graph for six robots.

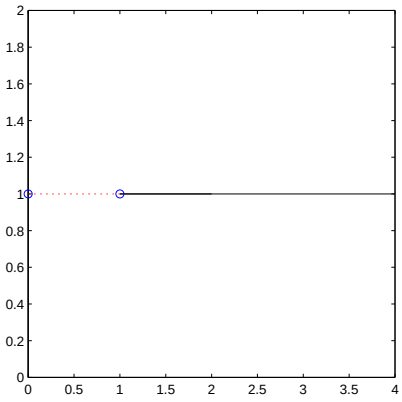

Figure 6.13: Simulation of three robots stabilizing to an equilibrium in $\mathcal{C}$. Note that one of the robots remains stationary and that robots 2 and 3 have the same final position.

we see that there are three zero eigenvalues and the rest have negative real parts from Theorem 6.2. Thus we can conclude that this formation is stable.

As in the undirected graph case, the set $\mathcal{C}$ defined in Section 5.2.1 is invariant. The simulation in Figure 6.13 of Example 6.1 where the three robots are initially collinear shows that the robots converge to a collinear equilibrium.

6.2.4 Conclusions on Directed Graphs

The stability results obtained for directed graphs are limited. However, in the event that a specific application requires the use of a directed graph it is possible using the technique outlined in Section 6.2.2 to build a graph that will be stable around the desired formation.

Chapter 7

Experiments

7.1 Experimental Model

The model in (5.6) is idealized and cannot represent a physical system. Let's implement the control from (5.6) to see how well it performs on real robots.

The results of Chapter 5 apply to a kinematic point model. As derived in the beginning of Chapter 3, it is possible to feedback linearize a kinematic unicycle model to obtain a point model. This feedback linearization will be the basis for our experiments.

As a preliminary step let's simulate the control (5.6) when the robots are feedback linearized kinematic unicycles. Recall that the kinematic unicycle has the following dynamical model

$$\dot{x} = u_1 \cos\theta$$

$$\dot{y} = u_1 \sin\theta$$

$$\dot{\theta} = u_2,$$

where (u_1, u_2) is the control input.

When we feedback linearize the unicycle about the outputs

$$\xi_x = x + l\cos\theta$$

$$\xi_y = y + l\sin\theta$$

then the $\xi := (\xi_x, \xi_y)$ dynamics are a kinematic point with $\dot{\xi} = v$. Define ξ_i to be output for robot i. Then using the ξ_i dynamics for robot i as z_i we have that the control inputs to the unicycle are

$$u_i = A(\theta_i)^{-1} v_i,$$

where

$$A(\theta) = \begin{bmatrix} \cos\theta & -l\sin\theta \\ \sin\theta & l\cos\theta \end{bmatrix}.$$

Note that in the unicycle formation problem we now have additional parameter l, the distance we used to feedback linearize the robots.

Let's perform some simulations of the feedback linearized system with various values of l to stabilized the robots to the equilateral triangle formation with unit side length. As a first step, let's choose l to be 0.01, two orders of magnitude smaller than the side length. Such a simulation is shown in Figures 7.1 and 7.2.

Next let's increase l to 0.1, one order of magnitude smaller than the side length of the triangle. A simulation of this case is shown in Figures 7.3 and 7.4.

Now let's selected l to be 0.5, half the side length of the triangle. A simulation for this case is shown in Figures 7.5 and 7.6. While the ξ for each robot forms an equilateral triangle, the actually positions of the robots are clearly not in an equilateral triangle. The performance in this case is not very satisfactory if we are trying to position the unicycles.

Finally, let's select l to be the same as the side length of the triangle, as shown in Figure 7.7. Again, the performance is not very satisfactory.

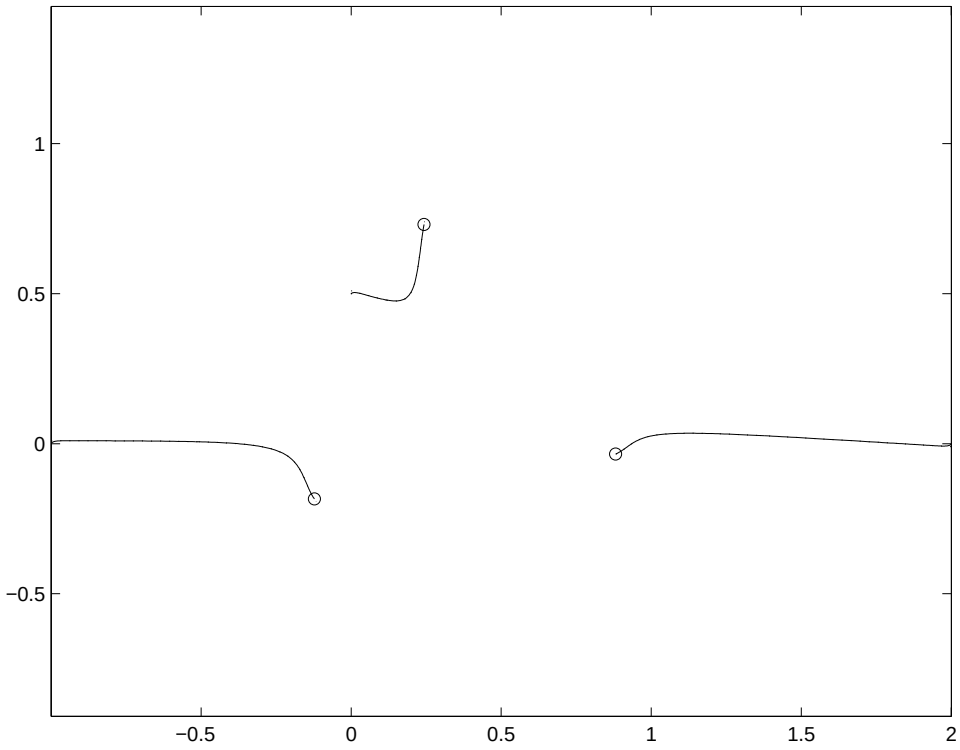

Figure 7.1: Simulation of three unicycle robots where the target formation is an equilateral triangle with unit length and $l = 0.01$. The trajectories of the unicycle robots in the plane are plotted with a solid line. The trajectories of the feedback linearized points ξ are plotted with a dotted line. In this simulation because l is small relative to the side lengths of the formation the two trajectories are almost coincident and appear in this figure as one line. Figure 7.2 shows the control signals for this simulation.

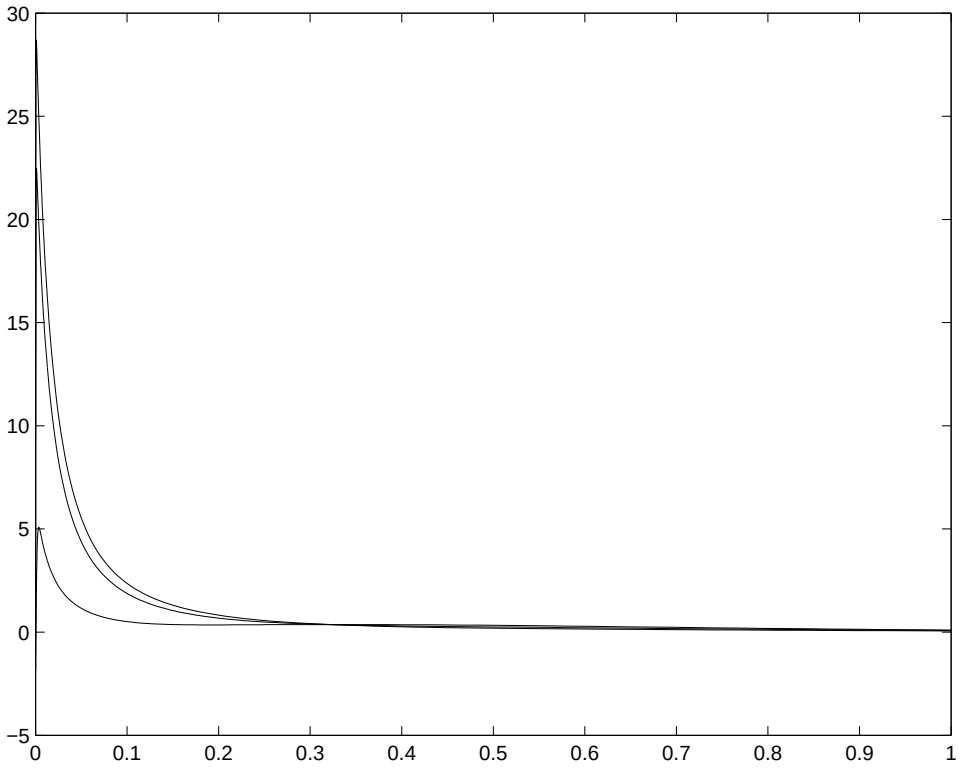

(a) Forward Velocities

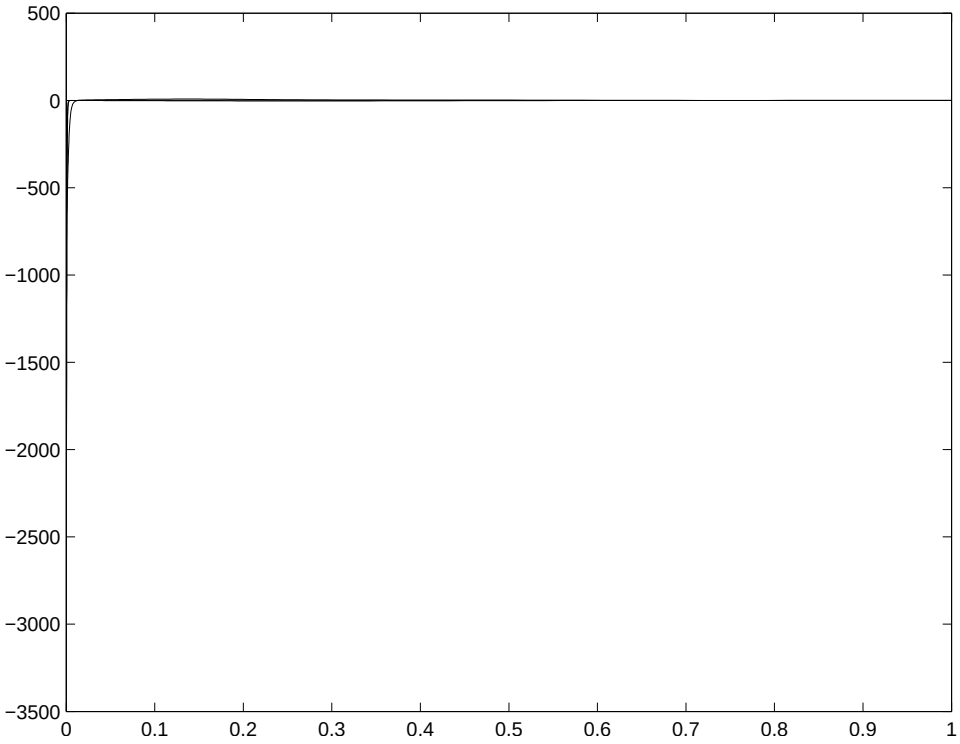

(b) Angular Velocities

Figure 7.2: Control signals for the simulation shown in Figure 7.1 where the goal formation is a equilateral triangle with unit length and $l = 0.01$. Figure 7.2(a) shows the control inputs u_1, the forward velocities of the robots. Figure 7.2(b) shows u_2, the angular velocities for each robot.

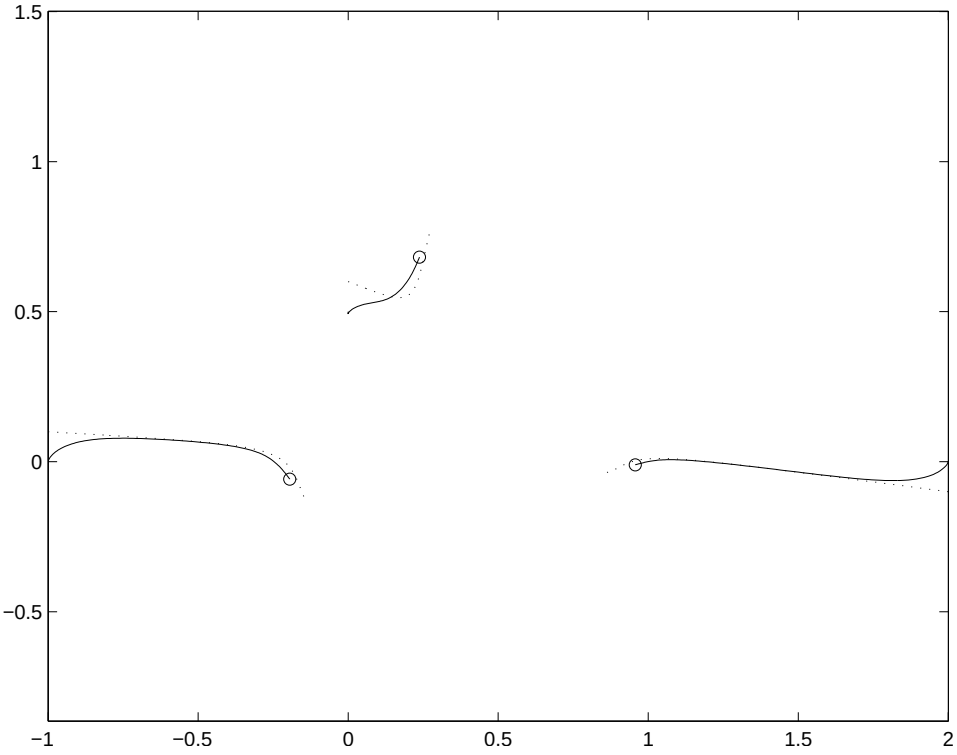

Figure 7.3: Simulation of three unicycle robots where the target formation is a equilateral triangle with unit length and $l = 0.1$. The trajectories of the unicycle robots in the plane are plotted with a solid line. The trajectories of the feedback linearized points ξ are plotted with a dotted line. Figure 7.4 shows the control signals for this simulation.

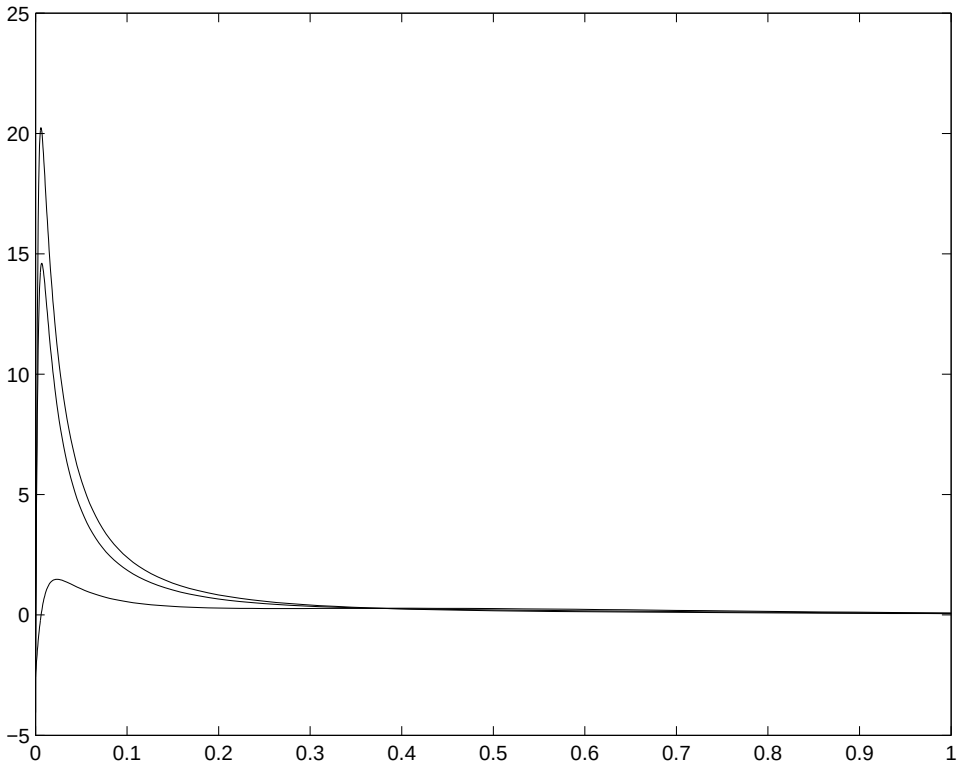

(a) Forward Velocities

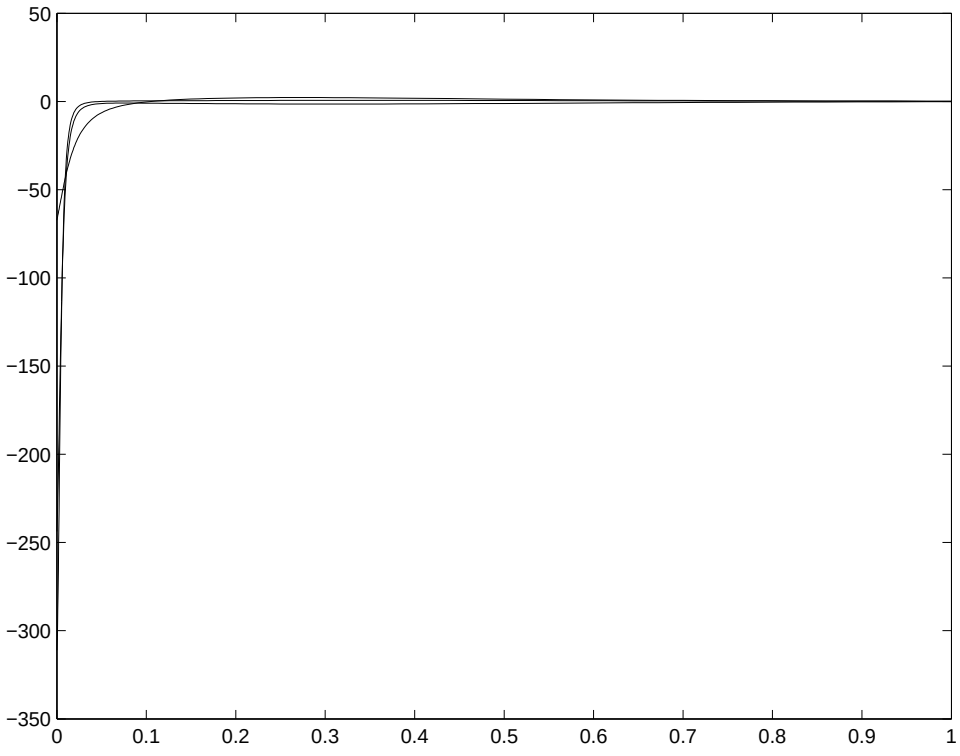

(b) Angular Velocities

Figure 7.4: Control signals for the simulation shown in Figure 7.3 where the goal formation is a equilateral triangle with unit length and $l = 0.1$. Figure 7.4(a) shows the control inputs u_1, the forward velocities of the robots. Figure 7.4(b) shows u_2, the angular velocities for each robot.

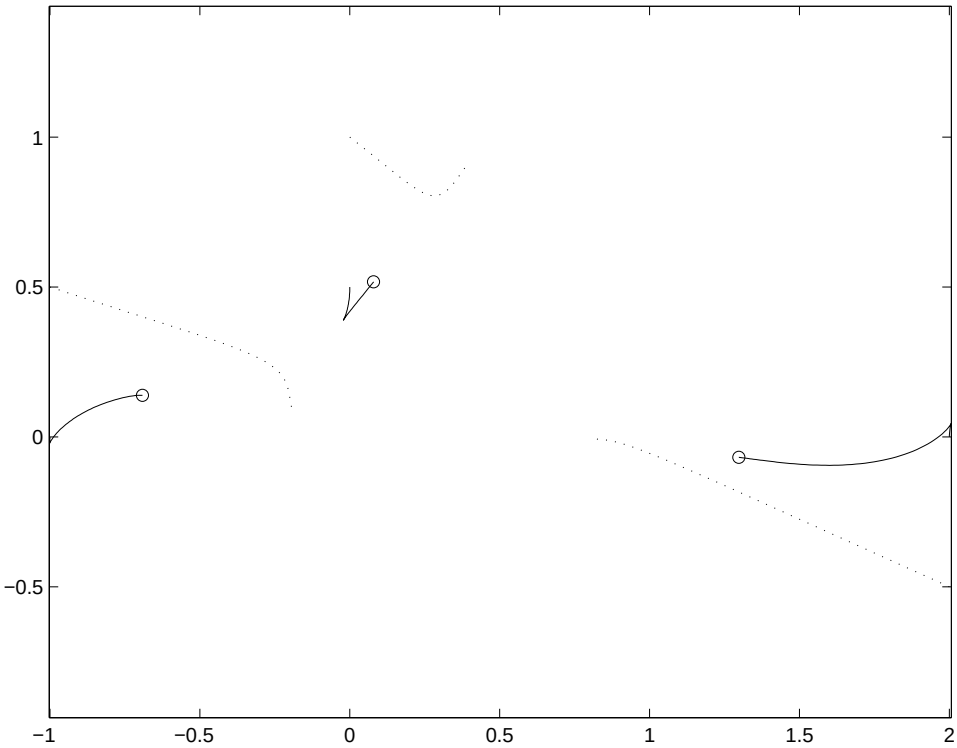

Figure 7.5: Simulation of three unicycle robots where the target formation is a equilateral triangle with unit length and $l = 0.5$. The trajectories of the unicycle robots in the plane are plotted with a solid line. The trajectories of the feedback linearized points ξ are plotted with a dotted line. Figure 7.6 shows the control signals for this simulation.

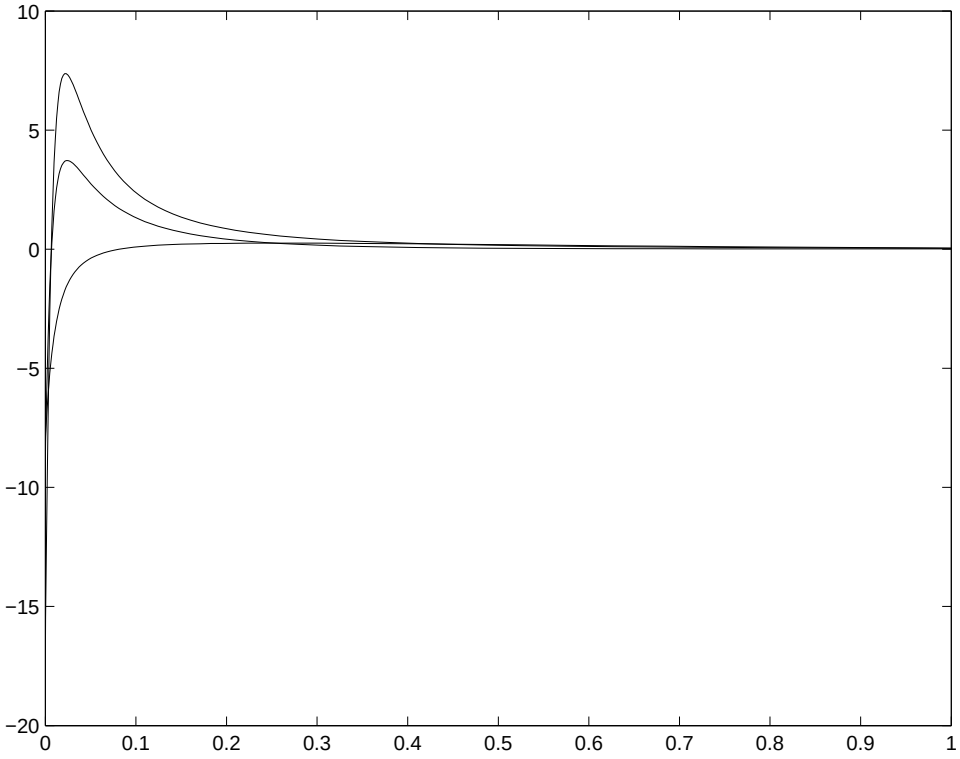

(a) Forward Velocities

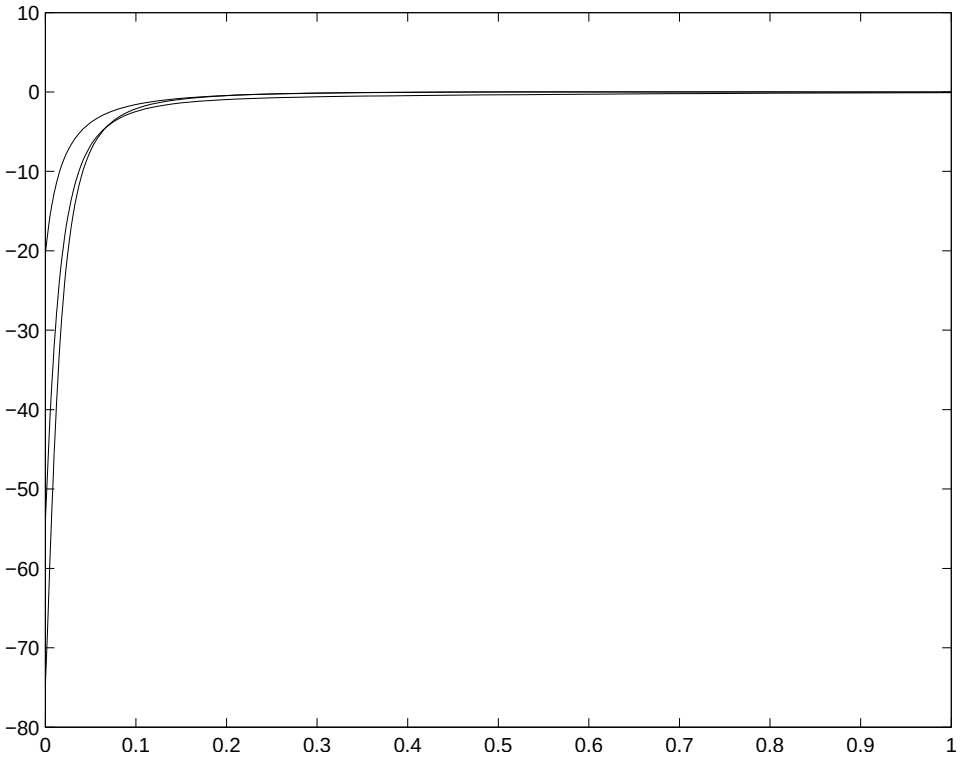

(b) Angular Velocities

Figure 7.6: Control signals for the simulation shown in Figure 7.5 where the goal formation is a equilateral triangle with unit length and $l = 0.5$. Figure 7.6(a)shows the control inputs u_1, the forward velocities of the robots. Figure 7.6(b) shows u_2, the angular velocities for each robot.

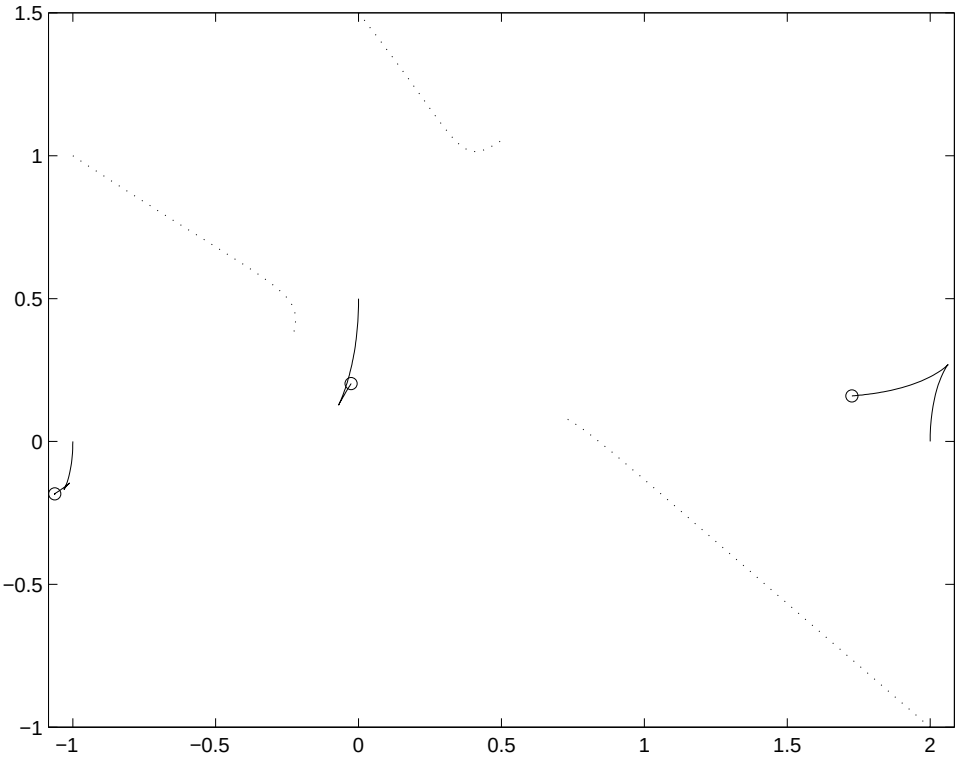

Figure 7.7: Simulation of three unicycle robots where the target formation is a equilateral triangle with unit length and $l = 1$. The trajectories of the unicycle robots in the plane are plotted with a solid line. The trajectories of the feedback linearized points ξ are plotted with a dotted line. Figure 7.6 shows the control signals for this simulation.

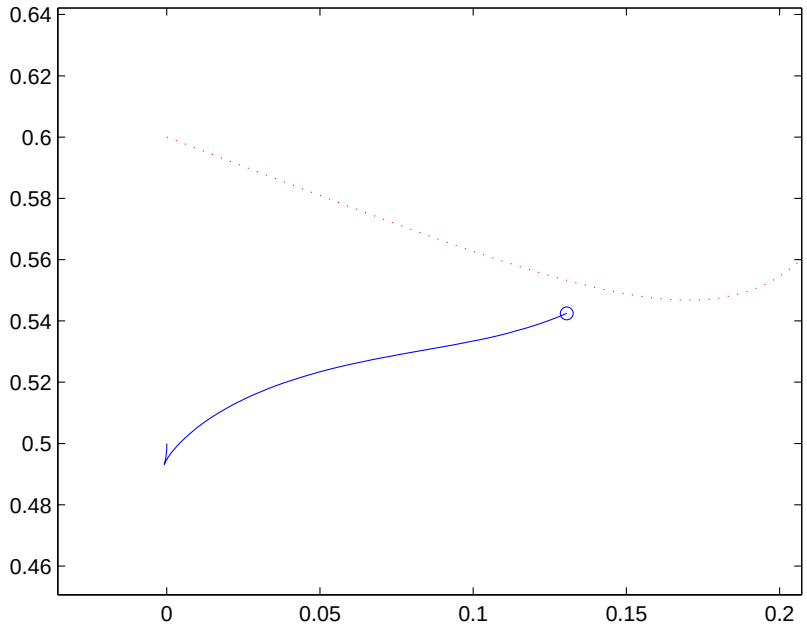

Figure 7.8: Enlargement of the trajectory of the upper robot in Figure 7.3 showing that the trajectory of the robot forms a cusp. The dotted line shows the trajectory of ξ for this particular robot.

In our experiment we will select l to be approximately an order of magnitude less than the smallest side of the figure. Although using a relatively small l value results in more accurate positioning of the robots, there is a trade off: the control signals can be very large when the unicycle makes tight turns. This phenomenon is especially obvious close to $t = 0$. If the unicycle's initial heading is not close to the direction of ξ's initial velocity, the unicycle will make a very tight turn when l is very small, resulting in a large initial angular velocity. This is the case in Figure 7.2 close to $t = 0$.

Additionally, these simulations show that the feedback linearization can result in the unicycle's trajectory having a cusp, as in Figure 7.8. This behaviour is a result of the feedback linearization. Although the behaviour of the robots is less ideal than when controlling the kinematic point, the simulations show that for a sufficiently small l, it is feasible to stabilize unicycles to a formation with the control from (5.6).

7.2 Experimental Set-Up

The mobile robot testbed used for our experiments consists of a collection of two wheeled vehicles, a bluetooth wireless server and a central supervisory computer connected to a camera. The testbed is reconfigurable and the system has been used to experimentally validate several multivehicle control designs. Although the experiment is run by a central computer, it is possible to simulate autonomous controls by using only local information in the computation of the control.

The central computer is needed to implement the control algorithm because the robots have limited processing and sensing capabilities. Each wheel on the robot is equipped with only an encoder that measures the distance the robot has traveled and so cannot measure any information about the other robots. The information from the wheel encoders is transmitted back to the computer via bluetooth wireless. So the central computer receives information about the robot position from two sources: the overhead camera and the wheel encoders. This information is combined using a sensor fusion algorithm. Specific details of the sensor fusion can be found in [27].

The overhead camera identifies each robot by its distinctive 'hat', as shown in Figure 7.9. The bright coloured circle is used to identify the robot and locate its position and the black stripe is used to determine its heading.

The robot inputs are calculated on the computer based on the position measurements obtained from the camera and the wheel encoders. The inputs are then transmitted to the robots via the bluetooth server using wireless communications. Further discussion of the communication protocol can be found in [27].

The robots have a separate gearbox and motor for each of the two wheels. The two motors mean that the wheels can be controlled independently. The central computer sends target velocities to each robot for each of its wheels, and an onboard proportional-integral-derivative controller (PID controller) and pulse width modulation (PWM) are used to control each motor to achieve the target wheel velocity based on information

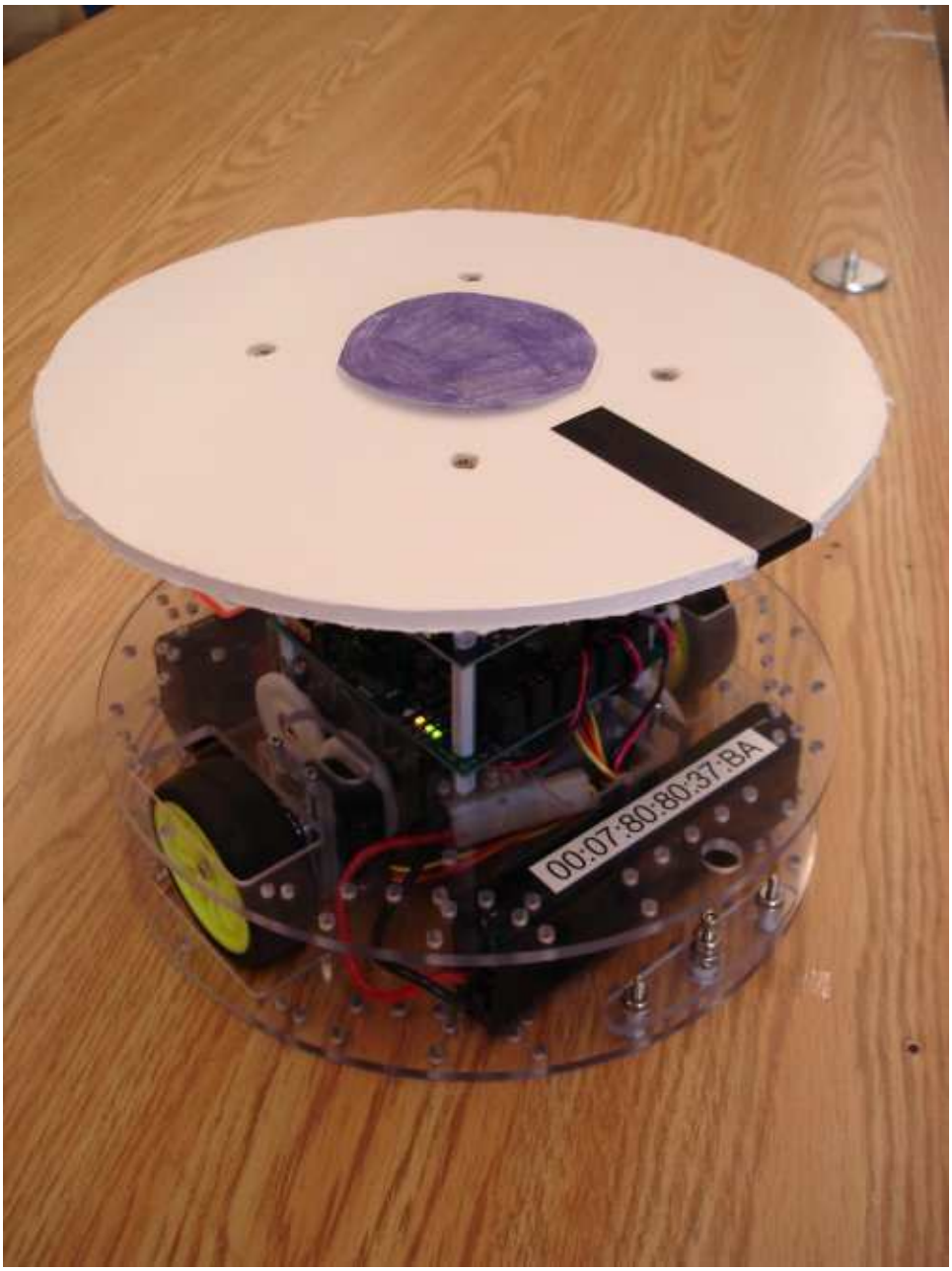

Figure 7.9: Robot used in the experiment. The distinctive top is used to identify the robot and the black stripe is used to determine the robot's heading by the central computer's vision algorithm.

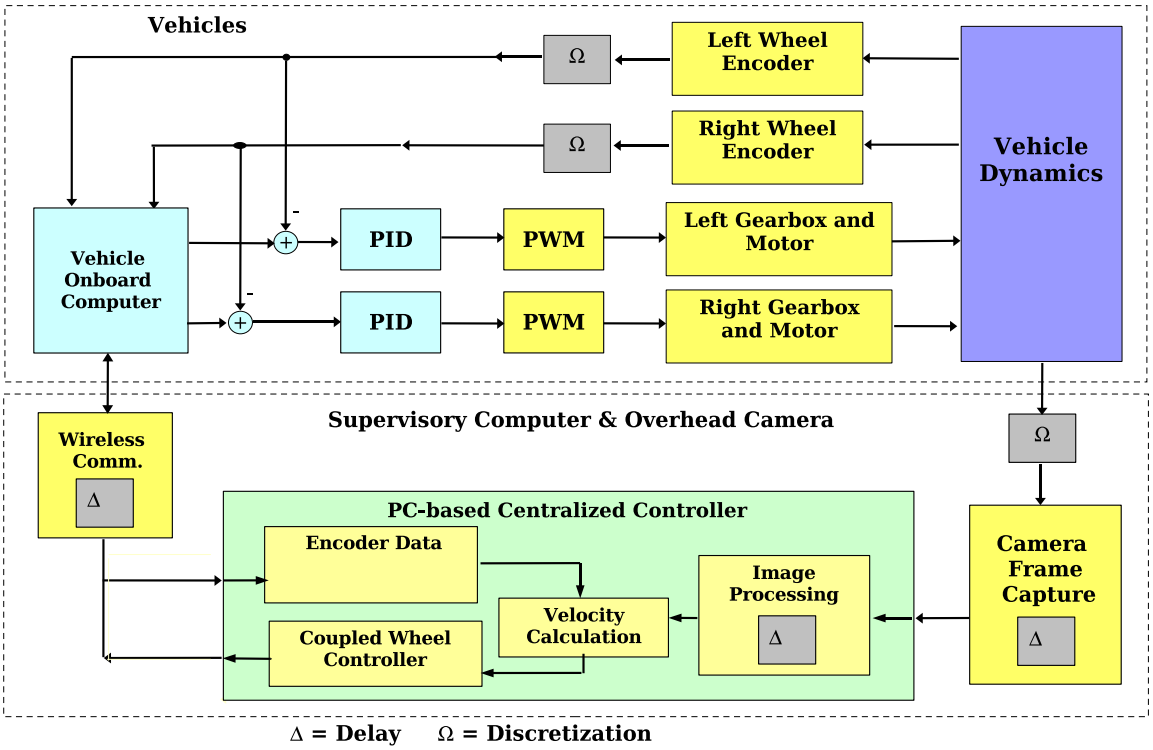

Figure 7.10: The feedback loop for the multivehicle experiment. Figure is from [27].

from the wheel encoders. The parameters for the PID controller can be adjusted at the start of the experiment via the central computer. For all the experiments that follow the following PID controller parameters were used: $K_p = 0.2$, $K_i = 5$, $K_d = 0$. The feedback loop for the experiment is shown in Figure 7.10.

The robots are very light, compared to the power of the motors, so a kinematic model closely describes the robot behaviour.

7.3 Sources of Error

There are several significant sources of error in the experiments. The first is the delays in the system shown in Figure 7.10. There is a considerable delay between the data collected from the overhead camera and when the position of the robots is available to

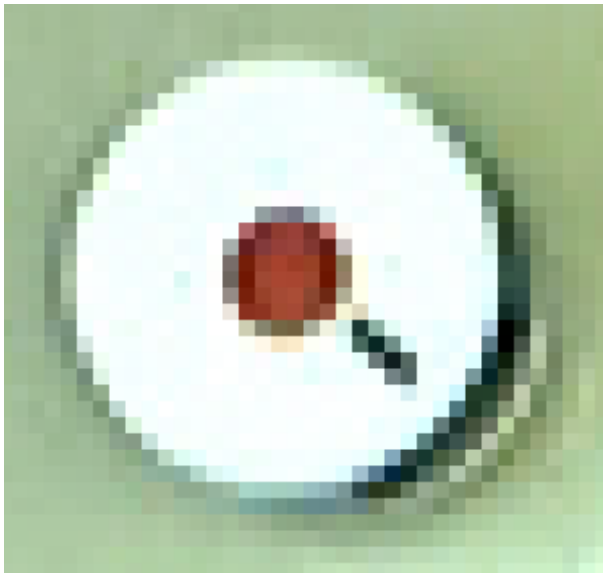

Figure 7.11: The top of the robot, as seen by the overhead camera. Figure is from [27].

calculate the control. This delay is approximately 180ms. The delay in transmitting the signals to the robots is 37ms. The delay in receiving information from the robot encoders is 178ms, [27]. The control loop runs every 200ms. So there is approximately a 400ms delay in the system.

The error in the position measurements of the robots from the camera is approximately 1 cm. Another significant source of error is the accuracy of the heading measurement for the camera. The camera has limited resolution, as shown see Figure 7.11, and the error in the heading measurement is $\pm 8^\circ$ [27]. This error is significant and creates an additionally uncertainty of $\pm$2cm in the location of the point ξ_i for robot i.

7.4 Implementation

The primary difficulty in implementing the control from Chapter 5 is that the control inputs are not bounded. If the robots are far from their target positions, or if the robot must make a very sharp turn, then the target wheel velocities may be very large. The physical limits of the motors that drive the robot wheels mean that the control cannot

achieve arbitrarily large values.

The control is designed for a robot with a unicycle model. The robots used in the experiment have two wheels. However, a two wheeled robot with independently controlled wheels can be made to behave like a unicycle. The target velocities for the two wheels are then calculated from the two unicycle control inputs u_1 and u_2. Define u_r and u_l to be the target velocities for the left and right wheels. Then

$$u_l = u_1 + \frac{1}{2}\rho u_2$$

and

$$u_r = u_1 - \frac{1}{2}\rho u_2,$$

where ρ is the distance between the two wheels of the robot. With these individual wheel controls, the forward velocity for the two wheeled vehicle is u_1 and the angular velocity is u_2, mimicking the unicycle model.

7.5 Experiment: Using the output values

Let's experiment using the control law derived from the minimally rigid graph with four vertices:

$$g(z) = \begin{bmatrix} ||z_1 - z_2||^2 \\ ||z_2 - z_3||^2 \\ ||z_3 - z_4||^2 \\ ||z_4 - z_1||^2 \\ ||z_3 - z_1||^2 \end{bmatrix} \text{ and } d = \begin{bmatrix} 1 \\ 1 \\ 1 \\ 1 \\ 2 \end{bmatrix}.$$

This control was simulated in Section 3.1. In this set of experiments we will calculate the control v_i based on the ξ_i positions of the other robots and then use the matrix $A(\theta)$ to calculate u_i.

Figure 7.12 shows the positions of the robots in the experiment and distances between them. It is clear from Figure 7.12(b) that the behaviour of the system is not the same as our simulations at the beginning of this chapter. In particular, the robots have a steady state oscillation. If we analyze the oscillatory portion using the Fourier transform we see that the frequency is 0.56 Hz. The period is 1.8s, a little more that four times the maximum delay of 400ms. Let's perform some more simulations to gain a better understanding of what is happening in the experiment. In particular, we will simulate a delay with the goal of recreating an oscillation with a period of four times the delay.

First let's simulate the unicycle model for the same initial conditions at the experiment shown in Figure 7.12. The value of 0.12m was selected for l. This is approximately one order of magnitude smaller than the side length of the formation. Additionally, the radius of the robot is 0.12m. So the point ξ_i corresponds to the tip of the black line shown in Figure 7.9 for robot i. The unicycle model simulation is shown in Figure 7.14. Note that the distances decrease much faster in the simulation than in the experiment. This is because we have limited the maximum velocity of the robots.

Figure 7.15 shows a unicycle simulation where the forward velocity of the unicycles has been limited at 0.1m/s, as in the experiment shown in Figure 7.12. This simulation looks more like the robot experiment. In the simulation the distance between the points ξ_i decreases linearly, similar to experimental observations in Figure 7.12(b). Note that both the experiment and the simulation converge to the target d values at similar times. However, the simulation does not have the oscillatory behaviour.

Let's try simulating a unicycle system with a delay. For a delay of 0.5s the system goes unstable with the same initial conditions of the experiment. Figure 7.16 shows a unicycle simulation with a delay of 0.2s that starts much closer to the equilibrium formation. This oscillation has a considerably larger amplitude than the one observed in the experiment.

Figure 7.17 shows a simulation with a delay of 0.5s and where the maximum velocity has been limited to 0.1m/s. This simulation closely resembles that of the experiment in

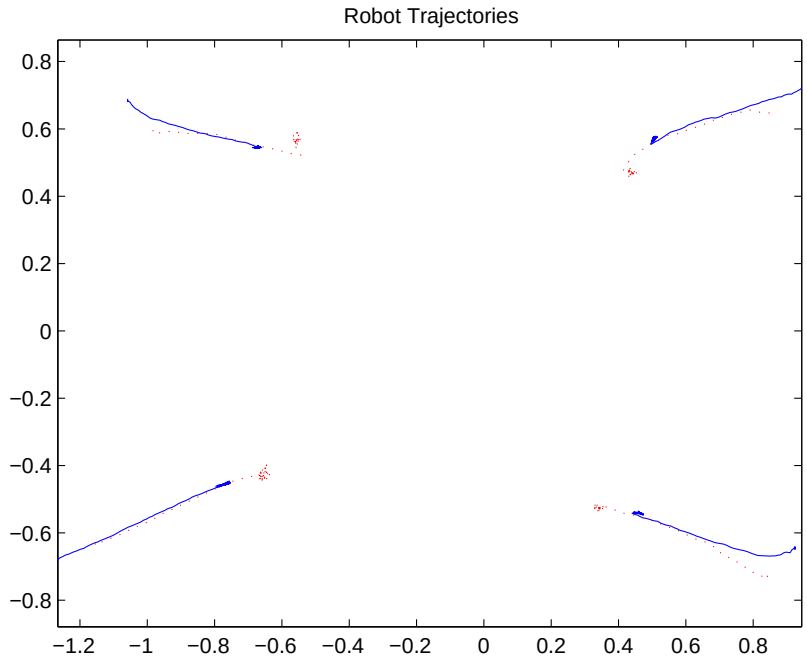

(a) Trajectories

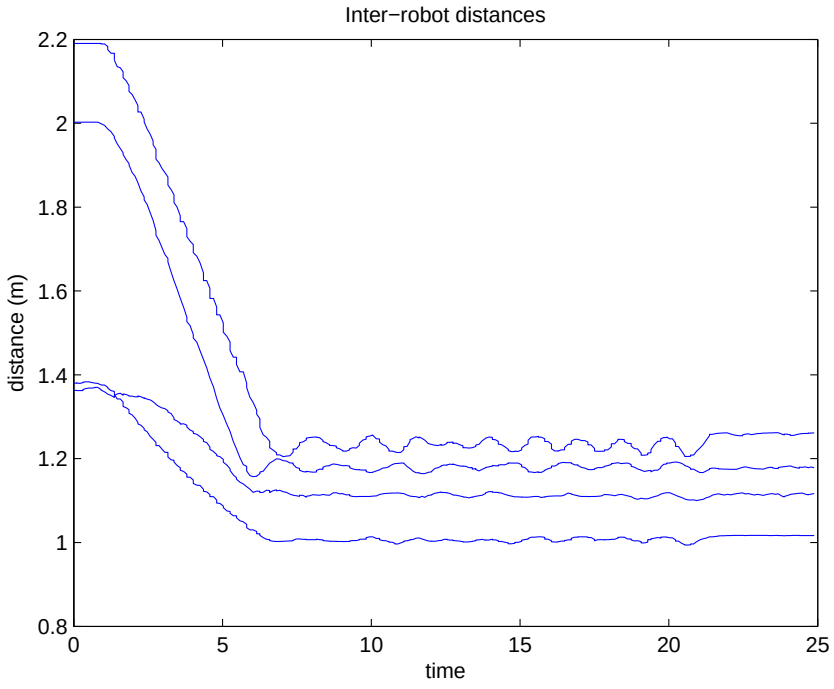

(b) Inter-robot distances

Figure 7.12: Experiment to form a square of side length 1m, and $l = 0.12$m. The velocity is limited at 0.1m/s. In Figure 7.12(a), the trajectories of the unicycle robots in the plane are plotted with a solid line. The trajectories of the feedback linearized points ξ are plotted with a dotted line.

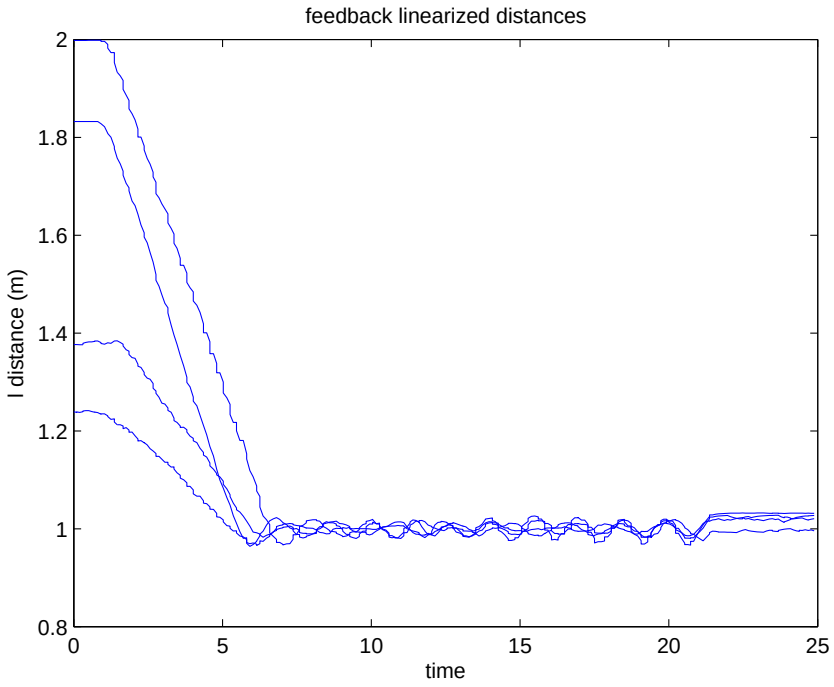

Figure 7.13: Distances between the feedback linearized points ξ for the experiment shown in Figure 7.12.

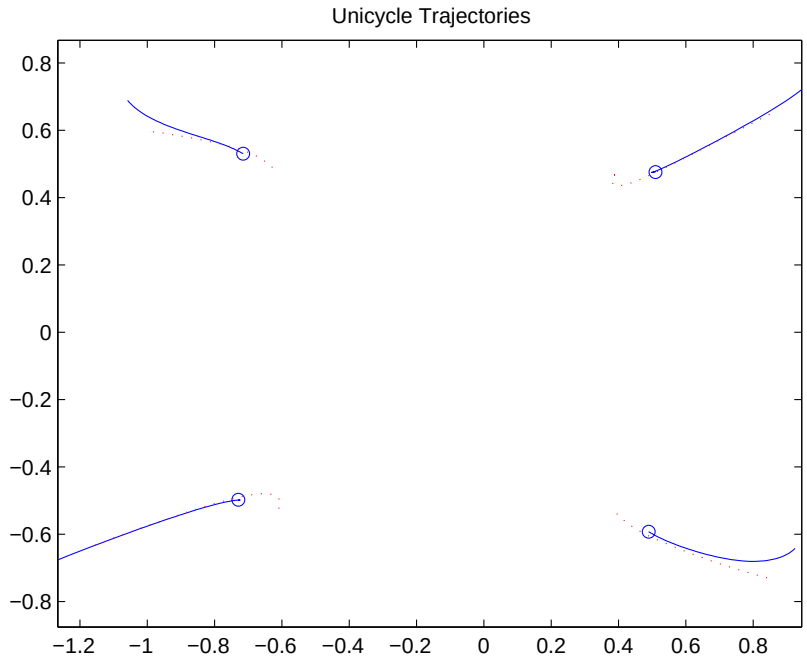

(a) Trajectories

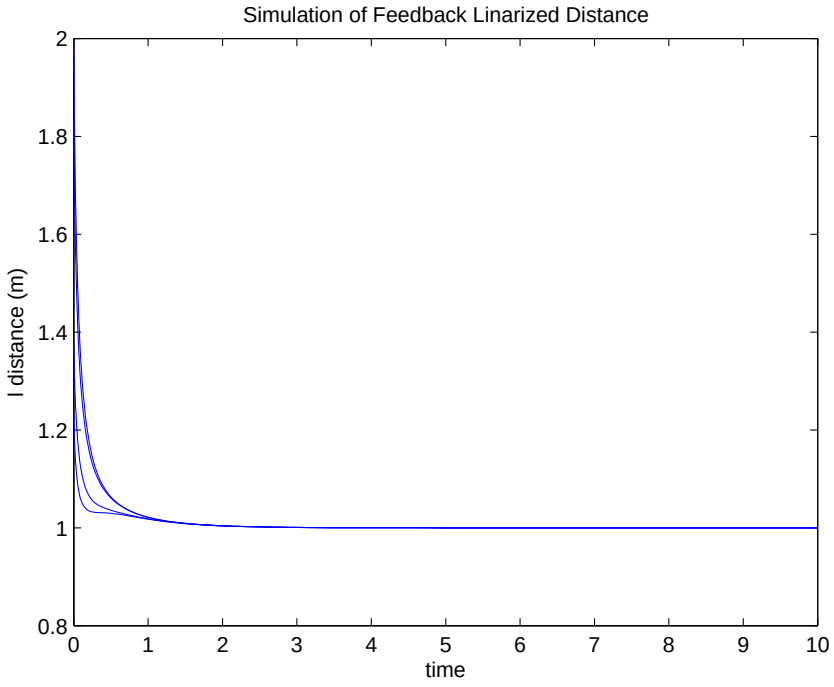

(b) Inter-robot distances

Figure 7.14: Simulation to form a square of side length 1m, and $l = 0.12$m. The velocity is limited at 0.1m/s and there is a delay of 0.5s.

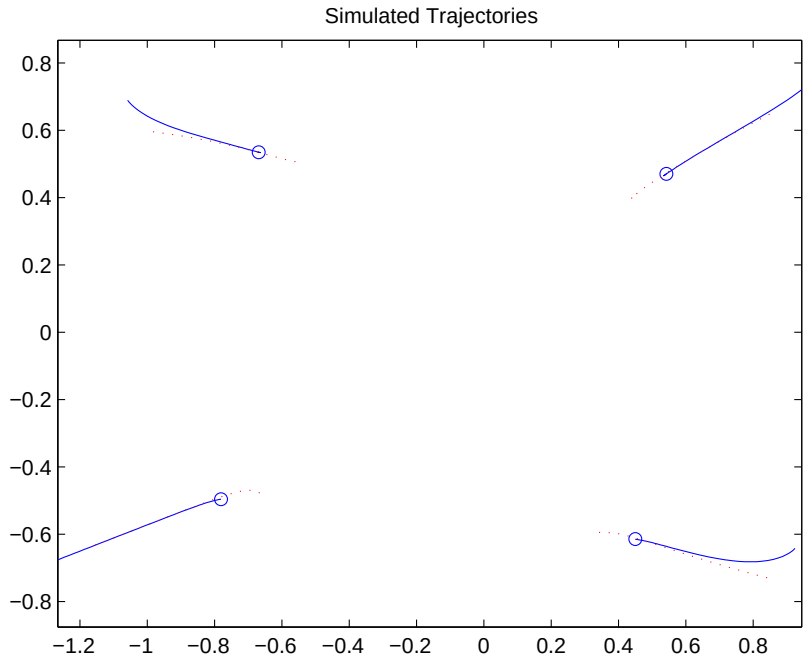

(a) Trajectories

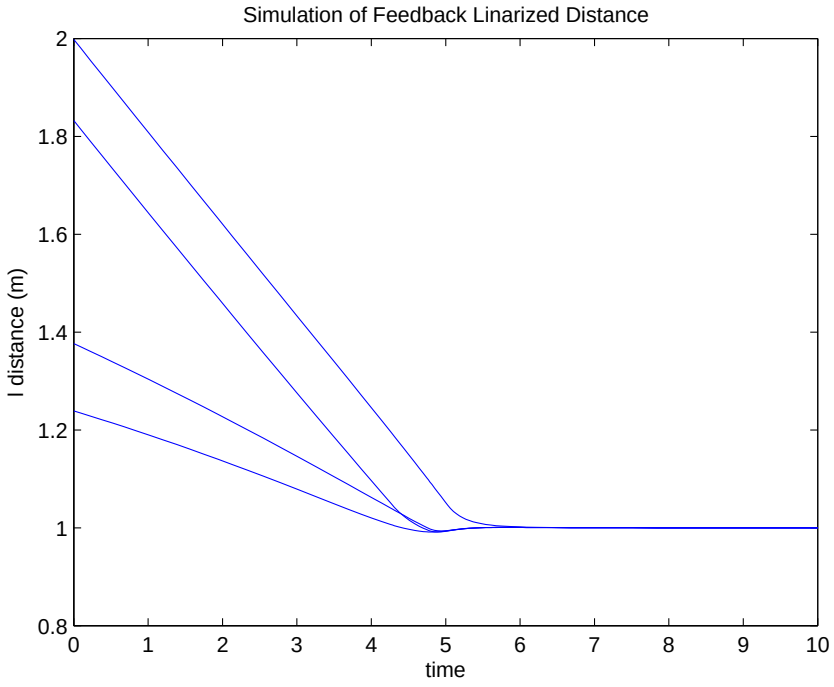

(b) Inter-robot distances

Figure 7.15: Simulation to form a square of side length 1m, and $l = 0.12$m. The velocity is limited at 0.1m/s.

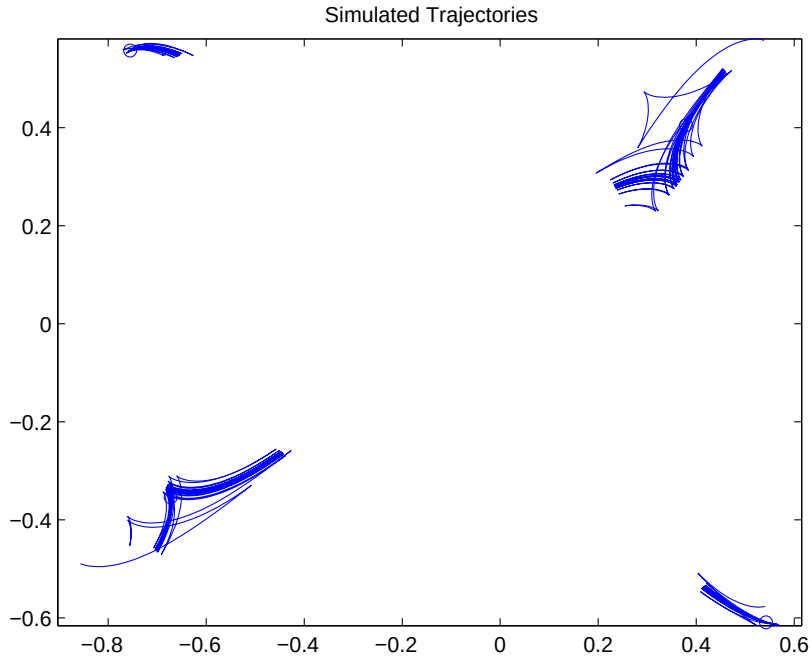

(a) Trajectories

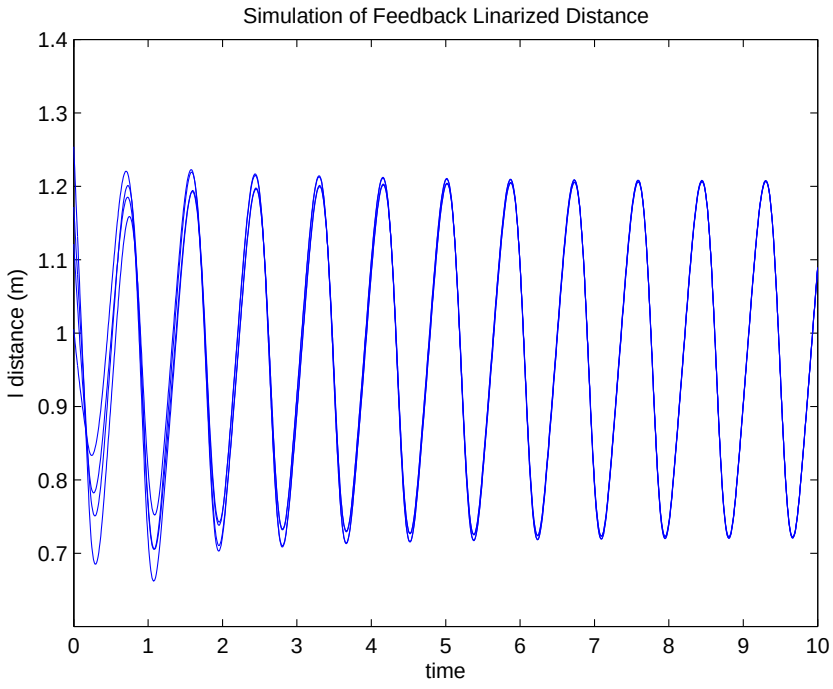

(b) Inter-robot distances

Figure 7.16: Simulation to form a square of side length 1m, and $l = 0.12$m. The control inputs are delayed by 0.5s.

7.12. In particular, there is a limit cycle. The period of the limit cycle is 2s; four times the delay. The experimental data is noisier than the simulation, but this discrepancy can possible be accounted for by the error in measuring the robots states.

In order to analyze this oscillation analytically, let's consider a simple case of one robot trying to position itself a distance $\sqrt{d}$ from a fixed beacon at the origin. Define

$$\phi(z) := \frac{1}{2}(\|z\|^2 - d)^2$$

as a the potential function for the single robot system. Then the resulting gradient system has the dynamics

$$\dot{z} = -(\|z\|^2 - d)z.$$

The system can be transformed into a single variable system by letting x be the distance from the origin to the robot. Then in these new coordinates the dynamics are

$$\dot{x} = -(x^2 - d)x.$$

If we linearize at $x^2 = d$ we see the linear dynamics are

$$\dot{\delta x} = -2d\delta x$$

Let's consider the linear system with a delay of τ. Then

$$\dot{\delta x} = -2d^2\delta x(t - \tau) \tag{7.1}$$

If we simulate this system we see that it does oscillate around the equilibrium, as shown in Figure 7.18.

The block diagram model for the system (7.1) is shown in Figure 7.19. If we study the Nyquist plot of $\frac{8e^{-s\tau}}{s}$ we see that when $d = 1$ the system becomes unstable when

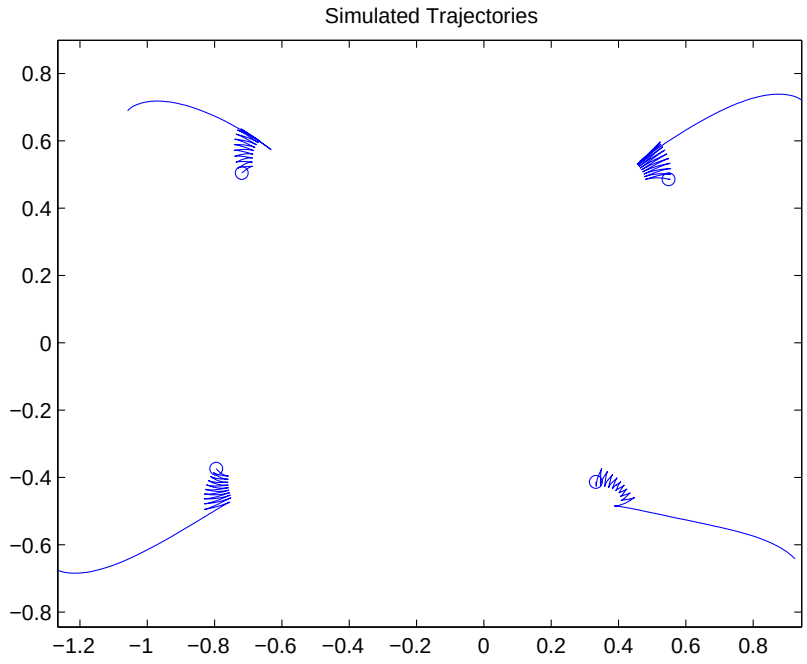

(a) Trajectories

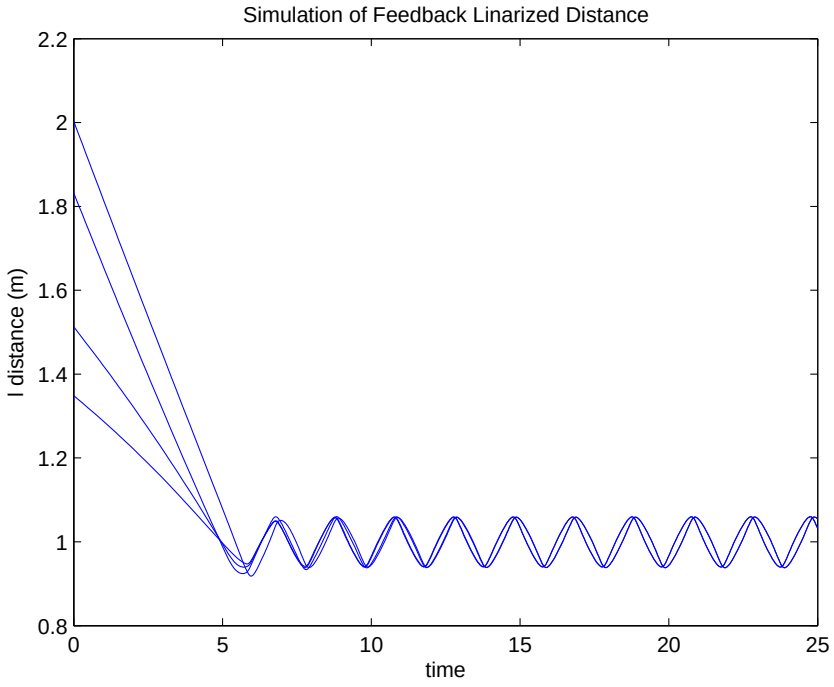

(b) Inter-robot distances

Figure 7.17: Simulation to form a square of side length 1m, and $l = 0.12$m. The velocity is limited at $0.1m/s$ and there is a delay of $0.5s$.

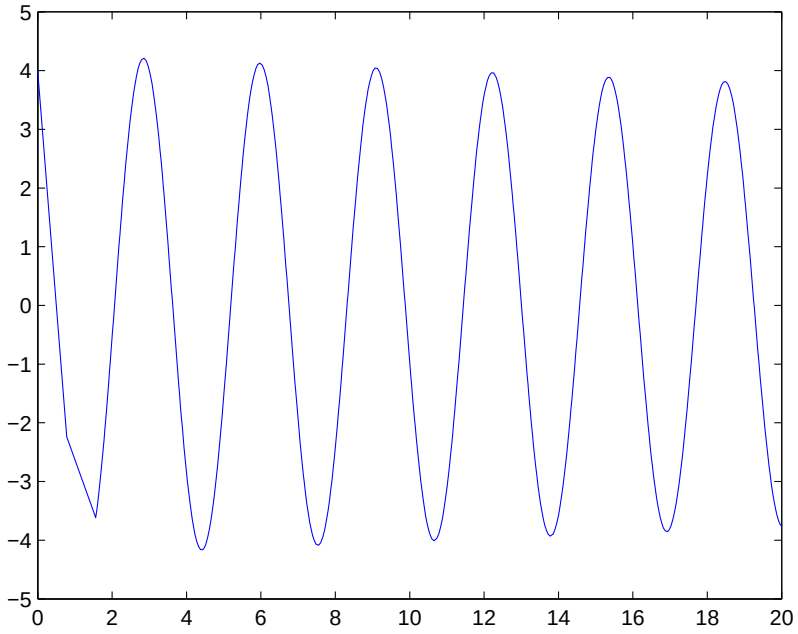

Figure 7.18: Simulation of the linear system in (7.1) with a delay of $\tau = 0.78$.

$\tau = \frac{\pi}{4} \approx 0.79$. The Nyquist plot when $\tau = 0.79$ is shown in Figure 7.20. So we can see that the delay that makes the linear system unstable is on the same order of magnitude as the delay in the robot system. In fact, when we simulated the experimental system with various delays we found that delays less than 0.79 would make the nonlinear system unstable if it was initialized too far from the equilibrium. However, this was not observed experimentally. Our hypothesis is that by limiting the maximum velocity of the robots the system stays stable for larger delays.

Now let's consider the experiments shown in Figures 7.21 and 7.22. The initial conditions for the two experiments are quite similar—but their behaviours are significantly different. In Figure 7.22 the robots converge to the target square formation. In Figure 7.21 the robots do not converge to a square and two robots have a collision. Both these formations are in the equilibrium set E_1. There are two distinct formations in the target equilibrium set because the formation was specified with a graph that is not globally

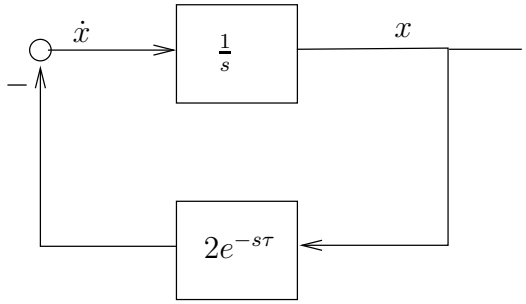

Figure 7.19: Linear system with a delay.

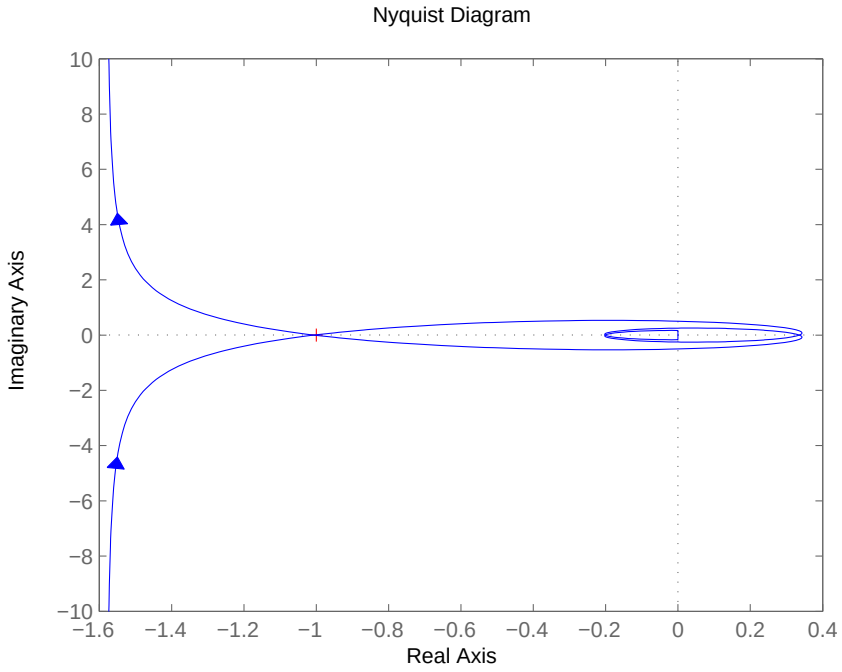

Figure 7.20: Nyquist plot of (7.1) with $\tau = 0.79$.

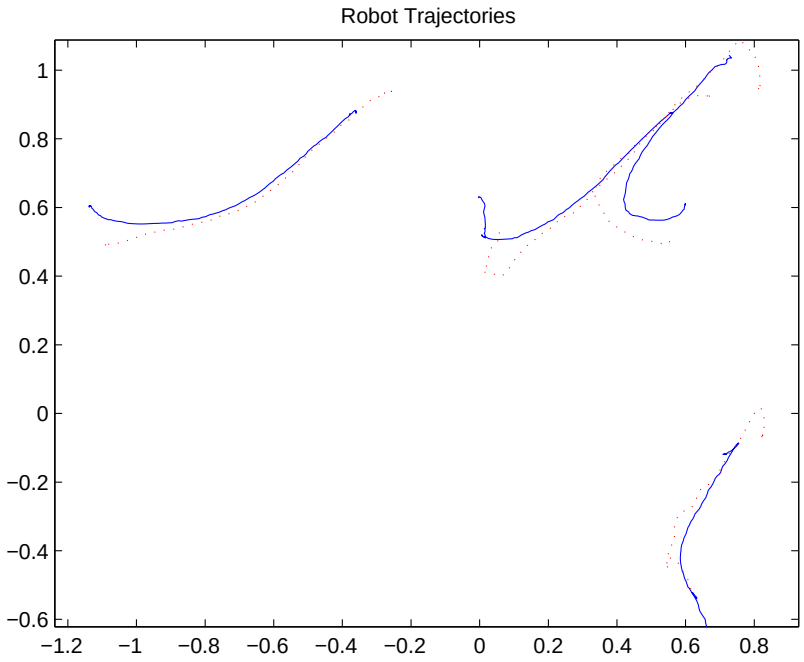

Figure 7.21: Experiment to form a square of side length 1m, and $l = 0.12$m. The velocity is limited at 0.1m/s. The trajectories of the unicycle robots in the plane are plotted with a solid line. The trajectories of the feedback linearized points ξ are plotted with a dotted line. In this experiment the robots do not converge to a square formation, but instead converge to a triangle formation—one of the other equilibria in E_1.

rigid. In fact, the graph specifying the target formation is minimally rigid and could have been generated using the Henneburg insertion technique outlined in Section 2.3.3. This experiment shows the limitations of using a minimally rigid graph to design the control.

7.6 Experiment: Using robot position values

The experiment in the previous section required the use of the points ξ_i. In order for the robots to know the location of these points, they must either know the heading of the robots, or they must track a beacon located a distance l in front of the robot. Both these solutions present implementation difficulties. It is difficult to gain information about the

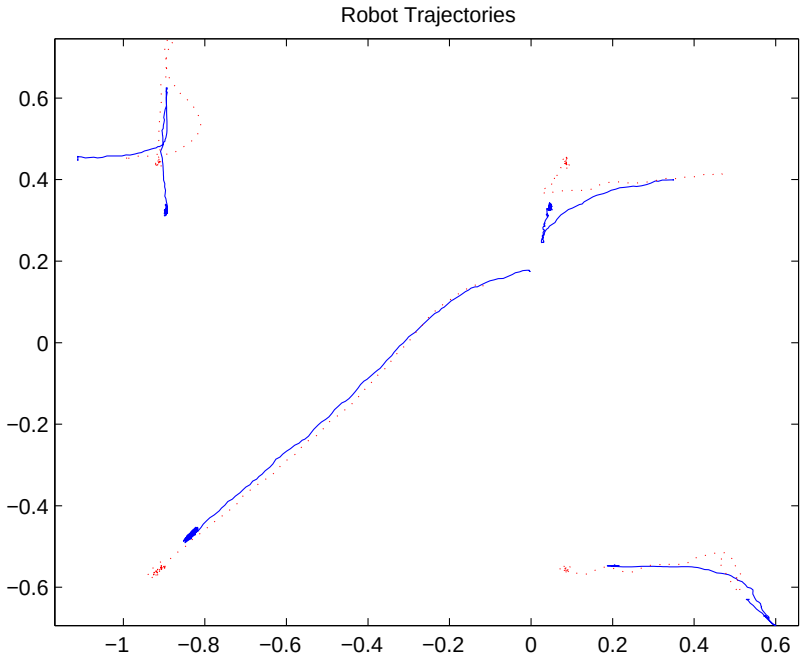

Figure 7.22: Experiment to form a square of side length 1m, and $l = 0.12$m. The velocity is limited at 0.1m/s. The trajectories of the unicycle robots in the plane are plotted with a solid line. The trajectories of the feedback linearized points ξ are plotted with a dotted line. The initial conditions of this experiment are very similar to those in Figure 7.21, however in this experiment the robots converge to a square formation.

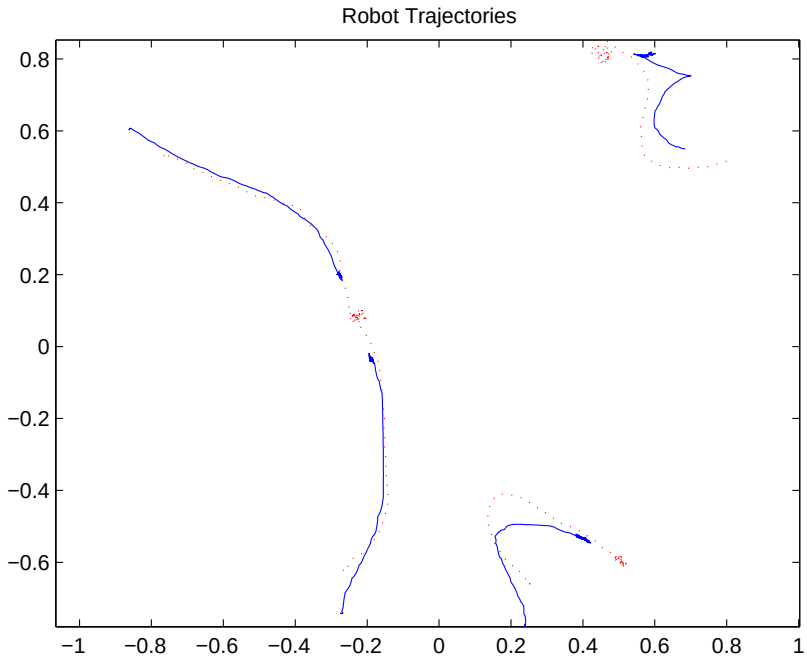

(a) Trajectories

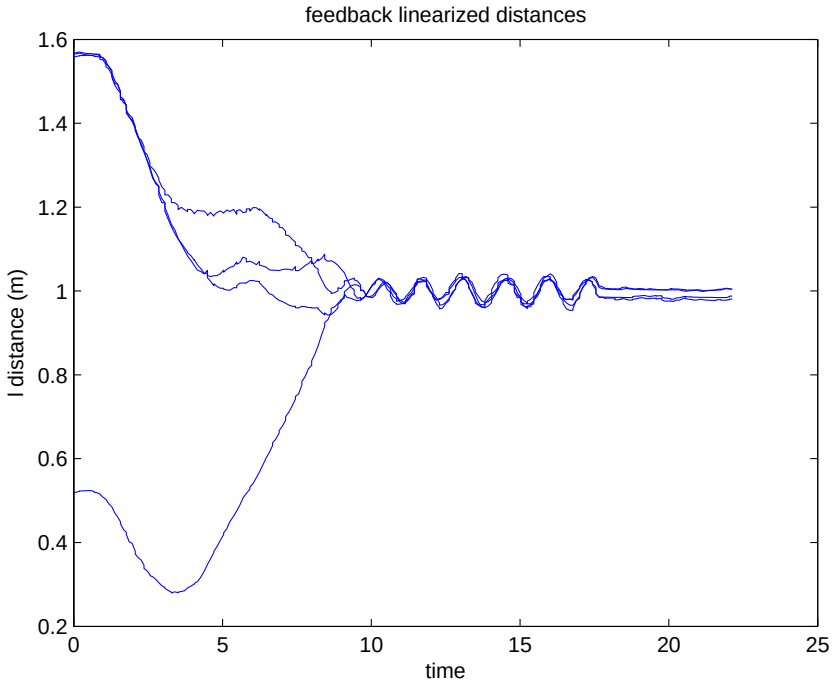

(b) Inter-robot distances

Figure 7.23: Experiment to form a square of side length $1m$, and $l = 0.12$. The velocity is limited at $0.1m/s$. In Figure 7.23(a), the trajectories of the unicycle robots in the plane are plotted with a solid line. The trajectories of the feedback linearized points ξ are plotted with a dotted line.

relative headings of the robots, so in general θ_i cannot be used in practice. In order to implement the beacon approach, the robots would have to be modified to have beacons attached to them. For some application this might not be feasible.

In the experiment shown in Figure 7.24, each robot calculates its control based on its ξ_i position and the z_j positions of the other robots. For experiments where $l = 0.12$m, like the experiments in the previous section, using z_i instead of ξ_i is equivalent to ξ_i having an additional error of 0.12m in its position. Due to this additional error, the ξ points do not reach their target separations, as demonstrated in Figure 7.25. However, the inter-robot distances is are similar to the experiments in the previous section.

7.7 Conclusions

The experimental behaviour of the controlled system (5.6) on the unicycle system had some unexpected results. In particular, a limit cycle was observed as the robots reached the target formation. Simulations showed that such a limit cycle occurs in systems where the maximum velocity of the robots is limited and the robots control is calculated based on delayed information. These sources of error were not modeled in our original analysis. However, the robots still converged to the target formation, showing that the control is robust to delays in the robot positions.

Additionally, experiments showed that using a combination of the robot's own ξ_i position and the x and y positions of the other robot still resulted in convergence to the target formation. This is an important observation because in a physical implementation of this control it might not be possible to obtain exact information on the ξ position of the robots. The experiments suggest that this control is suitable for implementation is some formation applications.

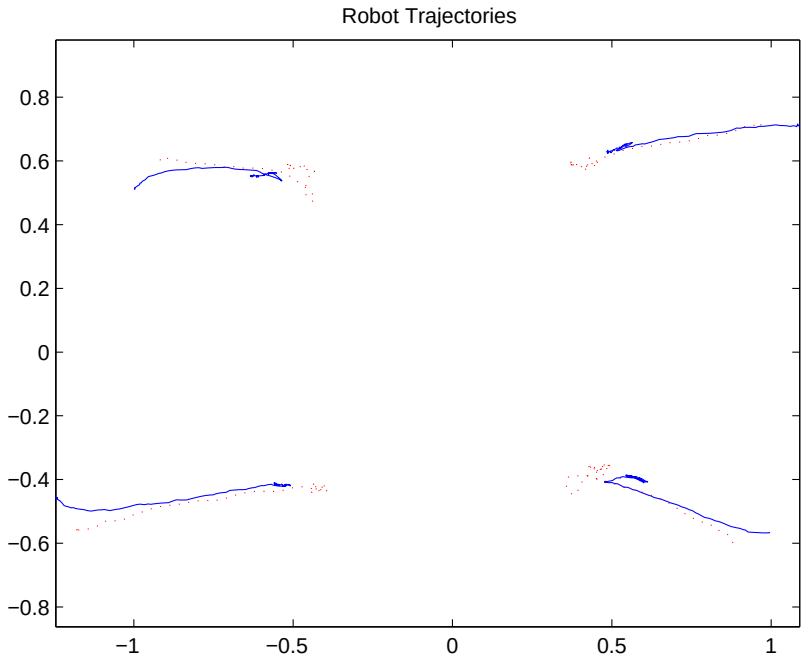

(a) Trajectories

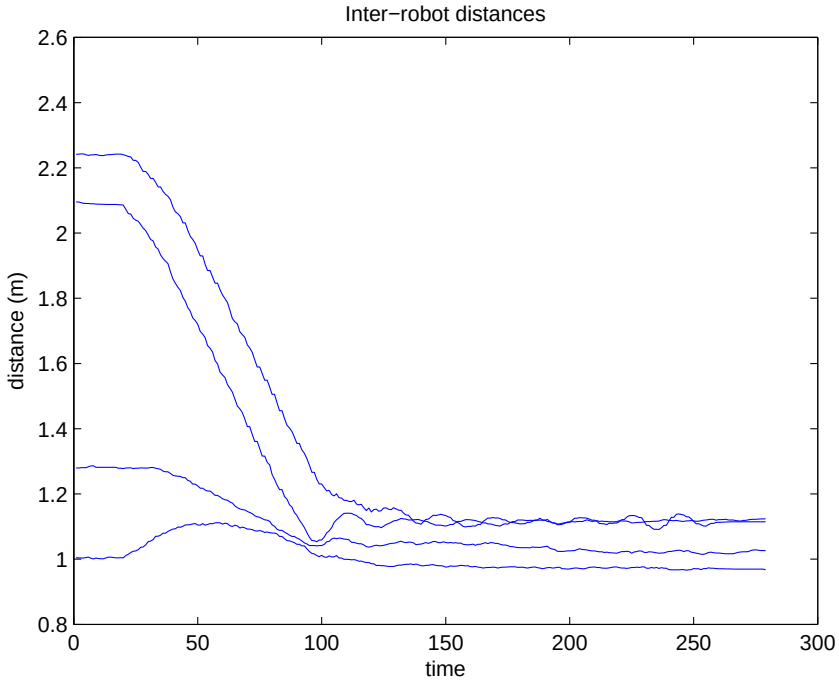

(b) Inter-robot distances

Figure 7.24: Experiment to form a square of side length $1m$, and $l = 0.12$. The velocity is limited at $0.1m/s$. In Figure 7.24(a), the trajectories of the unicycle robots in the plane are plotted with a solid line. The trajectories of the feedback linearized points ξ are plotted with a dotted line.

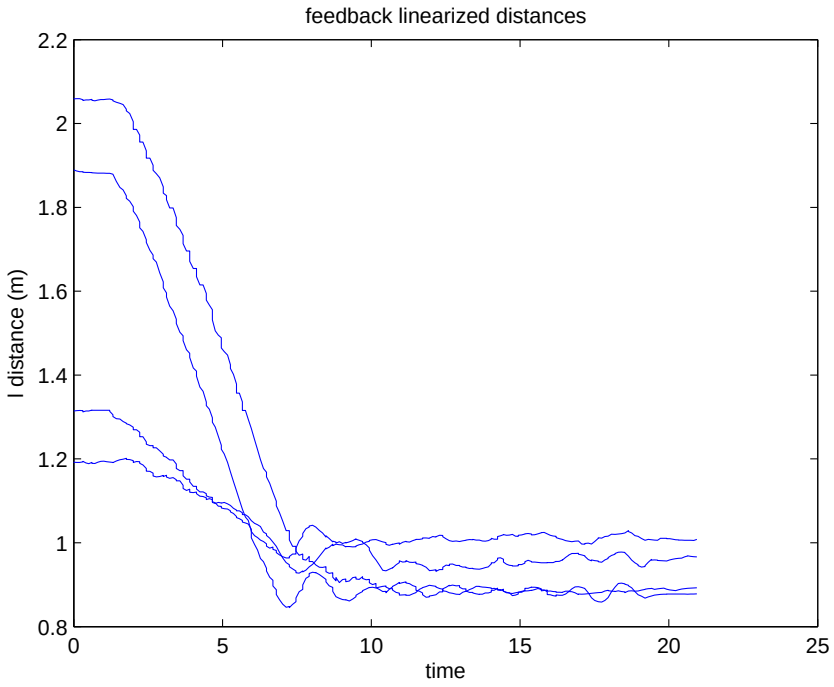

Figure 7.25: Distances between the feedback linearized points ξ for the experiment shown in Figure 7.24.

Chapter 8

Conclusions

This thesis studies the formation stabilization problem for multi-robot systems. In Chapter 3 we propose a control to solve the formation problem for nearly arbitrary formations, and in Chapter 5 we prove that the control in fact makes the target formation stable and that solutions exist for all time. In particular, we use the strong relationship between the stability of the target formation and the stability of equilibrium manifolds. The stability of equilibrium manifolds was studied in Chapter 4.

In Chapter 6 we extend the results of Chapter 5 to design a scalable control for the regular polygon problem as well as show how the results of Chapters 4 and 5 can be extended for a certain class of directed graphs.

Finally, experimental results validating the theory are presented in Chapter 7. The experimental equipment had several sources of error that are not modeled in our analysis. However, the robots still converged to the target formation, showing that the control is robust to delays and uncertainty in the robot positions.

The main results and contributions of this thesis are as follows:

- A gradient control to stabilize any infinitesimally rigid formation.
- The target formation was shown to be an embedded submanifold of the state space, which simplified the analysis of the formation stabilization problem.

- A rigorous treatment of stability of a manifold of equilibra was presented. The was based on [14] and [24], but there is some originality in the details and style.

- Design of a novel control to stabilize robots to a regular polygon formation.

- Design of a novel control to stabilize robots to a formation based on a directed graph.

- Experimental validation of the undirected formation control on a multi-vehicle system. These experiments show that the formation control is robust to significant delays in the experimental system.

8.1 Future Work

The results of this thesis could be extended in the following areas:

- If the control is implemented using cameras as sensors, uneven terrain could cause the robots to lose sight on one another. Making the control robust in these situations would be a particularly useful extension of this work.

- The formation control of the unicycles could be implemented by having the unicycle's trajectory track the path of steepest descent of the potential function instead of using the feedback linearization technique to control the unicycle.

- Necessary conditions for non-collinear equilibria in $E \setminus E_1$ could be investigated.

- The control could be modified so that the robots converge to a moving formation. Possibilities for extending the control in this way include assigning a leader that tracks a trajectory or by adding an additional term in the potential function. Using a leader would be a particularly suitable technique for the formation control based on a directed graph developed in Section 6.2.

- The results of Section 6.2 show that using individual potential functions results in a considerably more complicated control than the one obtained using a global potential function. In particular, further study is needed to understand why some infinitesimally persistent directed graphs result in closed loop systems with a Jacobian with four zero eigenvalues at the target formation. In particular, the possible relationship between these additional eigenvalues and cycles in the underlying directed graph warrants investigation.

Bibliography

[1] P.-A. Absil and K. Kurdyka. On the stable equilibrium points of gradient systems. *Systems & Control Letters*, 55(7):573–577, 2006.

[2] V.I. Arnold. *Mathematical Methods of Classical Mechanics*. Springer-Verlag, 1978.

[3] L. Asimow and B. Roth. The rigidity of graphs. *Transactions of the American Mathematical Society*, 245:279–289, November 1978.

[4] L. Asimow and B. Roth. The rigidity of graphs II. *Journal of Mathematical Analysis and Applications*, 68(1):171–190, 1979.

[5] J. Aspnes, T. Eren, D.K. Goldenberg, A.S. Morse, W. Whiteley, Y.R. Yang, B.D.O. Anderson, and P.N. Belhumeur. A theory of network localization. *IEEE Transactions on Mobile Computing*, 5(12):1663–1678, December 2006.

[6] B. Aulbach. Approach to hyperbolic manifolds of stationary solutions. In H.W. Knobloch, editor, *Equadiff 82 : Proceedings of the International Conference held in Würzburg, FRG, August 23-28, 1982*, pages 56–66. Springer-Verlag, 1983.

[7] S. Bereg. Certifying and constructing minimally rigid graphs in the plane. In *Proceedings of the Twenty-First Annual Symposium on Computational Geometry*, pages 73–80, Pisa, Italy, 2005. Annual Symposium on Computational Geometry.

[8] N. Biggs. *Algebraic Graph Theory*. Cambridge University Press, 1974.

[9] W.M. Boothby. *An Introduction to Differentiable Manifolds and Reimannian Geometry*. Academic Press Inc., 1986.

[10] J. Cortés, S. Martínez, and F. Bullo. Robust rendezvous for mobile autonomous agents via proximity graphs in d dimensions. *IEEE Transactions on Automatic Control*, 51(8):1289–1298, 2004.

[11] J. Cortés, S. Martínez, T. Karatas, and F. Bullo. Coverage control for mobile sensing networks. *IEEE Transactions on Robotics and Automation*, 2(2):243–255, 2004.

[12] D.K. Goldenberg, J. Lin, A.S. Morse, B.E. Rosen, and Y.R. Yang. Towards mobility as a network control primitive. In *Proceedings of the 5th ACM International Symposium on Mobile ad hoc Networking and Computing*, pages 163–174, Tokyo, Japan, 2004.

[13] V. Guillemin and A. Pollack. *Differential Topology*. Prentice-Hall, 1974.

[14] J.K. Hale. *Ordinary Differential Equations*. Wiley-Interscience, 1st edition, 1969.

[15] J.K. Hale and P. Massatt. Asymptotic behavior of gradient-like systems. In A.R. Bednarek, editor, *Dynamical systems II : Proceedings of a University of Florida International Symposium*, pages 85–101. Academic Press, Inc., 1982.

[16] J.M. Hendrickx, B.D.O. Anderson, J.-C. Delvenne, and V.D. Blondel. Directed graphs for the analysis of rigidity and persistence in autonomous agent systems. Unpublished manuscript. To appear, International Journal of Robust and Nonlinear Control.

[17] J.M. Hendrickx, B. Fidan, Y. Changbin, B.D.O. Anderson, and V.D. Blondel. Elementary operations for the reorganization of minimally persistent formations. In *Proceeds of the 17th International Symposium on Mathematical Theory of Networks and Systems (MTNS2006)*, pages 859–873, Kyoto, Japan, 2006.

[18] M. Hirsch. *Differential Topology*. Springer-Verlag, 1976.

[19] M. Hirsch and S. Smale. *Differential Equations, Dynamical Systems, and Linear Algebra*. Academic Press Inc., 1974.

[20] H.K. Khalil. *Nonlinear Systems*. Prentice Hall, 2002.

[21] J. Lin, A.S. Morse, and B.D.O. Anderson. The multi-agent rendezvous problem - the asynchronous case. In *Proceedings of the 43rd IEEE Conference on Decision and Control*, volume 2, pages 1926–1931, Atlantis, Bahamas, December 2004.

[22] Z. Lin, M.E. Broucke, and B.A. Francis. Local control strategies for groups of mobile autonomous agents. In *Proceedings of the 42nd IEEE Conference on Decision and Control and European Control Conference*, pages 3303–3308, Seville, Spain, 2003.

[23] S. Łojawiewicz. Sur le problème de la division. *Studia Mathmatica*, 18:87–136, 1959.

[24] I.G. Malkin. *Theory of Stability of Motion*. United States Atomic Energy Commission Technical Information Service, 1958.

[25] J.A. Marshall. *Cooperative Autonomy: Pursuit Formations of Multivehicle Systems*. PhD thesis, University of Toronto, September 2005.

[26] J.A. Marshall, M.E. Broucke, and B.A. Francis. Formations of vehicles in cyclic pursuit. *IEEE Transactions on Automatic Control*, 9(11):1963–1974, November 2004.

[27] J. Nawrot. Time optimal control for collision avoidance recovery of two unicycles. Master's thesis, University of Toronto, 2005.

[28] H. Nijmeijer and A.J. van der Schaft. *Nonlinear Dynamical Control Systems*. Springer-Verlag, 1990.

[29] R. Olfati-Saber and R.M. Murray. Distributed cooperative control of multiple vehicle formations using structural potential functions. In *Proceedings of the 15th IFAC World Congress*, Barcelona, Spain, 2002.

[30] E. Rimon and D.E. Koditschek. Exact robot navigation using artificial potential functions. *IEEE Transactions on Robotics and Automation*, 8(5):501–518, October 1992.

[31] L.B. Ryashko and E.E. Shnol. On exponentially attracting invariant manifolds of ODEs. *Nonlinearity*, 16:147–160, 2003.

[32] S.L. Smith, M.E. Broucke, and B.A. Francis. Stabilizing a multi-agent system to an equilateral polygon formation. In *Proceeds of the 17th International Symposium on Mathematical Theory of Networks and Systems (MTNS2006)*, pages 2415–2424, Kyoto, Japan, 2006.

[33] M. Spivak. *Differential Geometry*, volume 1. Publish or Perish Inc., 2nd edition, 1979.

[34] V. Sundarapandian. A geometric proof of Malkin's stability theorem. *Indian Journal of Pure and Applied Mathematics*, 34(7):1085–1088, July 2003.

[35] H. Tanner, A. Jadbabaie, and G.J. Pappas. Stable flocking of mobile agents, part ii: Dynamic topology. In *Proceedings of the 42nd IEEE Conference on Decision and Control and European Control Conference*, pages 2016–2021, Seville, Spain, December 2003.

[36] H. Whitney. Elementary structure of real algebraic varieties. *The Annals of Mathematics*, 66(3):545–556, November 1957.

[37] S. Wiggins. *Introduction to Applied Nonlinear Dynamical Systems and Chaos*. Springer-Verlag, 1990.

[38] S. Willard. *General Topology*. Addison-Wesley, 1968.

[39] W.M. Wonham. *Linear Multivariable Control*. Springer-Verlag, 3rd edition, 1985.

[40] F. Zhang and N.E. Leonard. Coordinated patterns on smooth curves. In *Proceedings of the 2006 IEEE International Conference on Networking, Sensing and Control*, pages 434–439, Fort Lauderdale, Florida, U.S.A., 2006.

[41] L. Zhi-Quan, M. Gastpar, L. Juan, and A. Swami. Distributed signal processing in sensor networks. *IEEE Signal Processing Magazine*, 23(4):14–15, July 2006.